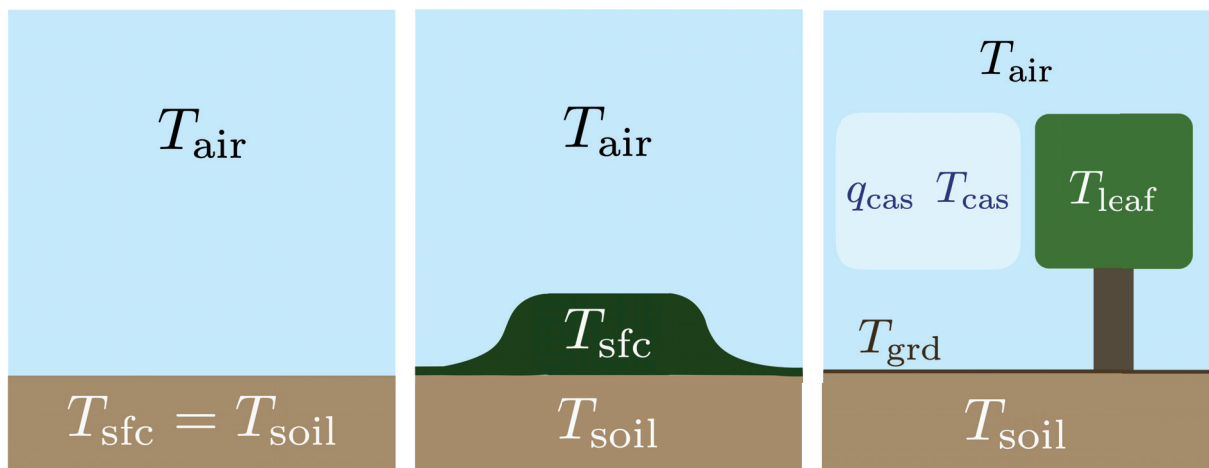# Studying land-atmosphere interactions in an Earth system model - The role of canopy heat storage and leaf thermoregulation

Marvin Heidkamp

Hamburg 2020

Hinweis

Die Berichte zur Erdsystemforschung werden vom Max-Planck-Institut für Meteorologie in Hamburg in unregelmäßiger Abfolge herausgegeben.

Sie enthalten wissenschaftliche und technische Beiträge, inklusive Dissertationen.

Die Beiträge geben nicht notwendigerweise die Auffassung des Instituts wieder.

Die "Berichte zur Erdsystemforschung" führen die vorherigen Reihen "Reports" und "Examensarbeiten" weiter.

Anschrift / Address

Max-Planck-Institut für Meteorologie
Bundesstrasse 53
20146 Hamburg
Deutschland

Tel./Phone: +49   (0)40 4 11 73 - 0
Fax: +49   (0)40 4 11 73 - 298

name.surname@mpimet.mpg.de
www.mpimet.mpg.de

Notice

The Reports on Earth System Science are published by the Max Planck Institute for Meteorology in Hamburg. They appear in irregular intervals.

They contain scientific and technical contributions, including Ph. D. theses.

The Reports do not necessarily reflect the opinion of the Institute.

The "Reports on Earth System Science" continue the former "Reports" and "Examensarbeiten" of the Max Planck Institute.
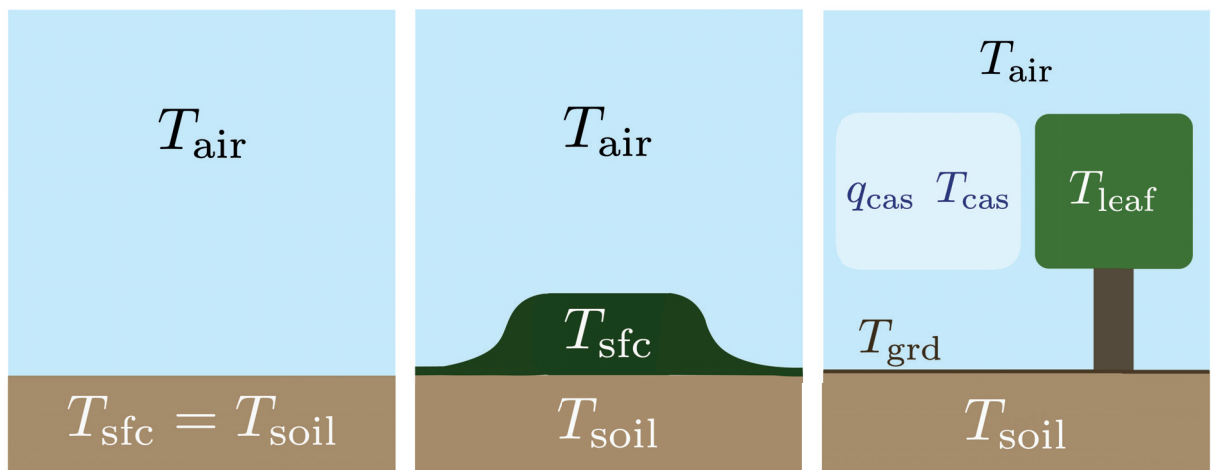
Layout

Bettina Diallo and Norbert P. Noreiks
Communication

Copyright

Studying land-atmosphere interactions in an Earth system model - The role of canopy heat storage and leaf thermoregulation

Marvin Heidkamp

Hamburg 2020

Marvin Heidkamp
aus Oldenburg i.H., Deutschland

Max-Planck-Institut für Meteorologie
The International Max Planck Research School on Earth System Modelling
(IMPRS-ESM)
Bundesstrasse 53
20146 Hamburg

Universität Hamburg
Geowissenschaften
Meteorologisches Institut
Bundesstr. 55
20146 Hamburg

Abstract

In this thesis, we investigate the role of the vegetation canopy in the climate system by analyzing two processes in the canopy layer. First, we study processes that control changes in thermal energy stored in the soil and the canopy layer to determine whether they affect the climate system over decadal time scales. Here we introduce a new approach to close the surface energy balance equation using a physically based estimation of the canopy heat storage (called SkIn$^+$ scheme). To test this scheme for the role of the heat storage, we perform an offline single-site experiment forced by observations as well as a coupled land–atmosphere experiment using the land component JSBACH of the MPI-ESM (Max Planck Institute - Earth system model). We find that SkIn$^+$ leads to warming during the day and to cooling at night, thereby improving the performance in the representation of the modeled surface fluxes on diurnal time scales. Compared to the old scheme, phase errors in surface temperature and heat fluxes are eliminated, and nocturnal heat releases that unrealistically destroy the stable boundary layer disappear. On the global scale, for regions with no or shallow vegetation and a pronounced diurnal cycle, the nocturnal cooling effect prevails because stable conditions at night maintain the delayed response in temperature, whereas the daytime turbulent exchange amplifies it.

Second, we investigate the process of *leaf thermoregulation*. Plants tend to keep their leaf temperature within an optimal range by regulating heat and water losses, which means that they are warmer in cool environments and generally colder in warm environments. This behavior has been found in laboratory and field experiments in previous studies. Here we address the question of whether a signature of leaf thermoregulation can also be found in a climate model and what is the impact on the global climate. To study the impact of leaf thermoregulation, we develop a new dual-source canopy layer energy balance scheme (CEBa) as a part of JSBACH. This scheme makes it possible to calculate the temperature and humidity in the

ambient canopy air space, the temperature of the ground surface, and the temperature of the leaf itself. The process of leaf thermoregulation is investigated in detail using different modeling approaches. These include a zero-dimensional instantaneous solution of the energy balance as well as offline FLUXNET site experiments and coupled global experiments. We find a negative correlation between the leaf temperature excess and the ambient air temperature as found in observations on the site level, but with a less pronounced magnitude. However, on a global scale, we find a positive correlation contradicting leaf thermoregulation theory at the leaf scale. Only in the case of unlimited water availability, we identify a negative correlation on the global scale. However, its magnitude is underestimated compared to observations and thus has a negligible impact on plant productivity.

Zusammenfassung

In dieser Arbeit untersuchen wir die Rolle der Vegetationsschicht (*canopy*) im Klimasystem, indem wir zwei Prozesse in der *canopy* analysieren. Erstens untersuchen wir Prozesse, die Veränderungen der im Boden und in der *canopy* gespeicherten thermischen Energie kontrollieren, um festzustellen, ob sie das Klimasystem über dekadische Zeitskalen hinweg beeinflussen. Hier stellen wir einen neuen Ansatz vor, um die Gleichung der Oberflächenenergiebilanz zu schließen, indem wir eine physikalisch basierte Schätzung der *canopy*-Wärmespeicherung (genannt SkIn$^+$-Schema) verwenden. Um dieses Schema im Hinblick auf die Rolle der Wärmespeicherung zu testen, führen wir ein durch Beobachtungen angetriebenes eindimensionales Standortexperiment sowie ein gekoppeltes Land-Atmosphären-Experiment mit der Landkomponente JSBACH des MPI-ESM (Max-Planck-Institut – Erdsystemmodell) durch. Wir stellen fest, dass SkIn$^+$ tagsüber zu einer Erwärmung und nachts zu einer Abkühlung führt, wodurch die modellierte Repräsentation der Oberflächenflüsse auf tageszeitlichen Skalen verbessert wird. Im Vergleich zum alten Schema werden Phasenfehler bei der Oberflächentemperatur und den Wärmeflüssen eliminiert, und nächtliche Wärmefreisetzungen, die die stabile Grenzschicht unrealistisch zerstören, verschwinden. Auf der globalen Skala überwiegt für Regionen ohne oder mit geringer Vegetation und einem ausgeprägten Tageszyklus der nächtliche Kühleffekt, weil stabile Bedingungen in der Nacht die verzögerte Reaktion der Temperatur aufrechterhalten, während der turbulente Austausch am Tag diese verstärkt.

Zweitens untersuchen wir den Prozess der *leaf thermoregulation*. Pflanzen neigen dazu, ihre Blatttemperatur durch die Regulierung von Wärme- und Wasserverlusten in einem optimalen Bereich zu halten, d.h. sie sind in kühler Umgebung wärmer und in warmer Umgebung im Allgemeinen kälter. Dieses Verhalten wurde in früheren Studien in Labor- und Feldexperimenten beobachtet. Wir befassen uns hier mit der Frage, ob ein Effekt

im Zusammenhang mit der *leaf thermoregulation* in einem Klimamodell gefunden werden kann und wie sich dies auf das globale Klima auswirkt. Um die Auswirkungen der *leaf thermoregulation* zu untersuchen, entwickeln wir im Rahmen von JSBACH ein neues Energiebilanzschema (CEBa) mit zwei Quellen für die *canopy*. Dieses Schema ermöglicht es, die Temperatur und die Feuchtigkeit im Luftraum der umgebenden *canopy*, die Temperatur der Bodenoberfläche und die Temperatur des Blattes selbst zu berechnen. Der Prozess der *leaf thermoregulation* wird mit verschiedenen Modellierungsansätzen detailliert untersucht. Dazu gehören eine nulldimensionale instantane Lösung der Energiebilanz sowie FLUXNET-Standortexperimente und gekoppelte globale Experimente. Wir finden eine negative Korrelation zwischen dem Temperaturüberschuss des Blattes und der Temperatur der Umgebungsluft, wie sie bei Beobachtungen auf Standortebene festgestellt wurde, jedoch mit einer weniger ausgeprägten Magnitude. Auf globaler Skala finden wir jedoch eine positive Korrelation, die der Theorie der *leaf thermoregulation* auf der Blattskala widerspricht. Nur im Falle einer unbegrenzten Wasserverfügbarkeit stellen wir eine negative Korrelation auf globaler Skala fest. Ihre Magnitude wird jedoch im Vergleich zu den Beobachtungen unterschätzt und hat daher einen vernachlässigbaren Einfluss auf die Pflanzenproduktivität.

Contents

1. Introduction

1.1. Motivation

The land surface plays a central role in the Earth System. It has a key function in controlling the interaction between the atmosphere and the terrestrial biosphere. Over two-thirds of this land surface are covered by vegetation (Huete et al., 2004). Due to its not negligible vertical extent, the vegetation is best described by using the concept of a so-called canopy layer. The canopy is commonly defined as "*the community of aboveground plant organs*" (Campbell et al., 1989). Due to its vast extent and its large variety, the canopy plays a key role in shaping the land surface and determining its characteristics. Via numerous biogeophysical and biogeochemical processes, the canopy substantially influences the exchange fluxes of energy, water, and momentum between the land surface and the overlying air mass. Furthermore, the complex structure of the canopy and the resultant shading also strongly affect the radiation budget of the land surface. The canopy, therefore, regulates to a large extent the distribution of incoming solar energy into the ground and turbulent heat fluxes, giving it a key role in controlling the surface and ground temperatures. The surface temperature, in turn, affects the diurnal variation of the boundary layer development. Via this coupling, important atmospheric processes such as cloud formation and convection can, therefore, strongly depend on the characteristics of the canopy, highlighting the need for an in-depth study of the involved processes.

Moreover, the afore-mentioned partitioning of radiation is closely linked to

the hydrological cycle, as the available energy at the surface strongly influences evaporation and transpiration, with evapotranspiration returning about half of the precipitated water to the atmosphere (e.g., Oki and Kanae, 2006). Quantifying the water exchange between atmosphere and land is an important task, as it influences the dynamics and thermodynamics of the climate system (Chahine, 1992). In this context, soil moisture plays a vital role as it is part of several feedbacks from local to global scale (Seneviratne et al., 2010). Most importantly, it constitutes an upper limit for transpiration, which represents the largest part of total land evapotranspiration (e.g., Lawrence et al., 2007). Knowledge of transpiration is essential for understanding not only the physical system but also the global carbon cycle. In particular, since the carbon uptake by photosynthesis in terrestrial plants is directly related to water loss by stomatal transpiration of leaves (e.g., Ball et al., 1987; Farquhar et al., 1980; Farquhar and Sharkey, 1982).

For a long time, it was controversial whether terrestrial processes exert an essential influence on the global climate (Pitman, 2003), but during the last decades, many studies and research papers have provided evidence that the land surface is indeed a key component of the climate system (e.g., Mintz, 1984; Chase et al., 1996; Betts, 2000; Feddes et al., 2001). Many of these studies rely on simulations that include Land Surface Models (LSM). These can be stand-alone models or a part of climate and Earth system models and are designed to represent a variety of climate-relevant surface as well as subsurface processes, realistically describing a wide range of land–atmosphere interactions (Sellers et al., 1997). Depending on the represented processes, these LSMs can be classified into three generations (Sellers et al., 1997; Pitman, 2003).

The first-generation models contained simple aerodynamic bulk transfer equations based on the concept of Budyko (1956), to describe the surface–atmosphere exchange, and the most important land surface parameters, namely albedo, aerodynamic roughness, and soil water availability, to represent key surface characteristics. Here the first LSM was implemented by Manabe (1969), who used a so-called "bucket scheme" to represent water

availability. This scheme is based on the theory that the soil has a constant depth and can store only a limited amount of water. A few years later, Blackadar (1976) developed a model with two soil layers: a thin variable surface layer affected by radiation, and a thick deeper layer whose temperature was determined by a prescribed solution of the heat equation.

The second generation of LSMs focused on biophysical processes and was introduced by the pioneering study of Deardorff (1978). He implemented a multi-layer soil model, including a single layer of vegetation, which represented evapotranspiration from four different sources (vegetation, bare soil, interception layer, and snow). These improvements became especially relevant on the global scale when general circulation models (GCM) incorporated land–atmosphere transfer schemes (including the biosphere). The Biosphere Atmosphere Transfer Scheme (BATS, Dickinson et al., 1986) and the Simple Biosphere Model (SiB, Sellers et al., 1986) were concurrently developed at this time and laid the foundation for many other LSMs, e.g., the Community Land Model (Dai et al., 2003). Another feature of the second-generation models was the introduction of the stomatal resistance, which is the additional resistance that water vapor molecules encounter when moving through the stomatal openings. This resistance was calculated by an empirical approach depending on solar radiation, vapor pressure deficit, temperature, and leaf water potential following Jarvis (1976).

The replacement of the empirical stomatal resistance by a physiological approach and the addition of carbon into LSMs formed the third generation (e.g., Sellers et al., 1996; Bonan, 1996; Knorr, 2000; Krinner et al., 2005; Raddatz et al., 2007). The stomatal conductance (the reciprocal of the stomatal resistance) was now calculated by the net leaf assimilation rate, which was determined as the minimum of three limiting factors: the amount of photosynthetically active radiation (PAR), the capacity to utilize the products of photosynthesis and the efficiency of the photosynthetic enzyme Rubisco (see, e.g., Farquhar et al., 1980; Collatz et al., 1991).

The need to evaluate LSM developments using observation-based data has

been recognized during the 1980s. The first systematic effort in this direction did not start before the 1990s with the Project for the Intercomparison of Land-Surface Parameterization Schemes (PILPS, Henderson-Sellers et al., 1993). Here they used synthetic data to improve the representation of the continental surface in a so-called "offline experiment", i.e., the LSM is not coupled to the atmospheric model but is forced with atmospheric data (e.g., observations and measurements). The widely quoted work of Chen et al. (1997) documented the first results of experiments forced with observed atmospheric boundary layer data, comparing 23 different land surface schemes. Two years later, a new project called Global Soil Wetness Project (GSWP, Dirmeyer et al., 1999), which requires processed atmospheric forcing data, extended the conclusions drawn by the point-based PILPS experiments to global scales. Only a year later, a new project was founded that followed the idea of combining PILPS with its local-scale character and GSWP, which is based on a global perspective; this ongoing joint project is called Global Land Atmosphere System Study (GLASS, Polcher et al., 2000). In the last decade and a half, GLASS has broadly expanded, and various other projects have joined. The main goal of this effort is to improve land surface schemes for the benefit of numerical weather prediction and climate models.

The last years have seen substantial progress in the modeling of land surface processes. However, despite its important role in the climate system, the canopy is often represented inadequately in present-day LSMs. For example, it is still common practice to neglect the heat storage in the canopy completely (e.g., Balsamo et al., 2011; Kowalczyk et al., 2013) or to close the surface energy balance within the uppermost soil layer of finite heat capacity, such as in JSBACH (Reick et al., 2013), the land component of the MPI-ESM (Max Planck Institute - Earth system model, Mauritsen et al., 2019). To overcome the possible shortcomings of this unphysical surface energy closure and to assess the added value of a more realistic scheme, we introduce a new, physically based concept of canopy heat storage into JSBACH, the model used in this study. Following Viterbo and

Beljaars (1995), we first neglect the soil heat storage and close the energy balance by implementing an infinitesimally thin layer at the land surface. This approach applies to areas with little or no vegetation and negligible heat storage. Conveniently, we abbreviate the new scheme with "SkIn", which stands for Surface is kept Infinitesimally thin, in addition to the fact that this scheme represents a canopy layer with a negligible vertical extent comparable with a thin "skin". For regions with tall vegetation, this approximation is not valid anymore because the energy stored in the canopy layer has to be considered. Therefore, in a second step, we reintroduce a heat storage, but this time we apply a physically based estimate of the canopy heat storage (following Moore and Fisch, 1986). This storage is associated with temperature changes in the biomass, which mainly consists of trunks, branches, litter, and leaves (e.g., dos Santos Michiles and Gielow, 2008), as well as in the canopy air, including changes in specific humidity (e.g., da Silva et al., 2012). The latter two are called sensible and latent heat storage. The SkIn scheme with a canopy heat storage depending on the heat capacity and the composition of the canopy layer is called SkIn$^+$.

The importance of the so-called "canopy heat storage" in connection with the solution of the energy balance equation has been demonstrated by many experimental studies at the site-level (e.g., Aston, 1985; Moore and Fisch, 1986; Jacobs et al., 2008; dos Santos Michiles and Gielow, 2008; Lindroth et al., 2010; Garai et al., 2010; da Silva et al., 2012; Kilinc et al., 2012; Burns et al., 2015). Several of these studies (e.g., Jacobs et al., 2008; dos Santos Michiles and Gielow, 2008; Lindroth et al., 2010) showed that the consideration of the canopy heat storage improves the energy balance closure calculated on the basis of observed data. The total change in stored energy of all different types of heat storages in the canopy layer (e.g., the energy flux for photosynthesis as well as the canopy heat storage in biomass and water content) can amount up to 40% of the net radiation (dos Santos Michiles and Gielow, 2008); and around 15% for crop sites (Meyers and Hollinger, 2004). Moreover, the extent of the canopy heat storage was investigated in a small number of modeling studies (e.g., Haverd et al.,

2007). However, as these modeling studies were focused on the local scale, this dissertation is the first study to investigate the climatic impact of the canopy heat storage on decadal time scales on the global scale using an Earth system model. Therefore, we ask the following two questions: Does the elimination of the soil heat capacity in the energy balance substantially affect the diurnal cycle of surface temperature and heat fluxes in the case of shallow vegetation at the site level? What is the climatological effect of the canopy heat storage on near-surface temperature on the global scale?

The canopy is not only a key component of the Earth system because of the role it plays in exchange of energy, moisture, and momentum, but also because substantial amounts of atmospheric carbon are taken up by leaves within the canopy layer. Woody plants have a significant share of the terrestrial carbon cycle and assimilate about 120 Gt carbon per year through the process of photosynthesis (e.g., Schimel et al., 2001). Since the net primary production (NPP) of plants correlates strongly with temperature, it is crucial to better understand the relation between leaf temperature and its environmental conditions, especially the air temperature surrounding the plant.

The first scientific studies on plant productivity and on the role of leaf temperature date back to the middle of the 19th century (e.g., Rameaux, 1843; Askenasy, 1875). These biochemical laboratory studies concentrated mainly on physiological processes and the metabolic properties of the plants. At the beginning of the 20th century, the physical processes of plants, such as transpiration, and the leaf temperature itself were given more attention. (e.g., Kusano, 1901; Askenasy, 1875; Ehlers, 1915). The first detailed studies about the energy balance of leaves and the heat transfer between the leaf and its environment started in the early 1960s. Gates (1962) showed that leaf temperatures – measured by an infrared radiometer – can exhibit a significant temperature range: Sunlit leaves were up to 20 °C warmer than the ambient air, while shaded leaves were found to be on average 1.5 °C colder than the air. This reduction of leaf temperature was mainly caused by transpiration, while, on the other hand, sensible heat transport played

a negligible role. These changes in leaf temperature occur on time scales ranging from seconds to minutes and can vary significantly throughout the day due to varying environmental conditions such as solar and thermal radiation, air temperature, wind speed, and water vapor content in the air (Gates, 1965). The measuring instruments used in these studies were either infrared thermometers or so-called "thermocouples", which generate a temperature-dependent potential difference. The difficulty in measuring the leaf temperature with an infrared thermometer is to obtain the correct estimate of the leaf's emissivity. In contrast, thermocouples have the disadvantage of additionally requiring the temperature of a reference junction. For that reason, Linacre and Harris (1970) proposed a new leaf thermometer in the form of a clamp thermometer called "Thermistor". It has the advantage of being a particularly small, mobile device that generates only a small current, ensuring negligible self-heating.

A rather sparsely cited paper from Linacre (1964) entitled "*A note on a feature of leaf and air temperatures*" laid the foundation for understanding what today is called the concept of "leaf thermoregulation". Linacre was the first to show that a significant relationship between the leaf temperature and the ambient air temperature exists. He analyzed this relation by plotting measured leaf temperatures of isolated plants (taken from different studies) against ambient air temperature in the form of a scatter diagram. For these measurements, intact leaves of photosynthetic plants were used, i.e., those exposed to bright sunlight (around midday) and not water-stressed. The leaf temperature excess of plants, which denotes the difference between leaf temperature and air temperature, shows a distinct negative correlation with air temperature (Fig. 1.1). This means, the leaf has the ability to be warmer than the air in cold environments, while it tends to stay colder than the air in warm environments. This implies that, at certain air temperature, the leaf excess temperature changes its sign. The temperature at which this happens is called "equivalence temperature". The regression line of the analyzed measured data from Linacre (1967) implied an equivalence temperature of 34 °C with a leaf temperature

around 12 °C above air temperature at the freezing point and around 8 °C below air temperature at 60 °C. Linacre hypothesized that the equivalence temperature could be interpreted as the optimum temperature for plant productivity and growth regarding plant metabolism; i.e., plants try to maximize their leaf net carbon gain by increasing carbon assimilation rate while simultaneously decreasing leaf mass per area (see Michaletz et al., 2016b). The equivalence temperature, and thus the optimum temperature varies between different plant species from 25 °C to 40 °C and averages around 30 °C.

The discussion of the process of leaf thermoregulation has been taken up again after the findings of Helliker and Richter (2008). They showed that the oxygen isotope ratio (δ^{18}O) of cellulose, which past studies used as a proxy for the ambient air temperature, exhibits a remarkably constant temperature of 21±2.2 °C ranging from boreal to subtropical regions. This indicates that, even on decadal time scales, the average leaf temperature

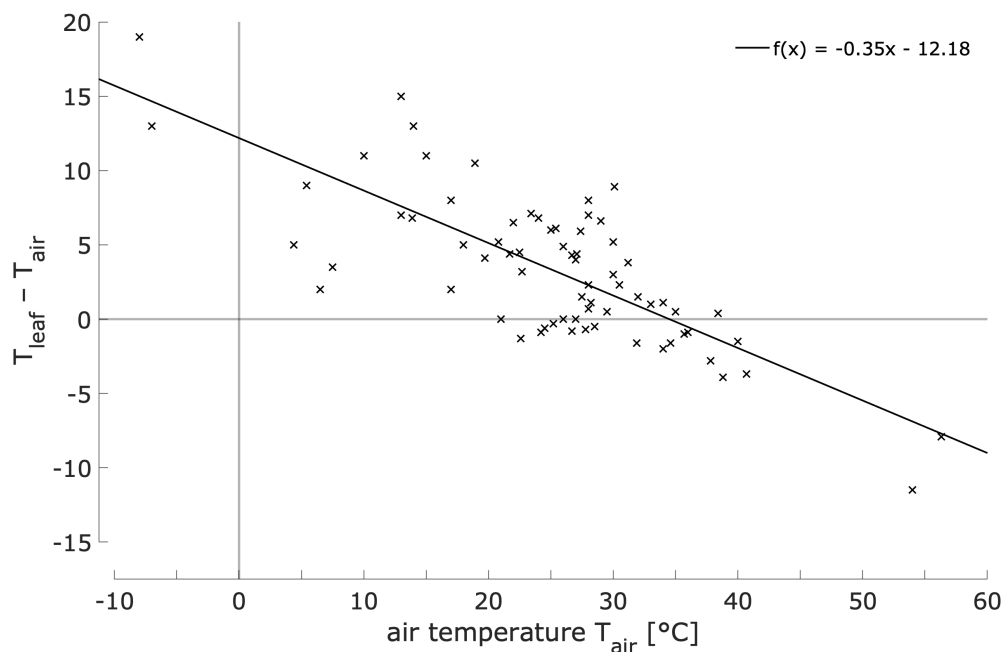
Fig. 1.1.: Relation between leaf temperature excess and air temperature, following the theory of leaf thermoregulation, based on short-term measurements of isolated and not water-stressed sunlit plants. Figure redrawn from Linacre (1967).

deviates from the ambient air temperature and tends to stay at a rather constant, optimal value, which results in maximal plant productivity. This hypothesis was tested by Michaletz et al. (2016b), who also invented the term "leaf thermoregulation". They collected and analyzed not only the long term $\delta^{18}O$ measurements, but also a large number of short-term point measurements of 1504 leaves from 185 different taxa (including the data of Linacre, 1964), consisting of mainly sunlit leaves but also shaded leaves. The regression line between the leaf temperature excess and the ambient temperature resulted in an equivalence point of 30.1 °C with a fitted slope of -0.27. Moreover, they concluded that leaf thermoregulation "originates from the optimization of leaf traits to maximize leaf carbon gain". Following the often-quoted paper of Michaletz et al. (2016b), there were further studies regarding leaf thermoregulation: Rey-Sánchez et al. (2016) quantified the leaf temperature fluctuations in a tropical forest and developed different empirical approaches to estimate leaf temperature variability by means of air temperature and photosynthetic activity for dry and wet seasons. Fauset et al. (2018) found different strategies of leaf thermoregulation and water use in three tree species in the Atlantic montane forest in Brazil.

In summary, the effect of leaf thermoregulation has been studied by numerous studies in recent decades to gain a better understanding of the thermal and photosynthetic response of the leaf to atmospheric conditions under the influence of various leaf functional traits. However, all these studies focused on the leaf scale, and the measured leaf temperatures and atmospheric conditions represented mostly short-term point measurements under optimized conditions (such as no water stress). They disregarded the process of leaf thermoregulation at the canopy scale and its impact on the climate system. Hence, leaf thermoregulation at the canopy scale has not yet been investigated in the context of a complex Earth system model, and its effect on the large scale climate and carbon cycle has not been estimated.

The standard model version of JSBACH (hereafter called Classic) and the extended SkIn$^+$ scheme are single layer vegetation schemes both based on

the big-leaf approach. This implies that only one temperature (called surface temperature) corresponding roughly to the temperature at the displacement height is used to characterize the temperature of the canopy air space, the ground under or next to the canopy, and the canopy leaves. To distinguish between all these different temperatures, we extend the big-leaf SkIn$^+$ scheme to a two-source scheme called "Dual-source Canopy Energy Balance" (CEBa). This scheme follows the basic idea of Shuttleworth and Wallace (1985) and Sellers et al. (1986) allowing evaporation from both the vegetation and the bare soil, at different temperatures, respectively (for a detailed description of the CEBa scheme, see the next chapter 2.3). With CEBa, which distinguishes between the temperature of the leaf and the air, it is possible to simulate the process of leaf thermoregulation in JSBACH. Here we want to determine whether leaf thermoregulation leads to a significant difference between the temperature of the leaf and the air at the canopy scale, as found in observations at the leaf scale.

With the new extended canopy scheme, we are able to study and better understand the process of leaf thermoregulation in the context of an ESM by answering the following questions: How do atmospheric conditions and leaf properties influence the leaf's ability to regulate its temperature? Specifically, does the negative correlation between the leaf temperature excess and air temperature observed at the leaf scale hold at the canopy and regional scale? Moreover, what is the impact of leaf thermoregulation on global climate and plant productivity?

1.2. Thesis Outline

As mentioned in the previous section, the main objective of this work is to investigate the role of the canopy in the climate system by analyzing two processes relevant for land–atmosphere interactions. First, we study changes in the energy stored in the canopy layer to better understand the underlying process and to determine whether it has an influence on the

climate on decadal time scales. Second, we investigate the leaf's ability to regulate its temperature and to assess whether the leaf thermoregulation signal (as described in the previous section) can be found in simulations with an ESM and whether it significantly influences the photosynthesis and the plant productivity. The scientific question that we addressed in the previous section are summarized as follows:

- Does the elimination of the soil heat capacity in the energy balance substantially affect the diurnal cycle of surface temperature and heat fluxes in the case of shallow vegetation at the site level? (Chapter 3)

- What is the climatological effect of the canopy heat storage on near-surface temperature on the global scale? (Chapter 3)

- How do atmospheric conditions and leaf properties influence the leaf's ability to regulate its temperature? Specifically, does the negative correlation between the leaf temperature excess and air temperature observed at the leaf scale hold at the canopy and regional scale? (Chapter 4)

- What is the impact of leaf thermoregulation on global climate and plant productivity? (Chapter 4)

To investigate these questions, we perform simulations on the site level as well as on the global scale with JSBACH3, the land component of the MPI-ESM.

First, in chapter 2, the standard version of JSBACH (also called JSBACH Classic) is described in detail, and the new SkIn$^+$ scheme using a physically based canopy heat storage is introduced to improve misrepresented processes in JSBACH Classic. In a further step, the model is extended to calculate an energy balance of the canopy, including separate sources of sensible and latent heat fluxes (soil and leaf). This new approach, called CEBa, allows to distinguish between two components of the canopy when calculating the near-surface temperatures and studying the process of leaf

thermoregulation.

In chapter 3, we evaluate the new scheme SkIn$^+$ by means of an offline simulation of the land component JSBACH of the MPI-ESM using measurements observed at the CASES-99 field experiment (see Sect. 3.1) in Kansas. In addition, a global coupled land–atmosphere experiment is performed with the MPI-ESM using a so-called AMIP (Atmospheric Model Intercomparison Project Gates, 1992) type simulation over 30 years to evaluate the regional impact of the new SkIn$^+$ scheme on decadal time scales.

In chapter 4, the process of leaf thermoregulation is analyzed using the new dual-source canopy energy balance scheme CEBa. This new scheme allows predicting four variables: the leaf temperature, the ground temperature, and the temperature and specific humidity in the canopy air space (CAS). First, the CEBa scheme is evaluated and compared to results obtained by JSBACH Classic for two sites located in a tropical and a temperate forest using observations from FLUXNET, a global network that provides time series data of measured atmospheric variables as well as sensible and latent heat fluxes (`https://fluxnet.fluxdata.org`). Moreover, with the new CEBa tool, we can establish – in a zero-dimensional experiment using the stationary solution of the energy balance – the influence of atmospheric conditions and leaf properties on the leaf's ability to regulate its temperature. Furthermore, we perform two FLUXNET site offline experiments with CEBa for a tropical and a temperate forest to identify the effect of leaf thermoregulation found in observations in a model framework at the canopy scale. Also, we perform a global coupled land–atmosphere AMIP model experiment with CEBa to establish whether the leaf thermoregulation signal can be found over a sizeable spatial area and over decadal time averages in a model simulation. Additionally, we quantify the impact of leaf thermoregulation on plant productivity, regarding gross primary production. In the last chapter, we summarize our results, discuss the limitations of our study, and the need and the possibilities for future research.

2. Models

In this chapter, the standard version of JSBACH (here we also refer to it as JSBACH Classic) is described in detail, and the strengths and shortcomings of the parameterization of the processes in the canopy layer are discussed (Sect. 2.1). One of the weaknesses is that the energy balance in JSBACH classic is closed within the uppermost soil layer. To improve this approach, the new SkIn$^+$ scheme using a physically based canopy heat storage concept is introduced and described (Sect. 2.2). In a further step, the model is extended to include a more realistic description of the energy balance of the canopy, including two separate sources of energy and water (soil and leaf), called CEBa, which is necessary to calculate the leaf temperature
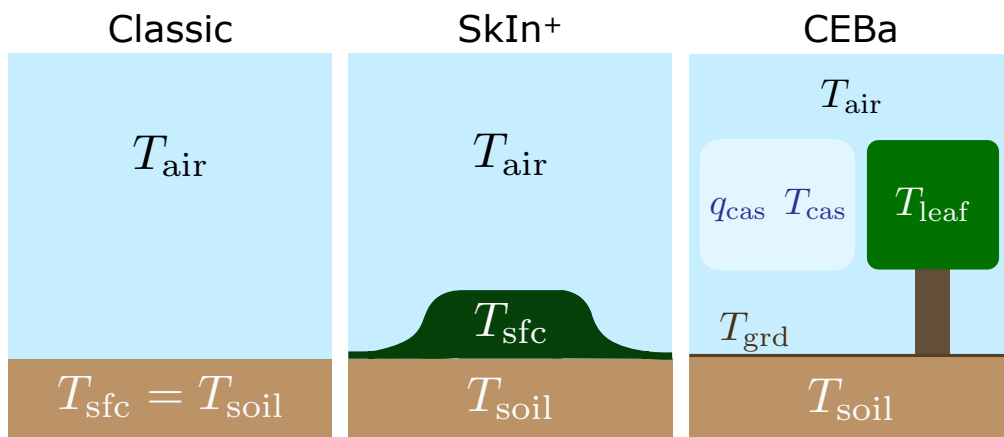
Fig. 2.1.: Evolution of JSBACH surface schemes: The standard version of JSBACH (Classic), where the temperature of the uppermost soil layer represents the surface temperature; the SkIn$^+$ scheme with an infinitesimally skin temperature in case of no vegetation and a canopy heat storage scaled with the vegetation height for large vegetation; and the CEBa scheme with the dual-source canopy energy balance and four variables in the canopy layer.

and to study the process of leaf thermoregulation (Sect. 2.3). A schematic overview of the evolution of the JSBACH surface schemes is depicted in Fig. 2.1.

2.1. JSBACH

JSBACH (version 3.11, Reick et al., 2013), the land component of the MPI-ESM (the Max Planck Institute - Earth system model, version 1.2, Mauritsen et al., 2019), serves as the starting point of this thesis. In the past, ECHAM (EC following ECMWF and HAM representing Hamburg, version 6.3, Stevens et al., 2013), the atmospheric component of MPI-ESM, included JSBACH. Since 2005, JSBACH is an independent, full representation of the global soil–vegetation–atmosphere transfer system (Raddatz et al., 2007) that can also be run alone in the so-called "offline" mode forced by meteorological data. The physical core components of the land processes (calculation of the energy balance, heat transports, and the water budget) are adopted from the ECHAM5 model (Roeckner et al., 2003), including a fully implicit land-surface–atmosphere coupling scheme (Schulz et al., 2001). This means that the mutual boundary conditions between the land surface and the atmosphere (temperature and specific humidity at the surface or the lowest atmospheric level, respectively) are formulated as implicit functions at the new time step. The surface radiation follows a scheme which allows albedo changes of the surface below the canopy (Vamborg et al., 2011), and the soil hydrology is calculated using a five-layer scheme (Hagemann and Stacke, 2015).

To represent the dynamics of land carbon uptake and release, JSBACH implemented the photosynthesis and canopy radiation from the prognostic phenology scheme BETHY (Biosphere Energy-Transfer Hydrology) (Knorr, 2000). Besides, JSBACH contains routines to calculate the uptake, storage, and release of carbon from vegetation and soils (Brovkin et al., 2009). Natural land cover changes are simulated prognostically by a dynamic vegetation

module, which includes the representation of the subgrid-scale heterogeneity of vegetation classes (Reick et al., 2013). Anthropogenic land use and land cover changes are prescribed either by maps or by forcing data from the New Hampshire Harmonized Protocol (Hurtt et al., 2011).

JSBACH simulates land surface and soil processes that take into account energy and water exchange at the surface and in the soil. These processes are described by the diffusion equations for enthalpy and water that are solved numerically on a multi-layer vertical grid extending to a depth of 10 m. The model contains five soil layers (Hagemann and Stacke, 2015) that grow in thickness with increasing soil depth (6.5 cm, 25 cm, 90 cm, 2.9 m and 5.7 m). The diffusion equation for heat

$$(\rho C)_{\text{soil}} \frac{\partial T_{\text{soil}}}{\partial t} = \frac{\partial}{\partial z}\left(\lambda_{\text{soil}} \frac{\partial T_{\text{soil}}}{\partial z}\right) \tag{2.1.1}$$

is solved numerically following the method from Richtmyer and Morton (1967). In Eq. (2.1.1) the term $(\rho C)_{\text{soil}}$ denotes the volumetric soil heat capacity [J/(m^{3}K)], λ_{soil} is the soil thermal conductivity [W/(m K)], and T_{soil} is the temperature of the soil. JSBACH applies a zero heat flux boundary condition at the bottom of the soil. At the top of the soil, it considers the temperature of the uppermost soil layer as the surface temperature. Therefore the ground heat flux is the heat exchange between the first and the second soil layers. An analogous equation, which governs the vertical diffusion for soil water, is represented by the one-dimensional Richards equation (that is described in detail by Hagemann and Stacke, 2015). To couple JSBACH and the atmosphere, the surface energy balance and surface water balance are solved to provide the boundary conditions for the two abovementioned diffusion equations; this represents a link between the atmosphere and the underlying soil. The water balance at the surface describes the changes in surface water caused by precipitation, evapotranspiration, snowmelt, surface runoff, and infiltration. Additionally, the snow budget and the interception reservoir of rain and snow is determined to close the entire water balance; the ECHAM5 documentation (Roeckner

et al., 2003) contains a detailed description of these processes.

The surface energy balance partitions the available net radiation R_{net} into the ground heat flux G, the turbulent sensible heat flux H, and the latent heat flux LE, where the latter two represent a forcing for the atmospheric component in the coupled system. In JSBACH Classic (the starting point of the model modifications in this thesis), the surface temperature T_{sfc} also represents the temperature of the uppermost soil layer T_{soil} (Fig. 2.2, left-hand side):

$$T_{\text{soil}} \ \hat{=} \ T_{\text{sfc}} \tag{2.1.2}$$

The surface energy balance is closed, i.e., calculated and evaluated, within the uppermost soil layer. Hence, the heat capacity of the canopy C_{cano} is approximated by the area-specific heat capacity of the uppermost soil layer C_{soil} [J/(m²K)]. This implies, that the soil heat storage S_{soil} (resulting in a change in stored energy of the uppermost soil layer) defined by

$$S_{\text{soil}} = C_{\text{soil}} \frac{\partial T_{\text{sfc}}}{\partial t} \tag{2.1.3}$$

is used as a proxy for the canopy heat storage S_{cano}. The soil heat storage corresponds to the term on the left-hand side of the energy balance equation that is proportional to the time derivative of the surface temperature:

$$S_{\text{soil}} = C_{\text{soil}} \frac{\partial T_{\text{sfc}}}{\partial t} = R_{\text{net}} + H + LE + G \tag{2.1.4}$$

The use of a non-physically motivated soil heat storage concept was chosen arbitrarily and is, in principle, not associated with the canopy layer. The terms on the right-hand side of Eq. (2.1.4) are positive if they represent an energy source for the system (here the uppermost soil layer) and negative if they represent an energy sink. The net radiation is the residual short-wave and long-wave part of downward or upward radiation respectively:

$$R_{\text{net}} = (1 - \alpha) \, S_{\text{in}} + L_{\text{in}} - \varepsilon \sigma T_{\text{sfc}}^4 \tag{2.1.5}$$

where α is the albedo, ε the surface emissivity, σ the Stefan-Boltzmann
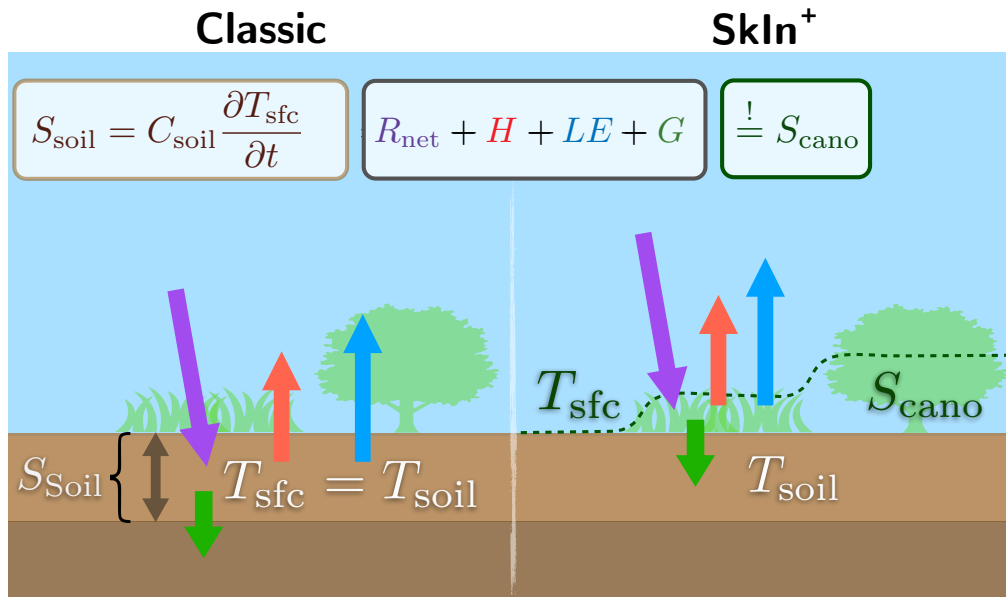
Fig. 2.2.: Simplified sketch of the modifications of the surface energy balance scheme: Comparison between the Classic scheme, which contains a heat storage term of the uppermost soil layer (S_{soil}), and the SkIn⁺ scheme, which considers a physically based estimation of the canopy heat storage scaled by vegetation height (S_{cano})

constant, L_{in} the incoming long-wave radiation, and S_{in} the incoming short-wave radiation. Consistently, in JSBACH Classic the ground heat flux G is the heat exchange between the first soil layer T_{soil} and the second soil layer $T_{soil,2}$:

$$G = \frac{\lambda}{\Delta z} \left(T_{soil,2} - T_{soil} \right) \tag{2.1.6}$$

where λ is the weighted average of the thermal conductivities for the first and second soil layer and Δz is the thickness between the centers of these layers. The surface fluxes of heat, water and momentum are defined using the bulk formulation based on the surface-layer similarity theory. The sensible heat flux H is parameterized as follow:

$$H = \rho c_p \frac{T_{air} - T_{sfc}}{r_{atm}} \tag{2.1.7}$$

where ρ is the density of humid air, $c_p = 1005$ J/(kg K) is the specific heat capacity of air at constant pressure, T_{air} is the air temperature of either the measurement height (offline run) or at the lowest atmospheric model

level (coupled run), and r_{atm} is the atmospheric resistance

$$r_{atm} = \frac{1}{c_h v} \tag{2.1.8}$$

which is the inverse product of the wind speed v and drag coefficient c_h. The latter characterizes the turbulent mixing processes, which are determined by the roughness of the underlying surface canopy layer and the influence of atmospheric stratification. Empirical stability functions derived by Louis (1979, 1982) that depend on the Richardson number quantify the atmospheric stability condition. Although the roughness lengths, as well as the drag coefficients, are assumed to be different for momentum and scalar quantities (Brutsaert, 1975), they are set equal in JSBACH.

The latent heat flux is composed of a vaporization part (the transition from liquid to gas) and a sublimation part (the transition from solid to gas):

$$LE = L_v E_{tot} + (L_{sub} - L_v)\chi_{sn}E_{pot} \tag{2.1.9}$$

where χ_{sn} is the snow covered fraction of the grid cell, $L_v = 2500.8$ kJ/kg is the latent heat for vaporization and $L_{sub} = 2834.5$ kJ/kg the latent heat for sublimation. Potential evaporation E_{pot} is defined as

$$E_{pot} = \rho\frac{q_{air} - q_{sat}}{r_{atm}} \tag{2.1.10}$$

while total evapotranspiration E_{tot} (including snow and interception reservoir) can be calculated as

$$E_{tot} = \rho\frac{c_{air}q_{air} - c_{sat}q_{sat}}{r_{atm}} \tag{2.1.11}$$

where q_{air} is the specific humidity of the lowest atmospheric level and $q_{sat} \mathrel{\hat{=}} q_{sat}(T_{sfc})$ is the saturated specific humidity at surface temperature. The difference between potential evaporation and total evapotranspiration can be expressed by two dimensionless factors (defined between 0 and 1) c_{air} and c_{sat}, which can be written as the sum of a vegetational and a

non-vegetational part (for the sake of simplicity neglecting snow and interception reservoir):

$$c_{\mathrm{sat}} = \frac{\chi_{\mathrm{veg}}}{1 + r_{\mathrm{cano}}/r_{\mathrm{atm}}} + (1 - \chi_{\mathrm{veg}})RH_{\mathrm{up}} \qquad (2.1.12\mathrm{a})$$

$$c_{\mathrm{air}} = \frac{\chi_{\mathrm{veg}}}{1 + r_{\mathrm{cano}}/r_{\mathrm{atm}}} + (1 - \chi_{\mathrm{veg}}) \qquad (2.1.12\mathrm{b})$$

where χ_{veg} is the grid cell's fraction of vegetation, $(1 - \chi_{\mathrm{veg}})$ is the fraction of bare soil, RH_{up} is the relative humidity of the uppermost soil layer, and r_{cano} is the so-called "canopy resistance". The latter describes the additional resistance that water vapor molecules encounter when moving through the stomatal openings. It depends on the carbon flux through the stomata and the leaf area index. In addition, it is modified by a water stress factor depending on the soil water within the root zone (Sect. 2.3 provides a more detailed description of the stomatal conductance and the canopy resistance).

The relative humidity of the uppermost soil layer is approximated by a cosine function:

$$RH_{\mathrm{up}} = \max\left\{\frac{1}{2}\left[1 - \cos\left(\pi\frac{\theta_{\mathrm{up}}}{\theta_{\mathrm{SFC}}}\right)\right],\ \min\left(1,\ \frac{q_{\mathrm{air}}}{q_{\mathrm{sat}}}\right)\right\} \qquad (2.1.13)$$

where θ_{up} is the volumetric soil moisture of the uppermost layer and θ_{SFC} the soil field capacity – a specific soil property. It describes the maximum amount of moisture held in the soil after the water has gravitationally drained away. Its value is depending on the soil type; generally, clay shows the highest soil field capacities, sand the lowest and loam something in between. Using these expressions and by rearranging the terms one can divide Eq. (2.1.11) into transpiration E_{trans} (evaporation through the plants' stomata) and into bare soil evaporation E_{bs}:

$$E_{\mathrm{trans}} = \rho\frac{q_{\mathrm{air}} - q_{\mathrm{sat}}}{r_{\mathrm{atm}} + r_{\mathrm{cano}}}\chi_{\mathrm{veg}} \qquad (2.1.14\mathrm{a})$$

$$E_{\mathrm{bs}} = \rho\frac{q_{\mathrm{air}} - q_{\mathrm{sat}}RH_{\mathrm{up}}}{r_{\mathrm{atm}}}(1 - \chi_{\mathrm{veg}}) \qquad (2.1.14\mathrm{b})$$

For a better overview, the above-mentioned relations were formulated disregarding snow or wet skin reservoir, but for the sake of completeness the total evaporation is condensed as a weighted average in Eq. (2.1.15):

$$
\begin{aligned}
E_{\mathrm{tot}} = {} & \left[\chi_{\mathrm{sn}} + \left(1 - \chi_{\mathrm{sn}} \right) \chi_{\mathrm{wet}} \right] E_{\mathrm{pot}} \\
& + \left(1 - \chi_{\mathrm{sn}} \right) \left(1 - \chi_{\mathrm{wet}} \right) \left[E_{\mathrm{trans}} + E_{\mathrm{bs}} \right]
\end{aligned}
\tag{2.1.15}
$$

where χ_{wet} is the wet skin fraction. All these parameterizations include variables which, in turn, are functions of the surface temperature. Moreover, the surface temperature appears to the fourth power in the description of the outgoing long-wave part of the net radiation. Also, the formulation of the latent heat flux exhibits a nonlinear temperature dependence. According to these dependencies, the energy balance equation (Eq. 2.1.4) and its alterations in the next two sections represent complex implicit nonlinear equations.

Over the last few years, JSBACH has been used for a considerable number of different applications, including being utilized in a coupled global context on decadal and millennial time scales. Various biogeochemical and biogeophysical aspects were studied: the carbon cycle (Raddatz et al., 2007; Claussen et al., 2013), natural and anthropogenic land cover change (Pongratz et al., 2008; Reick et al., 2013), vegetation cover and land surface albedo (Brovkin et al., 2013) and atmosphere-forest interaction and feedbacks (Brovkin et al., 2009; Otto et al., 2011). In addition to these aspects, the physical components, which regulate the exchange of energy, water, and momentum fluxes, have been studied (e.g., Knauer et al., 2015; Hagemann and Stacke, 2015; de Vrese and Hagemann, 2016). However, the performance of JSBACH on shorter time scales, such as the diurnal cycle, has not yet been investigated. An exception is a study by Schulz et al. (2001) who modified the numerical time integration scheme of JSBACH from a semi-implicit scheme, which does not conserve energy, to an energy-conserving implicit land–atmosphere coupling scheme. With the help of so-called "offline" experiments using data from the Cabauw (the Netherlands) tower on daily time scales, this scheme was found to improve the

representation and quality of modeled turbulent heat fluxes and of the surface temperature. In summary, the representation of the carbon cycle in JSBACH is state of the art (third generation). In contrast, the physical parameterizations, especially concerning the energy balance (first generation), can still be improved. Due to these weaknesses in the formulation (discussed in chapter 3) JSBACH Classic is extended to the SkIn$^+$ scheme (see next section).

2.2. SkIn$^+$

In the standard scheme of JSBACH, we close the surface energy balance within the uppermost soil layer of a finite thickness (6.5 cm) and heat capacity. This assumptions is inadequate in particular for shallow vegetation and areas covered with bare soil. In these cases, the absorption of radiation takes place in the uppermost micrometers of the soil, this assumption appears unrealistic. Therefore, in the SkIn (*Surface is kept Infinitesimally thin*) approach, a surface temperature T_{sfc} that corresponds to an infinitesimally thin interface between the canopy and the atmosphere is calculated. Here the exchange and storage of energy and water within the canopy are neglected for now. Hence, in this case, the prognostic energy balance (Eq. 2.1.4), which contains a heat storage term, is changed to a diagnostic energy balance equation where the surface energy balance is closed with the help of an infinitesimally thin surface:

$$R_{\text{net}} + H + LE + G = 0 \qquad (2.2.1)$$

This equation represents an immediate response of the surface temperature to the available energy. We note that the use of this instantaneous response is not a novel approach. This so-called "skin temperature" was introduced by Viterbo and Beljaars (1995) to replace the old ground-surface model of the ECMWF. This approach is also used in other land surface models, e.g., in the community Noah land surface model (Niu et al., 2011).

To solve the diagnostic energy balance (Eq. 2.2.1) explicitly, the nonlinear terms – which are related to the outgoing long-wave radiation described by the Stefan-Boltzmann law as well as to the temperature-dependent specific saturated humidity of the surface – have to be linearized. Here we chose a first-order Taylor approximation. Neglecting the heat storage term results in a loss of stability in the numerical solution because the storage term exerts a dampening effect. Therefore, the surface instantaneously reacts to variations in the forcing data, especially to intense fluctuations in solar radiation flux densities or to wind speed variations. As a consequence, the first guess of the solution using the linearizations is insufficient, and an iteration is needed to stabilize the system. For this implementation, we use a simple Newton iteration combined with a fixed-point iteration where the surface temperature of the previous time step serves as a first guess starting point. Further tests have shown that it is not sufficient to only update the outgoing long-wave radiation as a part of the net radiation and the saturated specific humidity every iteration step. Besides, the drag coefficient of heat must be included in the iteration loop as well, as it nonlinearly depends on the surface temperature. Taking the drag coefficient of heat into account in the iterative procedure exerts a negative feedback ensuring the stability of the numerical solution of the energy balance equation.

Besides, the implicit numerical scheme for the heat diffusion equation of the soil layer, which bases on the Richtmyer and Morton scheme (Richtmyer and Morton, 1967), has to be adjusted. That is because the ground heat flux no longer describes a conductive heat transfer between the two uppermost soil layers (Eq. 2.1.6), but instead, it depends on the heat exchange between the uppermost soil or snow layer and the overlying canopy air mass. Therefore, the ground heat flux

$$G = \Lambda_{\text{sfc}}\big(T_{\text{soil}} - T_{\text{sfc}}\big) \tag{2.2.2}$$

is assumed to be proportional to the temperature difference between the surface and the uppermost soil layer T_{soil}. The constant of proportionality represents an empirically determined factor, here so-called "heat transfer

coefficient" Λ_{sfc} [W/(m^{2}K)], which was introduced by Viterbo and Beljaars (1995), who used the notation skin conductivity. Different values are assigned – predominantly between 10 and 40 W/(m^{2}K) – for the heat transfer coefficient depending on the plant functional type (PFT). The values used for Λ_{sfc} in the present study can be found in Trigo et al. (2015).

The concept of the surface temperature characterizing an infinitesimally thin surface, in which we completely neglect the change in heat storage, is only valid for areas where bare soil or shallow vegetation prevails. It is considered as a special case that is analyzed in an offline single-site experiment located in Kansas' grassy landscape (for a detailed description, see Sect. 3.1). For the global evaluation experiment, which includes forest regions such as the tropical rain forest (that has a dense canopy of up to 45 m), this approach is insufficient. In this case, the change in total heat content (in short heat storage) of the canopy air, the water vapor, and the biomass itself is no longer negligible. Therefore, we introduce the canopy heat storage (S_{cano}), which bases on a formulation given by Moore and Fisch (1986), into the energy balance equation (see Fig. 2.2, right-hand side):

$$S_{\mathrm{cano}} = LE + H + G + R_{\mathrm{net}} \tag{2.2.3}$$

It is composed of the sum of three parts

$$S_{\mathrm{cano}} = S_T + S_{\mathrm{veg}} + S_q \tag{2.2.4}$$

where S_T denotes the heat storage in the canopy air space, S_{veg} represents the heat storage of biomass, and S_q represents the heat storage resulting from changes in specific humidity in the canopy layer (in short, the latent heat storage). The heat storage in the canopy air space S_T can be expressed as

$$S_T = C_T \frac{\partial T_{\mathrm{sfc}}}{\partial t} = c_p \rho z_{\mathrm{veg}} \frac{\partial T_{\mathrm{sfc}}}{\partial t} \tag{2.2.5}$$

where ρ is the density of humid air, C_T is the area-specific heat capacity of the canopy air, and z_{veg} is the vegetation height. The heat storage of

biomass in the canopy layer (S_{veg}) is determined as

$$S_{\mathrm{veg}} = C_{\mathrm{veg}} \frac{\partial T_{\mathrm{sfc}}}{\partial t} = c_{\mathrm{veg}} m_{\mathrm{veg}} \frac{\partial T_{\mathrm{sfc}}}{\partial t} \tag{2.2.6}$$

where C_{veg} is the area-specific heat capacity of the biomass, m_{veg} is the area specific mass of biomass, and c_{veg} is the specific heat capacity of moist biomass according to Moore and Fisch (1986). The latter is approximated by a weighted average between the specific heat capacity of dry biomass and the specific heat capacity of water $c_{\mathrm{w}} = 4184 \ \mathrm{J/(kg\,K)}$, assuming a constant water mixing ratio of 58%. For example, at a temperature of 25 °C the canopy biomass has a specific heat capacity of $c_{\mathrm{veg}} \approx 2650 \ \mathrm{J/(kg\,K)}$. The area specific mass of moist biomass (m_{veg}) can be estimated as a function of the vegetation height (z_{veg}) using a linear relationship, namely $m_{\mathrm{veg}} = \rho_{\mathrm{veg}} z_{\mathrm{veg}}$, where $\rho_{\mathrm{veg}} \approx 1.67 \ \mathrm{kg/m^3}$ is the partial density of moist biomass, i.e., the mass of moist biomass per one cubic meter of air estimated using values given by Moore and Fisch (1986).

The latent heat storage S_q can be calculated according to Moore and Fisch (1986) as follows:

$$S_q = L_{\mathrm{v}} \rho_{\mathrm{a}} z_{\mathrm{veg}} \frac{\partial q_{\mathrm{cas}}}{\partial t} \tag{2.2.7}$$

where $L_{\mathrm{v}} = 2.5 \cdot 10^6 \ \mathrm{J/kg}$ denotes the latent heat of vaporization and q_{cas} represents the specific humidity in the canopy air space. In contrast to the heat storages of the canopy air and the biomass – Eq. (2.2.5) and Eq. (2.2.6) – which are expressed using heat capacities related to the time derivative of surface temperature, the situation is more complicated regarding the latent heat storage. Changes in specific humidity can occur independently of temperature changes. This means that only considering changes in specific humidity due to changes in surface temperature would neglect other humidity sources and sinks. Thus, a different approach to parameterize the latent heat storage is required because the current schemes do not contain a prognostic variable for the specific humidity in the canopy air space. In this approach, we take the heat storage resulting from changes in specific humidity of the canopy air space into account by defining an effective surface

specific humidity q_{sfc}, which is the best proxy for the specific humidity in the canopy layer that we have. It represents a nonlinear weighted average between the specific air humidity above the canopy q_{air} and the saturated specific humidity at the surface temperature, $q_{\mathrm{sat}}(T_{\mathrm{sfc}})$, by demanding that

$$\frac{q_{\mathrm{air}} - q_{\mathrm{sfc}}}{r_{\mathrm{a}}} \overset{!}{=} LE\big(q_{\mathrm{air}},\, q_{\mathrm{sat}}(T_{\mathrm{sfc}}),\, r_{\mathrm{a}},\, r_{\mathrm{c}},\, ...\big) \tag{2.2.8}$$

where r_{a} is the atmospheric resistance, r_{c} is the canopy resistance, and LE is the latent heat flux as it is calculated in the energy balance equation. This means that q_{sfc} is calculated to represent the effective near-surface specific humidity that is required to reproduce the surface moisture fluxes due to turbulent exchange processes. In principle, the specific humidity of the boundary layer, q_{air}, could be used as a proxy for the canopy air space humidity, q_{cas}, as suggested by Moore and Fisch (1986). However, we are of the opinion that the usage of q_{air} would underestimate the latent heat storage in the current scheme. This leads to a modified formulation of the latent heat storage, S_q:

$$S_q = L_{\mathrm{v}} \rho_{\mathrm{a}} z_{\mathrm{veg}} \frac{\partial q_{\mathrm{sfc}}}{\partial t} \tag{2.2.9}$$

Because q_{sfc} is not a prognostic variable in the energy balance, its time derivative is approximated using values of q_{sfc} at previous time steps. That is an approximation that is inevitable in the current model framework and can only be avoided by developing an extended dual-source canopy layer scheme, which includes a prognostic specific humidity of the canopy air space, as mentioned in the discussion (see Sect. 2.3). Using these approaches, we replace the former unphysical canopy heat storage concept in the surface energy balance equation by a physically based estimation of the canopy heat storage.

When discussing heat storages within the canopy, it is also necessary to consider the change in energy stored in the form of chemical energy by carbohydrate bonds through the process of photosynthesis. Following Nobel (2009), the energy required to incorporate 1 mol CO_2 is 479 kJ. This means, a CO_2 flux of $1\,\mathrm{mg}\,CO_2/(\mathrm{m}^2\mathrm{s})$ corresponds to an energy flux of

about 11 W/m². This chemical heat storage has been evaluated in several experimental studies at the site-level (e.g., Jacobs et al., 2008; Meyers and Hollinger, 2004). In these studies, however, the focus was only on energy consumption through photosynthesis (GPP, i.e., gross primary production). So far, most studies neglected the heat release during the process of plant respiration (e.g., Wohl and James, 1942; Thornley, 1971). This simplification had led to an overestimation of the chemical heat storage. Thus, one has to consider not only the net primary production (NPP) but also all other processes that release CO_2, such as decomposition, harvest, or land cover change. Therefore, we added a term in the energy balance to estimate the magnitude of the heat stored in chemical bonds:

$$S_{\text{cano}} = LE + H + G + R_{\text{net}} + \beta F_{\text{CO}_2} \qquad (2.2.10)$$

where F_{CO_2} is the net CO_2 flux in kg/(m²s) and $\beta = 10.884 \cdot 10^6$ J/kg is the abovementioned conversion factor. The net CO_2 flux F_{CO_2} (negative during the day, positive at night) is calculated in JSBACH using the photosynthesis scheme of Farquhar et al. (1980) for C3 plants and the scheme of Collatz et al. (1992) for C4 plants. We note that the estimation of the chemical heat storage in our study is a first attempt to address this issue and should be investigated in more detail in future studies.

2.3. CEBa

In the standard scheme of JSBACH (JSBACH Classic) and the modified version SkIn⁺ (chapter 3), there is only one surface temperature representing the whole canopy. This approach is insufficient when looking more closely at the processes that determine leaf temperature. However, the leaf temperature is required to better understand the processes and environmental conditions that regulate leaf thermoregulation (LT). Therefore, we extend the approach of the SkIn⁺ scheme to a dual-source Canopy Energy Balance (CEBa), which generally follows the approach of Shuttleworth and

Wallace (1985), Sellers et al. (1986) and Vidale and Stöckli (2005). This type of models allows the calculation of four prognostic variables: the leaf temperature T_{leaf}, the ground temperature T_{grd}, the temperature in the canopy air space (CAS) T_{cas} and the specific humidity in the CAS q_{cas}. Many land surface schemes with a dual-source canopy layer, e.g., Samuelsson et al. (2006), solve the system of energy balances diagnostically for T_{cas} and q_{cas} without accounting for the heat capacity of the canopy air space, neglecting thermal energy storage as well as changes in enthalpy due to changes in the composition of the CAS. In contrast, we follow Vidale and Stöckli (2005) and consider heat and water storage in the CAS. As we will show in chapter 3, these are not negligible for tall vegetation. In CEBa, not only the change of one surface temperature is used to specify the different types of storages, as it was the case with SkIn^{+}. Now, the biomass heat storage S_{veg} depends correctly on the vegetation temperature, while T_{cas} is used to calculate the heat storage of the moist air in the canopy. Especially the latent heat storage S_q (i.e., heat storages resulting from changes in specific humidity in the canopy layer, see Eq. 2.2.9) no longer needs to be calculated by means of the effective surface specific humidity q_{sfc}. It is now calculated more realistically using the specific humidity q_{cas}, representing the moisture content in the CAS. However, the alternative approach is still valid for Earth system models using the single-source approach.

In literature, the temperature of the forest vegetation, not only of the leaves, but also for the tree stems and branches, is often referred to as the canopy temperature T_{c}. Since we do not distinguish these different parts of the forest vegetation in CEBa, i.e., the thermodynamic properties of branches, trunks, and leaves are all described by the same temperature, we use the canopy temperature as a proxy for the leaf temperature T_{leaf} in this study.

JSBACH uses the tile approach to describe the surface properties of the vegetation (such as vegetation type, leaf area index, albedo, and roughness length). The energy balance is solved using the parameter averaging method. This means that the tile properties are averaged over all vegetation types. In JSBACH, the distribution of the vegetation follows the

so-called "land tile" configuration. This means that the plants are clumped in one subgrid area of a grid box (vegetation fraction) and the open soil occupies the rest (non-vegetation fraction) getting the same amount of radiation (Lee, 2018). The total latent heat flux is then calculated using area-weighted means (compare Eq. 2.1.14). In addition, JSBACH calculates the surface albedo of the vegetated area and the canopy absorption of radiation (according to the two-stream approach of Sellers (1985) for three canopy layers with evenly distributed leaf densities) using a weighting factor between the canopy and the soil the so-called "sky-view factor" – a simple approach for estimating the fraction of the sky that the ground under the canopy "sees" (Verseghy et al., 1993)

$$\chi = 1 - \left[f_{\text{veg}}\left(1 - e^{-0.5 LAI_{\text{eff}}}\right)\right] \tag{2.3.1}$$

where f_{veg} is the vegetated fraction of the grid box and LAI_{eff} is the effective leaf area index taking into account the clumping of vegetation by canopy gaps (for more details see Loew et al., 2014).

Despite this distinction between vegetation and soil for the calculation of the albedo and the radiative transfer, the system consisting of both vegetation and soil receives the same average amount of net radiation in the energy balance of the Classic and the Skin$^+$ scheme. The sky view factor χ is used to partition the net radiation R_{net} in the energy balance of CEBa into a canopy surface $R_{\text{net,c}}$ and underlying ground surface $R_{\text{net,g}}$ part (Fig. 2.3). For the sake of simplicity, the index c for the canopy (which serves in this study analogously for the leaf) and the index g for the ground are used in the following:

$$
\begin{aligned}
R_{\text{net,c}} &= \left(1 - \chi\right)\left[\left(1 - \alpha_c\right)S_{\text{in}} + \varepsilon_c L_{\text{in}}\right] + \varepsilon_c\left(1 - \chi\right)\left(\sigma T_g^4 - 2\sigma T_c^4\right) \\
R_{\text{net,g}} &= \chi\left[\left(1 - \alpha_g\right)S_{\text{in}} + \varepsilon_g L_{\text{in}}\right] + \varepsilon_g\left(1 - \chi\right)\sigma T_c^4 - \varepsilon_g \sigma T_g^4
\end{aligned}
\tag{2.3.2}
$$

Here α is the albedo, ε the surface emissivity, σ the Stefan-Boltzmann constant, L_{in} the incoming long-wave radiation, S_{in} the incoming short-wave radiation. The factor 2 in $R_{\text{net,c}}$ follows the assumption that the
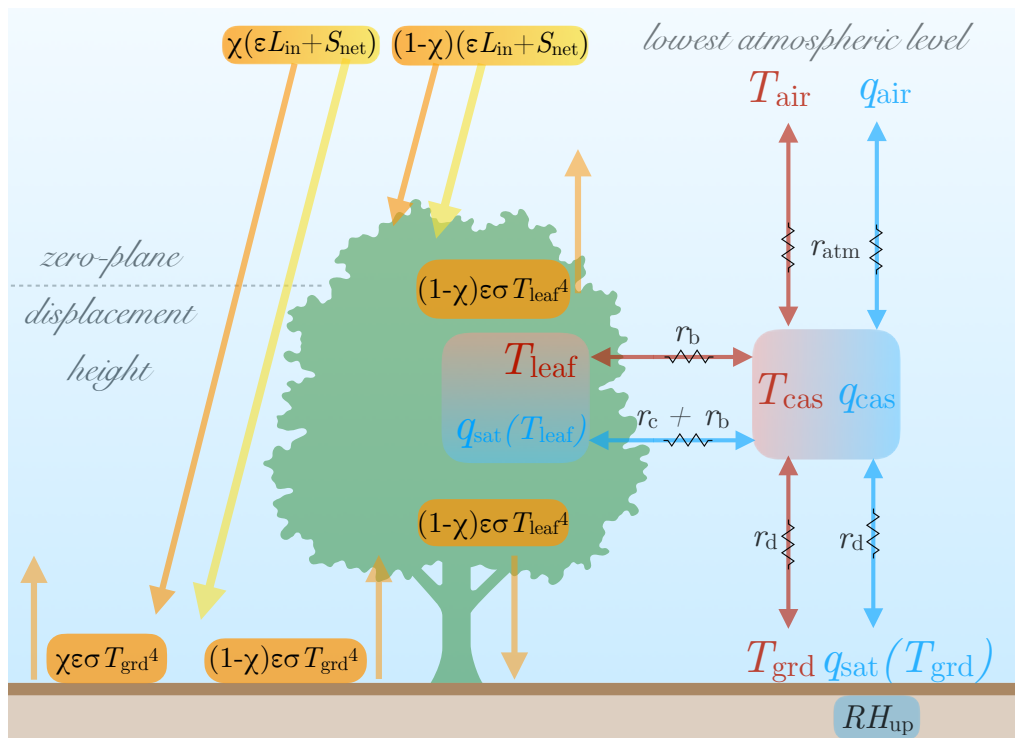
Fig. 2.3.: Principal sketch of the dual-source canopy energy balance scheme CEBa: Depicted are the radiative heat exchanges (yellow for short-wave radiation, orange for long-wave radiation), temperatures (red), specific humidities (blue), energy fluxes (red arrows), and water fluxes (blue arrows), including the resistances (black).

canopy layer emits radiation in two different directions: to the sky and to the soil surface. The radiation budget leads to two different cases of limit value calculation: For a negligible leaf area index ($LAI = 0$) the sky view factor is maximal ($\chi = 1$), which means that there would be no canopy at all leading to the known solution for bare soil:

$$
\begin{aligned}
R_{\mathrm{net,c}} &= 0 \\
R_{\mathrm{net,g}} &= \left(1 - \alpha_{\mathrm{g}}\right)S_{\mathrm{in}} + \varepsilon_{\mathrm{g}}L_{\mathrm{in}} - \varepsilon_{\mathrm{g}}\sigma T_{\mathrm{g}}^{4}
\end{aligned}
\tag{2.3.3}
$$

The second limiting case exists assuming a maximum leaf area index ($LAI \to \infty$) with a minimum sky view factor ($\chi = 0$) leading to an opaque canopy

layer that absorbs all incoming short-wave radiation:

$$R_{\mathrm{net,c}} = (1 - \alpha_{\mathrm{c}})S_{\mathrm{in}} + \varepsilon_{\mathrm{c}}\left(L_{\mathrm{in}} + \sigma T_{\mathrm{g}}^4 - 2\sigma T_{\mathrm{c}}^4\right)$$
$$R_{\mathrm{net,g}} = \varepsilon_{\mathrm{g}}\sigma T_{\mathrm{c}}^4 - \varepsilon_{\mathrm{g}}\sigma T_{\mathrm{g}}^4 \tag{2.3.4}$$

Here the soil surface still absorbs and emits long-wave radiation in interaction with the overlying dense canopy layer:

Figure 2.3 illustrates the energy and water exchange between the canopy, the ground, the canopy air space, and the lowest atmospheric level of the new CEBa system, including the temperatures, humidities, and resistances, respectively. The sensible and latent heat fluxes are parameterized using the common resistance formulation (for simplicity's sake snow and interception evaporation is not considered here):

$$H_{\mathrm{atm}} = \rho c_p \frac{T_{\mathrm{air}} - T_{\mathrm{cas}}}{r_{\mathrm{atm}}} \qquad LE_{\mathrm{atm}} = \rho L_{\mathrm{v}} \frac{q_{\mathrm{air}} - q_{\mathrm{cas}}}{r_{\mathrm{atm}}}$$
$$H_{\mathrm{g}} = \rho c_p \frac{T_{\mathrm{cas}} - T_{\mathrm{g}}}{r_{\mathrm{d}}} \qquad LE_{\mathrm{g}} = \rho L_{\mathrm{v}} \frac{q_{\mathrm{cas}} - RH_{\mathrm{up}}q_{\mathrm{sat}}(T_{\mathrm{g}})}{r_{\mathrm{d}}} \tag{2.3.5}$$
$$H_{\mathrm{c}} = \rho c_p \frac{T_{\mathrm{cas}} - T_{\mathrm{c}}}{r_{\mathrm{b}}} \qquad LE_{\mathrm{c}} = \rho L_{\mathrm{v}} \frac{q_{\mathrm{cas}} - q_{\mathrm{sat}}(T_{\mathrm{c}})}{r_{\mathrm{b}} + r_{\mathrm{c}}}$$

where ρ is the density of humid air, c_p is the specific heat capacity of air, L_{v} is the specific enthalpy of vaporization, r_{atm} is the atmospheric aerodynamic resistance, r_{b} is the aerodynamic resistance between the leaf and the CAS, r_{d} is the aerodynamic resistance between the ground surface and the CAS, r_{c} is the canopy resistance and RH_{up} is the relative humidity of the uppermost soil layer. The latter serves as a resistance for bare soil evaporation. The atmospheric resistance r_{atm} is calculated exactly in the same way as those used in JSBACH Classic (Eq. 2.1.8). However, the virtual potential temperature difference between the CAS and the atmospheric reference height, corresponding to the height of the lowest atmospheric level (LAL) – required for the calculation of the Richardson number – is now instead calculated between the surface and the LAL. In addition, the effective surface temperature q_{sfc}, which was the best humidity proxy for the estimation of the latent heat storage within the canopy layer using the
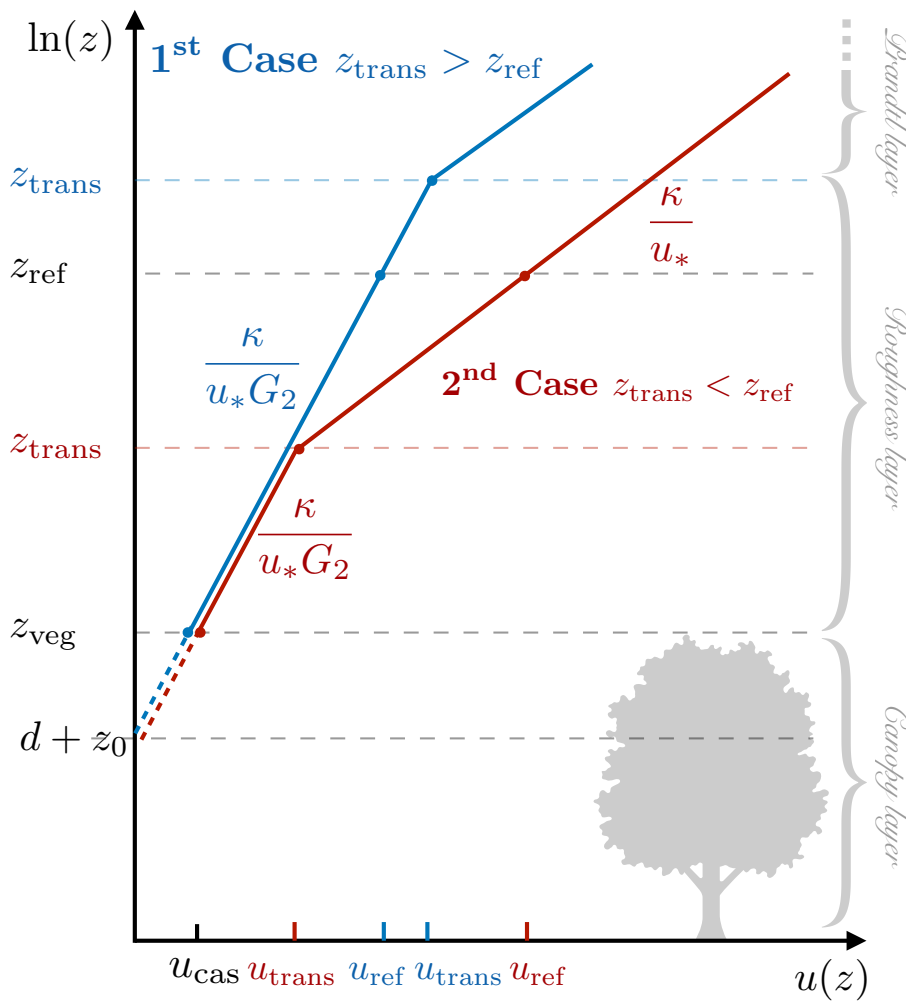
Fig. 2.4.: Logarithmic wind profile between the zero plane displacement height and the lowest atmospheric level: Comparison of wind profiles depending on the concept of the transition height for two different cases.

SkIn⁺ scheme, is replaced by the actual specific humidity of the CAS q_{cas}. Moreover, the roughness length of heat is not needed anymore in the drag coefficient because they are accounted[1] for in the aerodynamic resistances.

Since photosynthesis depends on the leaf temperature, in CEBa, the canopy resistance r_{c} depends on the leaf temperature instead of the temperature of the LAL. Both aerodynamic resistances between surfaces and the canopy air space have to be newly introduced. The resistance between the leaf and the canopy air space r_{b} (also called bulk resistance) is a function of the LAI, the leaf width, and the wind speed at the top of the canopy u_{cas}

and described the additional resistance induced by the turbulence in the leaf boundary layer (Choudhury and Monteith, 1988). It is modified with a free convection correction according to Sellers et al. (1986) depending on T_{leaf}, T_{cas} and the LAI. The parameterization of r_{d} follows a more complex approach depending on the vegetation height z_{veg}, the zero plane displacement height d (a function of z_{veg}, in turn), and u_{cas}. It is based on the general equation of an aerodynamic resistance for momentum transfer between the soil surface and the sink for momentum in the vegetation under neutral conditions (Choudhury and Monteith, 1988). We apply a stability correction for unstable cases following Sellers et al. (1986). For the estimation of the wind speed at the top of the vegetation height u_{cas}, we use an approach according to Xue et al. (1991). The basic idea is the concept of a so-called transition height z_{trans}. This height can be either below or above the reference height, depending on the height of the roughness layer, which is determined by the height of the vegetation. Figure 2.4 illustrates the concept considering two different cases for the transition height. For tall vegetation, the first case, the transition height exceeds the reference height of the LAL z_{ref}. For shallow vegetation, the transition height may be lower than the LAL. In this second case, the increase in wind speed of the logarithmic wind profile is scaled by an adjustment factor ($G_2 = 0.75$). Therefore, the wind speed in the CAS at the top of the vegetation z_{veg} can be calculated as

$$
u_{\mathrm{cas}} = \begin{cases} \frac{u_* G_2}{\kappa} \ln\left(\frac{z_{\mathrm{veg}}-d}{z_0}\right) & \Rightarrow z_{\mathrm{trans}} > z_{\mathrm{ref}} \\ u_{\mathrm{ref}} - \frac{u_*}{\kappa} \ln\left(\frac{z_{\mathrm{ref}}-d}{z_{\mathrm{trans}}-d}\right) - \frac{u_* G_2}{\kappa} \ln\left(\frac{z_{\mathrm{trans}}-d}{z_{\mathrm{veg}}-d}\right) & \Rightarrow z_{\mathrm{trans}} < z_{\mathrm{ref}} \end{cases} \quad (2.3.6)
$$

where

$$
u_* = \frac{\kappa}{G_2 \ln\left(\frac{z_{\mathrm{ref}}-d}{z_{0,\mathrm{m}}}\right)} u_{\mathrm{ref}} \quad (2.3.7)
$$

is the shear velocity and κ the Karman constant.

Considering all these expressions, we end up with a system of four coupled

equations:

$$C_c \frac{\partial T_c}{\partial t} = H_c + LE_c + R_{\text{net,c}} + \beta F_{\text{CO}_2}$$

$$0 = H_g + LE_g + R_{\text{net,g}} + G$$

$$C_T \frac{\partial T_{\text{cas}}}{\partial t} = H_{\text{atm}} - H_c - H_g \quad (2.3.8)$$

$$L_q \frac{\partial q_{\text{cas}}}{\partial t} = LE_{\text{atm}} - LE_c - LE_g$$

Here C_c and C_T are the area-specific heat capacities of the canopy and the CAS, respectively, L_q is the area-specific heat of vaporization for water, G is the ground heat flux, F_{CO_2} is the net CO_2 flux and β is a conversion factor (for the two latter see Eq. 2.2.10). Similar to the SkIn scheme, we assume an infinitesimally thin surface at the ground, which allows to neglect the ground heat storage. Analogously to the former model versions, the nonlinear terms within the system of equation in CEBa are linearized using a first-order Taylor approximation. To solve this linear system for the four prognostic variables, the inverse matrix has to be calculated and a Newton fixed-point iteration is applied.

In addition to the abovementioned modifications, which are mainly part of the surface energy balance equation, the CEBa scheme requires several changes to be applied in the surface and soil hydrology. The snow and skin reservoirs are distinguished between canopy and soil instead of representing the whole grid box. Moreover, the evaporative fluxes had to be adjusted consistently to maintain the water balance and soil water budgets. Finally, the coupling of the surface to the atmosphere had to be modified. The canopy layer and the ground represented in CEBa are connected radiatively to the lowest atmospheric level. The temperature and the humidity of the CAS are coupled, in contrast, by vertical turbulent diffusion to the atmospheric model. Therefore, the Richtmyer Morton coefficients of the implicit numerical diffusion scheme (Schulz et al., 2001) have been modified.

3. Canopy heat storage

This chapter has been published in a similar form regarding content as an article in the *Geoscientific Model Development* journal under the following authorship and title:

Heidkamp, M., Chlond, A., and Ament, F. (2018). Closing the energy balance using a canopy heat capacity and storage concept – a physically-based approach for the land component JSBACHv3.11. *Geoscientific Model Development*, 11:3465–3479

In present-day land surface models (LSM), the canopy is often represented inadequately. For example, it is still common practice to neglect the heat storage in the canopy completely or to close the surface energy balance within the uppermost soil layer of finite heat capacity, such as in JSBACH, the model used in this study. To be able to answer the research questions that motivate this work, a different approach to close the surface energy balance equation is investigated using a physically based estimation of the canopy heat storage (called SkIn$^+$). In order to test the performance of the scheme, we initially carry out an offline single-site experiment with the land component JSBACH of the MPI-ESM (for more information, see Sect. 2.1). In an offline experiment, the LSM is decoupled from its host model and forced by observation data; we then evaluate it against observed fluxes. For this purpose, initial data, forcing data, and verification data from the DICE project (Zheng et al., 2013) (for more information see Sect. 3.1) are used to compare energy- and water fluxes derived from eddy covariance measurements obtained during the CASES-99 field experiment in Kansas with simulated fluxes. In this first experiment, the aim is to determine whether the SkIn scheme would improve the performance in reproducing the diurnal cycle compared to the old heat storage concept in cases with shallow vegetation.

Following this, a global coupled land–atmosphere model experiment with the MPI-ESM is performed using the so-called AMIP (Atmospheric Model Intercomparison Project) protocol (Gates, 1992). In this experiment, the MPI-ESM (with T63 resolution, i.e., 1.9°) was run covering 30 years from 1979 to 2008 with prescribed sea surface temperatures. The objective of this experiment is to explore whether this scheme also has an impact on climatological time scales.

First, we describe the design of the experiments and the data used for them in detail (Sect. 3.1). Next, the results of both experiments are interpreted (Sect. 3.2) and the most important outcomes are discussed (Sect. 3.3) and summarized (Sect. 3.4).

3.1. Experiments and data

To address the first scientific question of this study, i.e., whether the heat storage concept correctly reproduces the coupling between the land and the atmosphere throughout the diurnal cycle in the case of shallow vegetation, we performed an offline single-site simulation with the JSBACH land surface model. We used observations from the Diurnal Land/Atmosphere Coupling Experiment (DICE, `http://appconv.metoffice.com/dice/dice.html`). This experiment was a joint effort between GLASS and GEWEX (Global Energy and Water Exchanges). The goal of DICE was to identify the complex interactions and feedbacks between the land and the atmospheric boundary layer. Koster et al. (2006) identified so-called "hot spot" regions characterized by a high coupling strength between the land surface and the atmosphere, which refers to the degree to which anomalies in land surface variables, for example, soil moisture, can affect the generation of precipitation or other atmospheric processes. Moreover, there has been disagreement among models for these regions in the past. One of these "hot spot" regions is located in the Great Central Plain of the United States. Therefore, DICE uses data from the CASES-99 (Coop-
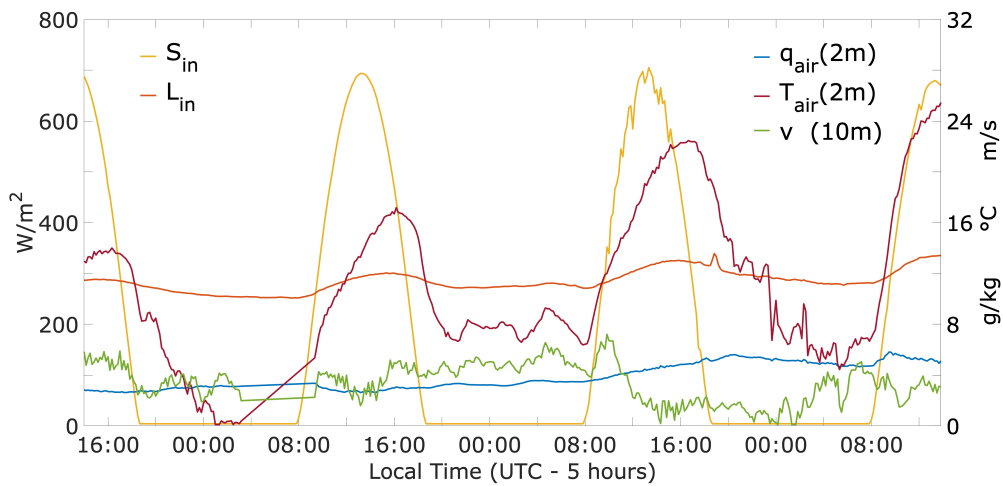
Fig. 3.1.: DICE forcing data used for the offline single-site experiment in the form of long-wave downward radiation (L_{in}, orange) and short-wave downward radiation (S_{in}, yellow) in W/m^2 (left axis), as well as the 10 m wind speed (v, m/s, green), the 2 m air temperature (T_{air}, °C, red) and the 2 m specific humidity (q_{air}, g/kg, blue) (right axis). Data are from the CASES-99 experiment in Kansas from October 23rd, 1999 to October 26th, 1999.

erative Atmosphere-Surface Exchange Study - 1999) field experiment in Kansas (37.7° N, 263.2° E). DICE principally follows the concept described in Steeneveld et al. (2006) and Svensson et al. (2011) regarding the same 3 days from the afternoon (19 UTC, 14:00 local time) of October 23rd 1999 to the 26th. For these 3 days, DICE provides forcing data (precipitation, air pressure, air temperature, specific humidity, and wind, as well as short-wave and long-wave incoming radiation) and verification data (surface temperature as well as sensible and latent heat fluxes) with a high temporal resolution of 10 minutes (Fig. 3.1). Also, 10-year forcing data of lower resolution (3 hours) are available for an initialization.

The measurement site was located near Leon, representing a relatively flat homogeneous terrain with dry soils. The area is situated far from the ocean or large bodies of water and is dominated by a continental climate. Following Köppen climate classification, it belongs to the northern limits of North America's humid subtropical climate zone (Cfa). Its climate features hot, humid summers and cold, dry winters. Without any substantial moderating influences such as mountains, there are often extreme weather events

such as thunderstorms or tornados in the spring and summer months. The average annual precipitation is comparably high, with 993 mm distributed over 147 rain days because convective precipitation prevails over stratiform or orographic precipitation; this means that rain events in these regions are generally severe and short-lasting, rather than weak and long-lasting.

The actual experiment of DICE contains the abovementioned three days from the afternoon of October 23rd, 1999 to the 26th. The three days were part of a 25-days drought and exhibited an increasing trend in temperature without any precipitation and permanent clear skies. The value of the air temperature of the first day and particularly the first night was below the October average, whereas the second night was relatively warm (Fig. 3.1). These different conditions during the nights indicate various turbulence and atmospheric stability regimes: intermittent turbulence (transition from lightly unstable to lightly stable conditions) for the first night, continuous turbulence or fully turbulent (neutral, tendency to lightly stable) for the second night with high wind speeds, and radiative (hardly any turbulence and very stable) for the third night including a temporary calm.

For the first offline single-site experiment, an almost 10-year spin-up is run to ensure an equilibrium temperature and moisture in deeper soil layers. This initialization is done using forcing data of the Water and Global Change (WATCH) project (Weedon et al., 2014), which bases on the 40-year ECMWF reanalysis (ERA-40) data. We replace the last year of the spin-up by a local measurement site in Smileyberg, Kansas, ending with the first day of the actual 3-day experiment. Gaps in this last year are filled by values from the WATCH data so that the time series does not contain missing values. In summary, the spin-up data contains 3583 days with a time step of three hours, which was interpolated to an hourly model time step. The actual 3-day simulation is performed with a model time step of 10 minutes. We adjusted the surface and soil parameters of the model (such as root depth or roughness length) to the site's properties.

The second evaluation experiment is run in a global coupled model con-

figuration for thirty years from 1979 to 2008 with a T63 resolution (i.e., 1.9°) using MPI-ESM. The simulation follows the AMIP project (Gates, 1992), which means that the sea surface temperature is prescribed. The soil and surface parameters of the model are the standard values (Hagemann, 2002), and the time step of the model is 450 seconds. Data from the WATCH project (Weedon et al., 2014) are used to compare the model results with observations.

3.2. Results

In this section, we evaluate the results of SkIn in an offline single-site experiment located in Kansas, where shallow vegetation prevails, and the canopy heat storage is negligible. Next, we discuss the extended SkIn$^+$ scheme, including the effect of the canopy heat storage, in the form of a global experiment.

3.2.1. Single-site experiment

Figure 3.2 shows results from the numerical experiments by displaying a time series of various quantities in the surface energy balance equation for the three specific days of the DICE experiment. Plotted are calculated fluxes of net radiation, sensible heat, latent heat, and ground heat flux using the standard version of JSBACH (upper panel, Fig. 3.2a), as well as the modified version SkIn (lower panel, Fig. 3.2b). In addition, observational data (dashed lines), which serve as verification data, are also plotted. The energy in the form of net radiation (violet) is divided into the sensible (red), the latent (blue), and the ground heat flux (green). Concerning the sign convention of the fluxes, we note that negative (positive) turbulent fluxes are pointing downwards (upwards) and are related to an uptake (release) of surface energy. Positive (negative) ground heat fluxes constitute an energy gain (loss). Heat fluxes measured by the eddy covariance method usually do
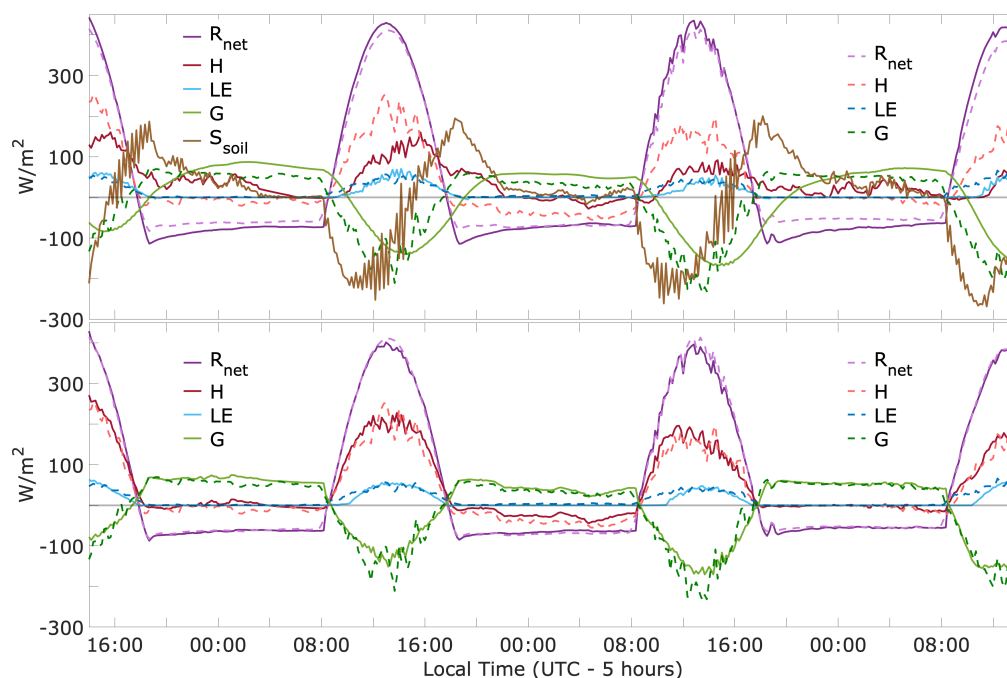
Fig. 3.2.: Performance of the classic JSBACH scheme and SkIn on diurnal time scales: Comparison of the time series of the components of the surface energy balance equation between the reference model (a) and the observations, and SkIn (b) and the observations (dashed lines). Plotted are the net radiation (R_{net}, violet), sensible heat flux (H, red), latent heat flux (LE, blue), ground heat flux (G, green), and heat storage term (S_{soil}, brown). Data are from the CASES-99 experiment in Kansas from October 23rd, 1999 to October 26th, 1999.

not close the energy balance, which means that their sum is smaller than the available energy (net radiation minus ground heat flux, e.g., Twine et al., 2000). Normally, this imbalance is distributed to the heat fluxes weighted by the Bowen ratio (see, e.g., Ingwersen et al., 2015). However, as there are no measurements of the ground heat flux during the DICE experiment, there is no other possibility except to calculate it as the residuum, including the stated imbalance. Therefore, we consider the ground heat flux only as an approximation, especially during the day when the largest residuals of the energy balance closure can occur.

At daytime, the net radiation is positive with a maximum when the sun is at its zenith, whereas at night, it stays at a constant negative value, which results in heat loss from the soil corresponding to a positive ground

heat flux pointing upward. During the first and third night, the sensible and latent heat fluxes disappear because turbulent motions are suppressed under stable conditions, whereas on the second night, a negative sensible heat flux prevails – meaning that the atmosphere releases heat to the soil.

The latent heat flux reaches only about $50 \, \mathrm{W/m^2}$ during these three days, which is the result of the 25-day drought. Thus, at about $250 \, \mathrm{W/m^2}$, the sensible heat flux represents a large part of the available energy (about $400 \, \mathrm{W/m^2}$) leading to a high Bowen ratio of about 5:1. Regarding the reference run, the sensible, the latent, and the ground heat flux react slower to the increase in net radiation. The cause of this delay is the presence of the thermal energy storage S_{soil} within the uppermost soil layer, which amounts to $250 \, \mathrm{W/m^2}$. This energy is stored (negative flux) during the day and released (positive flux) during the night. Therefore, the assumption that the energy will be absorbed in a layer of soil 6.5 cm thick results in a phase shift of about two to four hours.

In nature, radiation is absorbed within the first few micrometers of the soil–vegetation system and is then transported via thermal conduction further downwards. As a consequence, the uppermost soil layer is heated up during the first part of the day and releases a part of its energy content during the second half: As soon as the net radiation starts to increase, the heat is instantly stored in the uppermost soil layer resulting in an absolute maximum of the thermal energy change of up to $250 \, \mathrm{W/m^2}$. After a delay of about two hours, this energy is partly released by the sensible heat flux and partly conducted into deeper layers by the ground heat flux. Thus, the uppermost soil layer continuously absorbs less energy until around 16:00 (local time) when the situation reverses, and the layer releases the accumulated amount of energy it had previously absorbed. In some cases, a part of this energy transfer persists until nighttime, resulting in nocturnal heat releases that destroy the stable boundary layer. A further weakness of the reference scheme is related to its susceptibility to amplify fluctuations. Such behavior is evident, for example, when the time series shows jumps of the heat storage term by about $150 \, \mathrm{W/m^2}$ from one time step to another.
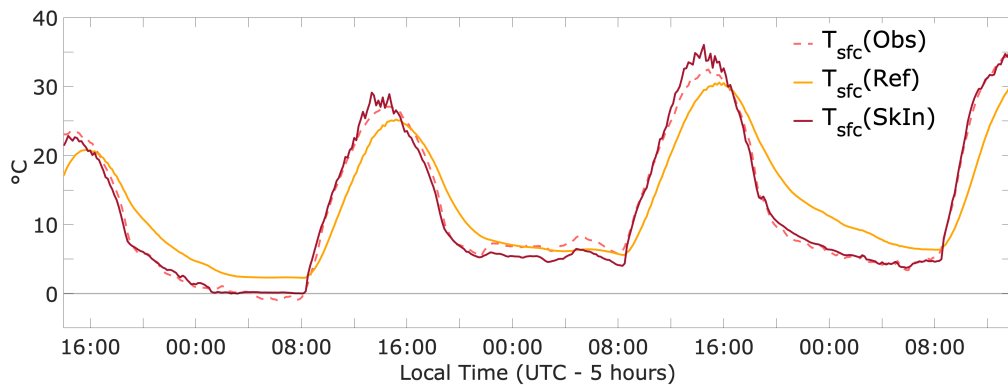
Fig. 3.3.: Performance of the classic JSBACH scheme and SkIn on diurnal time scales: Comparison of time series of the surface temperature T_{sfc} between the reference model (orange line) and SkIn (red line) plotted against observations (dashed line). Data are from the CASES-99 experiment in Kansas from October 23rd, 1999 to October 26th, 1999.

Comparing the results of the modified SkIn model version with those of the reference run (JSBACH Classic), we note that the first improvement is the disappearance of the nightly heat releases. The sensible heat flux of SkIn follows the observations almost perfectly, even on the second night when negative heat fluxes occur. In the SkIn simulation, where per definition no heat storage exists, we find that all fluxes immediately react to variations in the radiative forcing, and the phase shift found in the reference simulation vanishes.

The surface temperature exhibits a similar phase shift (Fig. 3.3): in the reference simulation the surface temperature is underestimated by up to 4 K in the case of heating and overestimated by up to 8 K in the case of cooling with respect to the observations. The simulation of SkIn only shows some minor disagreement with the observations. In particular, SkIn overestimates the surface temperature maximum on the second and third day, but apart from that, it fits the observation quite well. The behavior of the surface temperature in the reference run exhibits a phase shift, as it is equal to the soil temperature at about 3 cm depth. Here the ground heat flux, as the heat exchange between the first and second soil layers of the reference run, shows the same inertial lagging (Fig. 3.2). In addition, it is quite smooth and overestimates the nightly ground heat flux (partic-

ularly on the first night). Betts et al. (1993) found the same phase shift in temperature and the delayed response in the heat fluxes.

Interestingly, the phase error in surface temperature – caused by the dampening effect due to the heat storage term – exhibits an asymmetric behavior. The phase shift between the surface temperature and the observed temperature increases with time and is more pronounced during the night than during the day. In the SkIn scheme, the adjustment to an equilibrium temperature, which is determined by the radiative forcing, is achieved instantaneously. In contrast, in the heat storage based approach, the temperature difference between the simulated temperature and the equilibrium temperature decreases over time according to an exponential rate. The time required to reach the equilibrium state is determined by a time constant, which depends on the turbulence conditions in the atmosphere. During the day, the turbulent motions intensify the turbulent exchange and reduce the time needed to reach the equilibrium. In contrast, at night, the exchange is strongly reduced under stable conditions resulting in longer relaxation times. Thus, the simulated temperature in the SkIn run is always lower than that in the reference run. That is the case in the afternoon as well as during the night.

Moreover, the skin conductivity like the drag coefficient – in contrast to the heat capacity – acts to reduce the relaxation time to reach the equilibrium. However, the skin conductivity and the drag coefficient damp the amplitude of surface temperature to variations in the forcing. Overall, we deduce that based on a daily average, the cooling effect of SkIn outweighs its warming effect during the day for regions where shallow vegetation prevails (here SkIn leads to a cooling of 0.6 K).

In the next section, this finding will be further examined using an AMIP experiment. Moreover, we will address the extent to which the surface processes of regions with tall vegetation or regions located at high latitudes without a pronounced diurnal cycle will respond to the formulation of the land–atmosphere coupling.

3.2.2. Results of the AMIP run

A key aspect of the SkIn$^+$ scheme is the introduction of a physically based canopy heat storage S_{cano}. Since the latent heat storage S_q is not associated with a temperature tendency, it is not possible to compare the heat capacities related to different processes; however, it is necessary to compare different heat storages. Because heat storages have the nature to compensate each other over decadal time scales, we only compare the negative (stored energy) contributions of the heat storages to estimate their magnitude. That could be interpreted as the average amount of energy stored in the canopy. The same amount will also be released. The 30-year mean of the canopy heat storage ranges between roughly 5 and 15 W/m^2 for tall vegetation (Fig. 3.4a). The total canopy heat storage S_{cano} amounts to 3.7 W/m^2 in the global land mean. This value appears relatively small since the regions with no or shallow vegetation account for negligible storages (around 0 W/m^2) and do not contribute to the mean. The heat storage in the canopy air space S_T amounts to 19 % of the total canopy heat storage, and the latent heat storage S_q constitutes 22 %. The most significant contribution to the total storage, with around 60%, comes from the heat storage of the moist biomass S_{veg}. In the warm and humid tropics, where tall vegetation prevails, we find the largest values for the canopy heat storage. Here the latent heat storage partly shows a similar magnitude as the biomass heat storage. In the tropics the total canopy heat storage averages 12 W/m^2 (15 W/m^2 at maximum), whereas in the taiga mean values of 5 W/m^2 are observed, and in deciduous forests mean values of 3 W/m^2 are found.

Comparing the latent heat storage S_q qualitatively on diurnal scales with the other two storage terms, which are directly related to the surface temperature tendency, we find that the temperature-related heat storages tend to react like an ordinary heat storage. An ordinary heat storage exhibits a negative peak during the first half of the day (energy stored) and a positive during the second half of the day (energy released, compare the soil
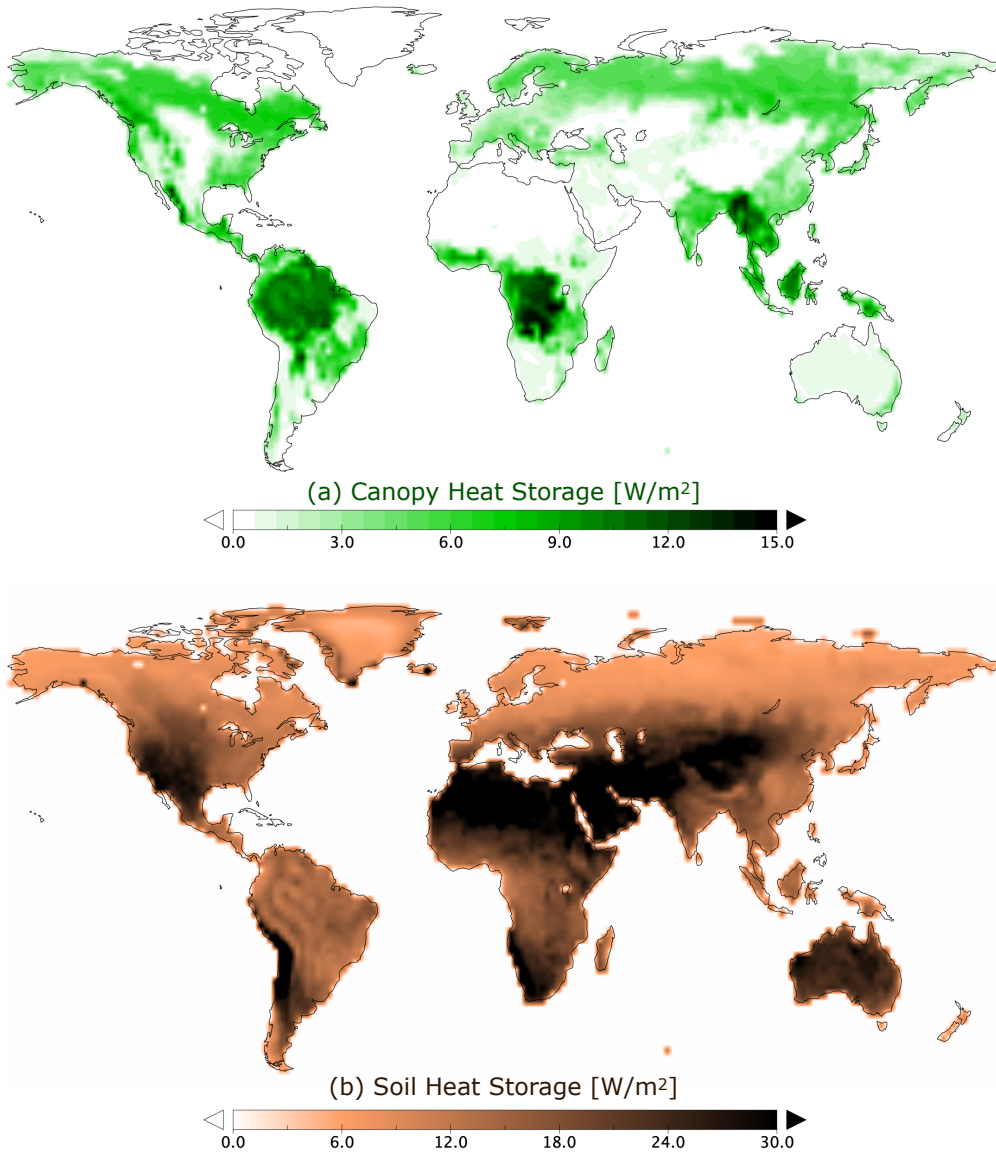
(a) Canopy Heat Storage [W/m²]

| 0.0 | 3.0 | 6.0 | 9.0 | 12.0 | 15.0 |

(b) Soil Heat Storage [W/m²]

| 0.0 | 6.0 | 12.0 | 18.0 | 24.0 | 30.0 |

Fig. 3.4.: Comparison of the canopy and the soil heat storage: Global
distribution of the negative contributions of the canopy heat storage S_{cano} (a)
and the soil heat storage S_{soil} (b), both in W/m² as a 30-year mean (1979-2008).

heat storage in Fig. 3.2), whereas the latent heat storage, does not show
this temporal course. It shows positive as well as negative changes in heat
storage throughout the day. That corresponds to the fact that the specific
humidity does not follow a strict diurnal pattern like the surface tempera-
ture. On the contrary, there are different kinds of days that represent either
a positive or negative trend in humidity, depending on dry or wet periods.

The negative part of the chemical heat storage βF_{CO2} follows the same regional pattern as the other canopy heat storages, whereas the temporal course on diurnal scales differs. In particular, the chemical heat storage follows the PAR (photosynthetically active radiation) part of the incoming solar radiation and results in energy consumption during the day and energy release due to respiration at night. With 0.64 W/m^2 on global average, it amounts to 17% of the total canopy heat storage S_{cano} and is slightly smaller than S_T. Nevertheless, it should not be neglected because the sum of all of these supposedly small terms could be important. As previously mentioned, we think that the chemical heat storage is an interesting process which should also be investigated in connection with the interaction between the carbon cycle and the climate on decadal time scales.

The soil heat storage in the reference model JSBACH Classic (Fig. 3.4b) is related to the soil heat capacity of the uppermost soil layer, which is determined by the present soil type based on the FAO (Food and Agriculture Organization of the United Nations) soil classification guidelines. The soil heat storage varies spatially in the range between 5 and 50 W/m^2 and amounts to 17 W/m^2 on global average. For regions with tall vegetation, it reaches values of about 10 W/m^2, which corresponds to the same order of magnitude as the canopy heat storage in the SkIn$^+$ scheme: for tropical forests, it is slightly smaller, and for Northern hemisphere forests it is slightly larger. However, the soil heat storage significantly exceeds the canopy heat storage in regions with no or shallow vegetation. In general, the magnitude of the canopy heat storage, as well as the soil heat storage, is proportional to the temperature tendency. The regions with no or shallow vegetation exhibit the largest diurnal ranges in temperature. Therefore, the largest discrepancy appears in these areas and amounts to up to 50 W/m^2. Thus, we expect that the primary influence of the SkIn$^+$ scheme occurs in regions where bare soil or shallow vegetated regions dominate, such as grasslands or savanna, while we expect a rather small effect in forested regions.

Figure 3.5a illustrates the performance of the SkIn$^+$ scheme in terms of the

(a) ΔT(SkIn⁺ — Classic) [K]
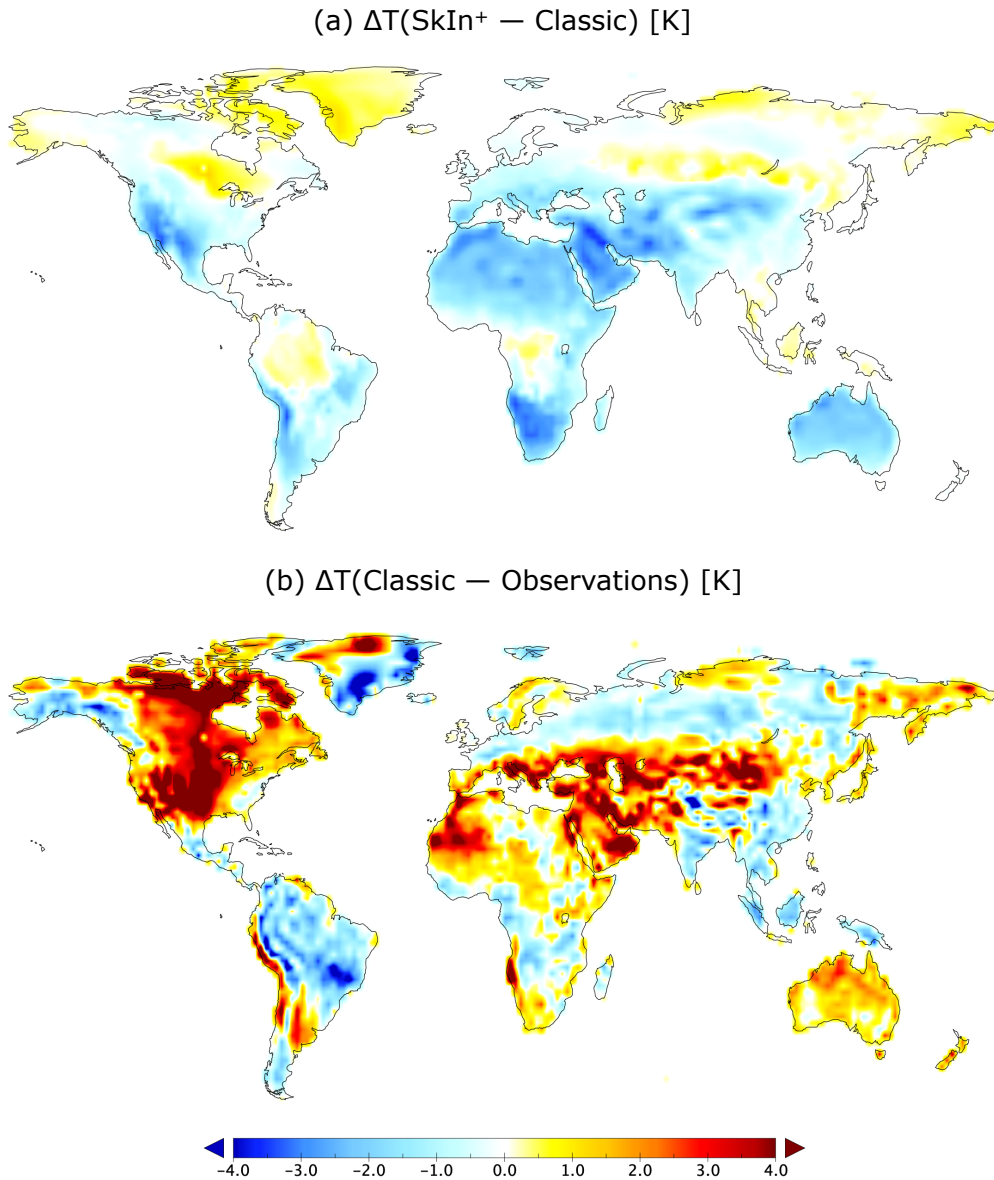
(b) ΔT(Classic — Observations) [K]

Fig. 3.5.: Performance of SkIn⁺ scheme on regional scales: Thirty-year (1979-2008) summer half-year (Apr-Sep) average of the difference of near-surface temperatures between SkIn⁺ and the reference run (JSBACH Classic, a) as well as between reference run and observations (in short model bias, b).

simulated 2m-temperature, which includes the canopy heat storage S_{cano}, on regional scales using a 30-year average for the summer season (April to September) by displaying the difference of the near-surface temperature between SkIn⁺ and the reference run (JSBACH Classic). Based on our experience with the offline version, we know that SkIn leads to warming

during the day and cooling at night due to its instantaneous response to the radiative forcing. Thus, the sign of the local mean temperature difference between SkIn$^+$ and the reference run depends on whether the night effect prevails or whether the daytime effect and other processes predominate, such as clouds and precipitation. In the global mean, SkIn$^+$ leads to a cooling of 0.22 K. Almost all regions characterized by no or shallow vegetation and a pronounced diurnal cycle, where mostly well-mixed conditions during the day and very stable conditions during the night occur, show an overall cooling in SkIn$^+$ relative to the reference scheme (with a maximum of up to -3.5 K). This effect is visible in Australia, the southwestern United States, the Gran Chaco region in South America, the Sahara, the Middle East, and central Asia.

In the tropics, the SkIn$^+$ and the reference scheme show much smaller differences, which suggest that the canopy heat storage in SkIn$^+$ roughly corresponds to that of the uppermost soil layer. Only in some parts of the tropics is SkIn$^+$ slightly warmer than the reference scheme, indicating an opposite SkIn effect with higher temperatures at night and lower temperatures during the day. Consequently, an absence of the canopy heat storage would lead to a slight cooling in the tropics. With respect to the mid and high latitudes of the Northern Hemisphere, we note that north of fifty degrees SkIn$^+$ leads to a warming in summer relative to the reference scheme because the daytime effect prevails in this region and is caused by the supply of heat during the longer insolation period in these regions during Northern Hemisphere summer.

Figure 3.5b depicts the difference in near-surface temperatures between the reference run and the observations (WATCH dataset). A comparison of the patterns of the upper and the bottom panel in Fig. 3.5 shows that for certain regions, where the reference model tends to be too warm, SkIn$^+$ produces a cooling and vice versa. Not all biases disappear entirely (see appendix Fig. B.1), especially as the existing biases are much larger than the effects due to SkIn$^+$, but the SkIn$^+$ scheme improves the overall performance of the land surface exchange by reducing the model bias. Thus, the root mean

square error of the global average temperature bias over land is reduced by 0.19 K, which corresponds to a bias reduction of about 9%. SkIn$^+$ leads to significant improvements in the southwestern United States, the Gran Chaco region, western and central Africa, and particularly in the Middle East, Central Asia, and Australia. In some other regions, such as parts of South Africa or in North America's boreal forests, the SkIn$^+$ scheme seems to be unable to reproduce the temperature patterns. Therefore, further refinements are required to improve the treatment of various land–atmosphere interaction processes, in particular over boreal forests and in snow-covered regions. Moreover, other biases that are not related to land processes, for example, those caused by the atmosphere and its large-scale circulation patterns, may be responsible for the apparent shortcomings of the SkIn$^+$ scheme.

3.3. Discussion

In this study, we demonstrate that the soil heat storage approach appears to be too simple and is unable to correctly reproduce the coupling between the land surface and the atmosphere concerning the simulation of diurnal cycles of energy fluxes and the near-surface temperature in regions with shallow vegetation. SkIn$^+$ does not show an unambiguous effect in one direction but causes both cooling and warming depending on the time of day. One could debate that the heat storage approach only induces phase errors in the diurnal cycle of surface fluxes and of near-surface temperatures producing errors that cancel each other when averaged over decades. However, this assumption appears to be untrue because we find a temperature signal of up to 3.5 K in the 30-year temperature average differences. Moreover, the calculation of the correct timing of heat fluxes is an important issue per se because it influences and triggers convection, which governs the formation of clouds and precipitation and, in turn, affects the energy fluxes. Therefore, we recommend that the SkIn$^+$ scheme should be used not only for models that operate on short time scales but also for Earth system

models with decadal time scales or longer.

However, in some regions, the SkIn⁺ scheme shows worse performance than its predecessor, likely because some existing biases only emerge in the SkIn⁺ scheme. In addition, we believe that the SkIn⁺ scheme, which considers the canopy heat storage, would take full effect in cases where subgrid-scale surface temperature variations in a grid cell are taken into account. At the moment, we solve the surface energy balance for the whole grid box using the parameter averaging method implying that the same surface temperature represents the whole grid cell. A more promising approach, which would be more suitable for the SkIn⁺ scheme and would allow a better representation of spatial subgrid-scale heterogeneity, would be a flux aggregation method (Best et al., 2004; de Vrese and Hagemann, 2016). An example of the use of the flux aggregation method is the Tiled ECMWF Scheme for Surface Exchanges over Land model (TESSEL, Balsamo et al., 2009). Moreover, future developments of land surface exchange schemes should also take the vertical discretization of the thermal structure within the canopy layer into account, which is important in the case of tall vegetation. Here the temperature of the tree crown, the surface temperature under the trees, the ambient air space temperature within the canopy, and the leaf temperature itself are differentiated (e.g., Vidale and Stöckli, 2005, see CEBa). The development of the SkIn⁺ scheme is only the first step to decoupling the surface energy balance from the soil layer. We believe that future studies, taking more processes within the canopy layer into account to address the role of the leaf temperature and its relation to evapotranspiration within the forest, will be capable of improving our understanding of land–atmosphere exchange processes (see next chapter).

3.4. Conclusion

In several current climate models, it is common practice to use a prognostic procedure to close the surface energy balance within the uppermost soil

layer of finite thickness and heat capacity. In this study, we investigate a different approach by closing the energy balance diagnostically at an infinitesimally thin surface layer (SkIn). We address the question of whether the classic heat storage concept correctly reproduces the coupling between the land and the atmosphere throughout the diurnal cycle regarding shallow vegetation. Therefore, we performed an offline site experiment with JSBACH, the land component of the MPI-ESM, using observations from the CASES-99 field experiment in Kansas. Analyzing the surface energy balance in both schemes, we find the following:

- The surface temperature simulated in JSBACH Classic is underestimated in the case of heating during the day and overestimated in the case of cooling at night.

- The turbulent exchange during daytime counteracts the delayed response in near-surface temperature whereas, during stable conditions at night, a significant phase shift occurs.

- SkIn removes these phase errors in the time-dependent behavior of the heat fluxes and surface temperatures that were caused by the dampening effect of the soil heat storage.

- With the new scheme, nocturnal heat releases, which previously destroyed the stable boundary layer unrealistically, disappear.

Here we demonstrate that the SkIn scheme leads to significant improvements in the representation of exchange processes and removes almost all biases.

Following this, we investigate the effect of the SkIn scheme on decadal time and global spatial scales. The questions we address are whether the SkIn scheme shows a regional impact on decadal time scales, and if so, whether the current biases in near-surface temperature are at least partly caused by the former oversimplified parameterization of the surface energy balance. To answer these questions, we performed a global coupled land–

atmosphere experiment covering the years from 1979 to 2008 (AMIP run) with prescribed sea surface temperature. For this global run, the standard heat storage concept is replaced by a physically motivated approach that describes heat storage of the canopy layer in the surface energy balance (SkIn$^+$). In this method, not only the heat storage of the biomass itself is taken into account, but the heat storage of the moist air within the canopy layer is also included. In addition, we want to determine if the daily warming or the nightly cooling, which occurs in the offline site-level version of SkIn, also prevails in the coupled run and, if so, which effect dominates in which region. Comparing the simulated summer near-surface temperatures of the SkIn$^+$ scheme with those of the reference run as well as with the WATCH data we find the following:

- The heat storage of the canopy layer must be taken into account in regions with tall vegetation (especially in the tropics). Here the heat storage of the canopy layer is larger than that of the uppermost soil layer.

- For most regions – especially those with no or shallow vegetation and a pronounced diurnal cycle – the night effect of SkIn$^+$ prevails, leading to a cooling in the near-surface temperature relative to the standard scheme.

- For the tropics, where the heat storage of the canopy layer is larger than that of the uppermost soil layer the SkIn$^+$ scheme leads to a slight warming.

- For high latitudes, SkIn$^+$ tends to warm the near-surface air temperature due to the extended day length in the Northern Hemisphere in summer.

In summary, the SkIn$^+$ scheme also shows a significant global effect on decadal time scales and a reduction of the model bias in several regions.

4. Leaf thermoregulation

This chapter focuses on the understanding of the process of leaf thermoregulation (LT), which was first detected by Linacre (1964) and later investigated in detail by Michaletz et al. (2016b). Leaf thermoregulation is the ability of plants to buffer its temperature against temperature extremes of the air. This means, the leaf can be warmer than the air in cold environments, while it tends to stay colder than the air in warm environments. When depicting the measurements of leaf and air temperature, it leads to a negative correlation between the plants' leaf temperature excess (the difference between leaf temperature and environmental temperature) and air temperature (LT signal). The process of leaf thermoregulation is analyzed by means of the new dual-source canopy energy balance scheme (CEBa). As described in chapter 2, this scheme allows the calculation of four prognostic variables: the leaf temperature, the ground temperature, and the temperature, as well as the specific humidity in the canopy air space (CAS). With this new tool, we are able to identify the influence of atmospheric conditions and leaf properties on the leaf's ability to regulate its temperature. To this end, we perform zero-dimensional experiments in which we solve the CEBa energy balance stationarily (steady-state case) as a function of the air temperature. Here we determine the equivalence point of leaf thermoregulation (where leaf and air temperature are equal) under prescribed atmospheric conditions and leaf properties. Furthermore, we perform two offline single-site experiments with CEBa using forcing data from a FLUX-NET tower in Brazil's tropical forest and the temperate Tharandt forest in Germany. We do so to identify the effects of leaf thermoregulation in an Earth system model framework at the canopy scale similar to the results

of Michaletz et al. (2016b) at the leaf scale. In addition, we conduct a global coupled land–atmosphere model experiment with CEBa using the same AMIP framework as in section 3.2.2 to establish whether leaf thermoregulation leads to large simulated leaf temperature excesses as found in observations. Finally, we quantify the impact of leaf thermoregulation on plant productivity regarding gross primary production.

4.1. Physical explanation

The physical explanation behind the negative correlation between the leaf temperature excess and the air temperature – especially the lower leaf temperature in a warm environment – can be explained by the energy balance of the leaf as follows (assuming constant net radiation that is absorbed by the leaf surface): With increasing air temperature, the leaf temperature also increases to maintain the energy equilibrium by keeping a constant temperature difference and sensible heat flux. While the leaf temperature increases linearly, the saturated specific humidity of the leaf $q_{\mathrm{sat}}(T_{\mathrm{leaf}})$ increases exponentially following Clausius–Clapeyron theory. Thus, the transpiration increasingly outweighs the sensible heat flux leading to decreasing Bowen ratios. Above a certain air temperature, the latent heat flux of the leaf exceeds the available energy flux (mainly in the form of the net of thermal and solar radiation absorbed, emitted and reflected from the leaf), resulting in a sensible heat flux towards the leaf (Fig. 4.1). This behavior is known as the oasis effect and has also been found for vegetated canopies (Taha et al., 1991). To explain this process quantitatively, we consider the energy balance of the leaf and solve it analytically for the temperature difference $T_{\mathrm{leaf}} - T_{\mathrm{air}}$. Ignoring heat storages within the leaf, the energy balance can be written by

$$R_{\mathrm{net}} = LE_{\mathrm{leaf}} + H_{\mathrm{leaf}} \qquad (4.1.1)$$

where R_{net} is the net radiation, LE_{leaf} is the latent heat flux of the leaf and H_{leaf} the sensible heat flux of the leaf. The latent and sensible heat
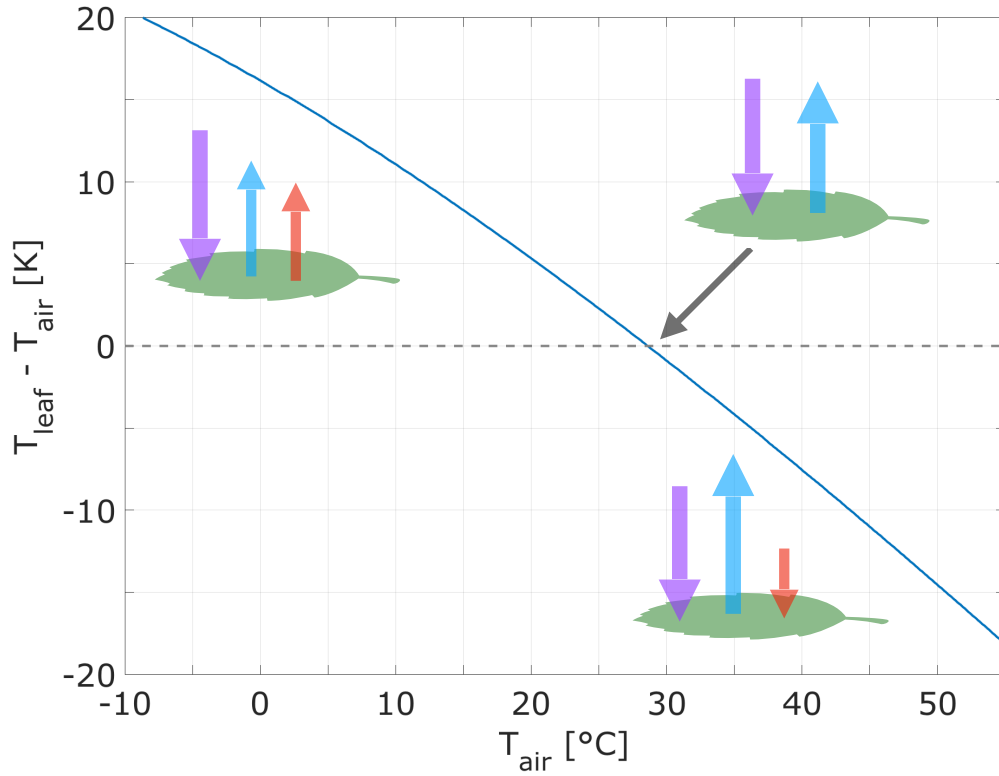
Fig. 4.1.: Example case for the analytically solved leaf energy balance equation: Negative correlation between leaf temperature excess and air temperature as well as three different cases of the energy balance (R_{net} in violet, H_{leaf} in red and LE_{leaf} in blue, atmospheric conditions and resistances are prescribed: $R_{\text{net}} = 700\,\text{W/m}^2$, $q_{\text{air}} = 20\,\text{g/kg}$, $r_{\text{b}} = r_{\text{s}} = 10\,\text{s/m}$) according to Eq. (4.1.4).

flux can be expressed as

$$LE = c_1 \frac{q_{\text{sat}}(T_{\text{leaf}}) - q_{\text{air}}}{r_{\text{b}} + r_{\text{s}}}$$
$$H = c_2 \frac{T_{\text{leaf}} - T_{\text{air}}}{r_{\text{b}}} \tag{4.1.2}$$

where q_{air} is the specific humidity of the air, r_b is the aerodynamic leaf resistance and r_s the stomatal resistance. The terms $c_1 = \rho L_{\text{v}}$ as well as $c_2 = \rho c_p$ can be seen as constant, in first order. Here ρ denotes the air density, L_{v} the enthalpy of vaporization, and c_p the specific heat capacity of air at constant pressure. The saturated specific humidity of the latent

heat flux can be linearized at $T = T_{air}$ as

$$LE \approx c_1 \frac{q_{sat}(T_{air}) - q_{air}}{r_b + r_s} + c_1 \alpha \frac{T_{leaf} - T_{air}}{r_b + r_s} \qquad (4.1.3)$$

where α is the slope of the saturation specific humidity at T_{air}. With the abovementioned approximations, the leaf energy balance can be solved analytically and written in terms of the leaf temperature excess, as follows

$$(T_{leaf} - T_{air}) = \frac{r_b}{c_2} R_{net} - \frac{c_1}{c_2} \frac{1}{c_3 + r_s/r_b} q_{sat}(T_{air})(1 - RH) \qquad (4.1.4)$$

with $c_3 = 1 + \alpha c_1/c_2$. With this equation, we can quantify the atmospheric conditions and leaf properties that lead to an equilibrium between the leaf and the air temperature (equilibrium point). Equation 4.1.4 shows that an increase in net radiation or relative humidity decreases the leaf temperature excess and the plant's ability to buffer its temperature against air temperature. A more detailed investigation of these relationships is carried out in a steady-state experiment (Sect. 4.4.1).

4.2. Experiments and data

To understand the process involved in leaf thermoregulation (LT) under different atmospheric conditions and for various leaf specific properties, we solve the system of equations of the CEBa energy balance for different air temperatures from –20 °C to 60 °C. This method makes it easier to understand the cause of the negative correlation between leaf temperature excess and air temperature in terms of equivalence point and slope. For this simplified experiment, we bypass the framework of the complex Earth system model and extract only the most important subroutines regarding the CEBa energy balance. We use surface parameters of a forest with tall vegetation and assume no water stress, i.e., unlimited soil water availability for transpiration. The specific humidity of the air required as forcing is replaced by the saturated specific humidity for the respective air tem-

Fig. 4.2.: Location of the FLUXNET tower site located in the tropical evergreen broadleaf forest, Brazil, photo taken from `https://fluxnet.fluxdata.org` (01 Nov 2019, URL: `http://sites.fluxdata.org/files/media/images/br-sa1-primary_forest_tower.jpg`)

perature multiplied by the relative humidity. The latter, as well as the wind speed and the incoming solar radiation (in the form of the angle of inclination), are prescribed and kept constant for the respective experiment over the entire forced temperature range. In a further step, we analyze how the equivalence point and the slope of the leaf temperature excess depend on different values of relative humidity, incoming solar radiation, canopy resistance, and aerodynamic leaf resistance. Although the leaf temperature excess as a function of air temperature represents a nonlinear curve, we approximate it by a linear function, reducing the complexity to two degrees of freedom (i.e., slope and equivalence point).

To address the second scientific question, i.e., whether we are able to identify a negative correlation of leaf temperature excess and air temperature at the canopy scale, we performed two offline single-site experiments with CEBa using forcing data from a FLUXNET tower in Brazil's tropical forest and the temperate Tharandt forest in Germany. Both sites exhibit a

Fig. 4.3.: Location of the FLUXNET tower site located in the evergreen needleleaf forest in Tharandt, Germany, photo taken from `https://tu-dresden.de` (01 Nov 2019, URL: `https://tu-dresden.de/bu/umwelt/hydro/ihm/meteorologie/ressourcen/bilder/forschung/projekte/turbefa/bilder/aufbau_13?lang=en`)

forest with a dense canopy and a large vegetation height. The tropical site (ID: `BR-Sa3`, -3.0° N, -55.0° E, 100 m elevation) is located in an evergreen broadleaf forest (Fig. 4.2) with a vegetation height of around 35-40 m, while the measurement height is at 64 m. The average annual temperature is 26.1 °C and the annual mean precipitation is 2044 mm. The Tharandt FLUXNET tower (ID: `DE-Tha`, 51.0° N, 13.6° E, 385 m elevation) is located in an evergreen needleleaf forest (Fig. 4.3) with a vegetation height of around 30 m, while the measurement height is at 42 m (Delpierre et al., 2009). The annual mean temperature is 8.2 °C and the annual mean precipitation is 843 mm. For both locations, the surface and soil settings are extracted from the standard settings of the respective JSBACH grid box and adapted to the properties of the site. For the tropical site, data are only available from September 2001 to October 2003. Therefore, these
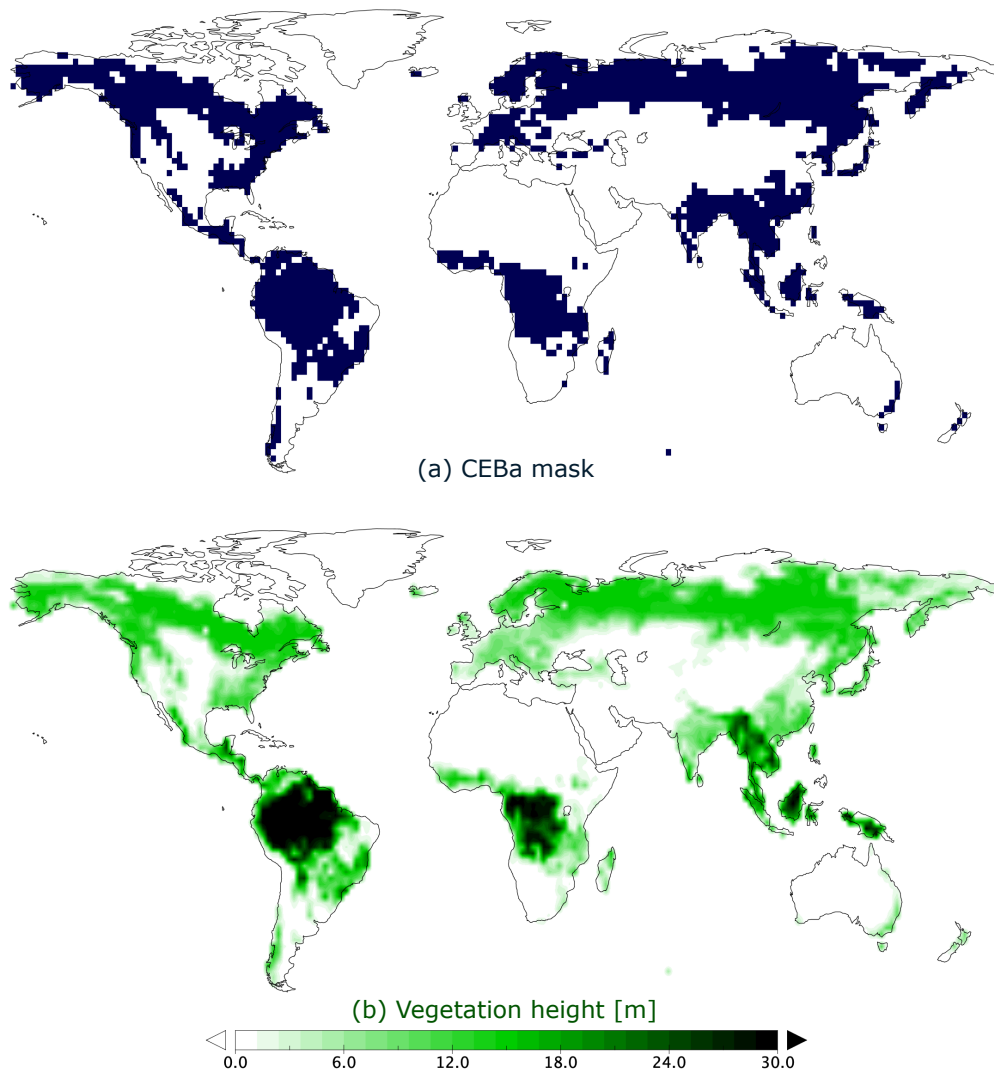
(a) CEBa mask

(b) Vegetation height [m]

0.0   6.0   12.0   18.0   24.0   30.0

Fig. 4.4.: CEBa 5-m vegetation height mask indicating for which grid cells the CEBa scheme is used (a) and average vegetation height in JSBACH (b)

years are randomly resampled for a 10-year initialization period to ensure equilibrium with respect to the temperature and moisture content in the soil. Since the Tharandt site provides a long period of data, the data from 1996 to 2005 are used for the spin-up of the model and the data from 2006 to 2014 for the actual experiment.

To investigate the leaf temperature on a global scale, we performed an AMIP run with the same settings as in chapter 3 for thirty years from 1979 to 2008 (for more details, see Sect. 3.1). The CEBa scheme requires an

estimate of the wind speed profile in the canopy layer to properly simulate the exchange of heat and water between the CAS and the leaves or the ground, respectively. It is possible to run the CEBa scheme for shallow or even no vegetation, like deserts or glaciers (the latter with an average vegetation height of z_{veg} = 0). However, the simulations with CEBa for these extremes have not shown adequate results. Therefore, in the framework of this study, the CEBa scheme is applied for grid boxes with an averaged vegetation height greater than 5 meters. The resulting mask is depicted in Fig. 4.4. For all other land grid points, the SkIn$^+$ scheme is used instead. The T63 grid contains a total of 192×96 = 18432 grid points, one-third of which are land points (6222). For around 30% (ca. 2000 grid points) of these land points, the CEBa scheme is used. In this regard, the current model version of CEBa rather represents an extended SkIn$^+$ scheme in regions with tall vegetation than a completely independent scheme. Before performing experiments to investigate the effect of leaf thermoregulation, the new CEBa scheme is evaluated at the site- and global scale in the next section.

4.3. Evaluation of CEBa

To test the performance of the new CEBa scheme compared to the standard JSBACH Classic, we use both FLUXNET tower sites to compare the simulated sensible and latent heat fluxes with measured eddy covariance fluxes at the tower. Therefore, we perform two single-site offline experiments with Classic and CEBa, respectively. Since the FLUXNET observations lack leaf temperature measurements, we compare the emitted outgoing long-wave fluxes instead. The radiative flux is converted into a radiative temperature T_{rad} using the Stefan-Boltzmann law and assuming the same emissivity of ε = 0.996 as used in JSBACH Classic. Figure 4.5 shows the comparison of the averaged diurnal cycle for the summer season (April to September) between JSBACH Classic (red) and JSBACH CEBa (blue) against observations (black dashed lines). Plotted are the radiative temperature T_{rad}
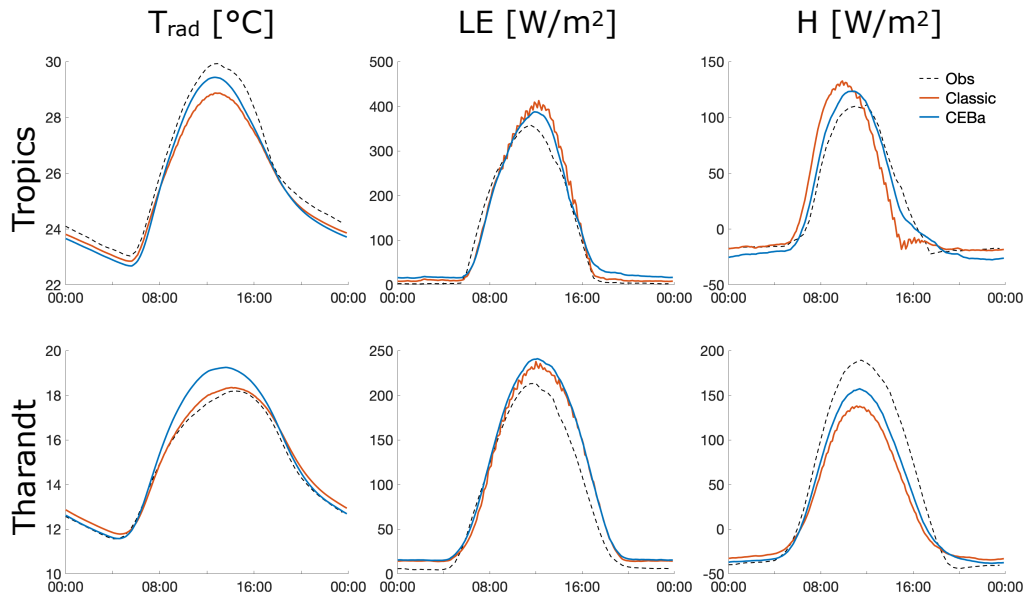
Fig. 4.5.: Performance of the classic JSBACH scheme and JSBACH CEBa. Displayed are comparisons of the summer season (Apr–Sep) mean diurnal cycles of the components of the canopy energy balance between JSBACH Classic (red) and JSBACH CEBa (blue) against observations (black dashed lines). Plotted are the radiative temperature T_{rad} (left column), total latent heat flux LE (middle column) and total sensible heat flux H (right column). Data are from two FLUXNET tower sites: tropical forest in Brazil (Sept 2001 to Oct 2003, top row) and needleleaf forest in Tharandt, Germany (2006-2014, bottom row).

(left column), total latent heat flux LE (middle column) and total sensible heat flux H (right column). The upper row of Fig. 4.5 shows the comparison of fluxes for the tropical forest in Brazil for around two years from September 2001 to October 2003; the bottom row depicts the results for the needleleaf forest in Tharandt, Germany, for the years 2006 to 2014. Since the observed energy balance in Tharandt exhibits a large non-closure of almost $100 \, \text{W/m}^2$, the excess energy is assigned to the latent heat flux during the day and to the sensible heat flux during the night, similar to the so-called "energy residual" closure correction technique (Ershadi et al., 2014). Overall, the simulated fluxes of Classic, as well as of CEBa, fit the observations quite well. At the tropical site, Classic underestimates the daytime maximum in radiative temperature, while CEBa overestimates it for Tharandt. In general, the Classic scheme shows numerical induced fluc-

tuations in the heat fluxes even in the average over multiple years, while CEBa exhibits smooth curves such as seen in the observations. For the tropics, the Classic scheme shows in this regard an unusual phase shift in the sensible heat flux compared to the observations and the CEBa scheme. Since the radiative temperature is not phase-shifted, it could be caused by the abovementioned numerical instabilities rather than by incorrectly simulated heat storages. For Tharandt, both schemes show a significant difference in the Bowen ratio: the latent heat flux is overestimated, and the sensible heat flux underestimated. The cause of this bias could not be explained in this study and should be further investigated in the future.

In addition to the offline single-site experiments, we evaluate the performance of CEBa with respect to the simulated 2m-temperature in a global coupled experiment over 30 years (from 1979-2008) with the AMIP framework as used in chapter 3. We find a similar pattern in the difference of the simulated near-surface temperature between CEBa and Classic as in the difference between SkIn$^+$ and Classic (3.5a). Only a yet unexplained slight temperature increase in the high latitudes (mainly over Siberia) remains. That also leads to a significant bias reduction in the near-surface temperatures simulated by the CEBa scheme. However, despite the potentially more realistic representation of the processes in the canopy layer, the CEBa scheme does not achieve the same model bias reduction (7.4%) as the SkIn$^+$ scheme (8.8%).

4.3.1. Conclusion

We find that the new CEBa scheme correctly reproduces the diurnal cycle of T_{sfc}, H and LE at the site-level for a temperate as well as for a tropical forest. Only for the daytime maximum in radiative temperature in Tharandt, CEBa shows a larger temperature bias than JSBACH Classic, but it removes the unrealistic drop in sensible heat storage during the afternoon at the tropical forest site.

Regarding the performance of the CEBa scheme on regional and global scales, we conclude that CEBa leads to a significant bias reduction in simulated near-surface temperatures (7.4%) compared to JSBACH Classic, but has a slightly weaker performance than SkIn$^+$. To improve the results of the CEBa scheme, an extensive tuning and technical effort would be necessary, which is beyond the scope of this study. However, in general, the CEBa scheme provides, due to the more realistic treatment of energy exchange and its larger number of degrees of freedom, the possibility of a deeper understanding of the complex processes in the canopy layer.

4.4. Results

To get a better understanding of the influence of atmospheric conditions and leaf properties on the leaf thermoregulation (LT), we calculate the zero-dimensional steady-state solution of the CEBa energy balance equations for different air temperatures. Then we investigate whether we can find the negative correlation between leaf temperature excess and air temperature related to leaf thermoregulation, which can be found in measurements at the leaf scale, also at the canopy and global scale. Therefore, we depict and interpret the results of single-site offline experiments as well as of a global run.

4.4.1. Steady state experiment

To understand the underlying physical mechanisms responsible for the leaf thermoregulation curve, we numerically solve the system of the four energy balance equations of the new JSBACH CEBa scheme. Hereby, we calculate the stationary solution (without heat or water storages) as a function of the air temperature to determine the equivalence point and the slope of the linear regression line describing the negative correlation of leaf thermoregulation. This steady-state experiment can be interpreted as a zero-
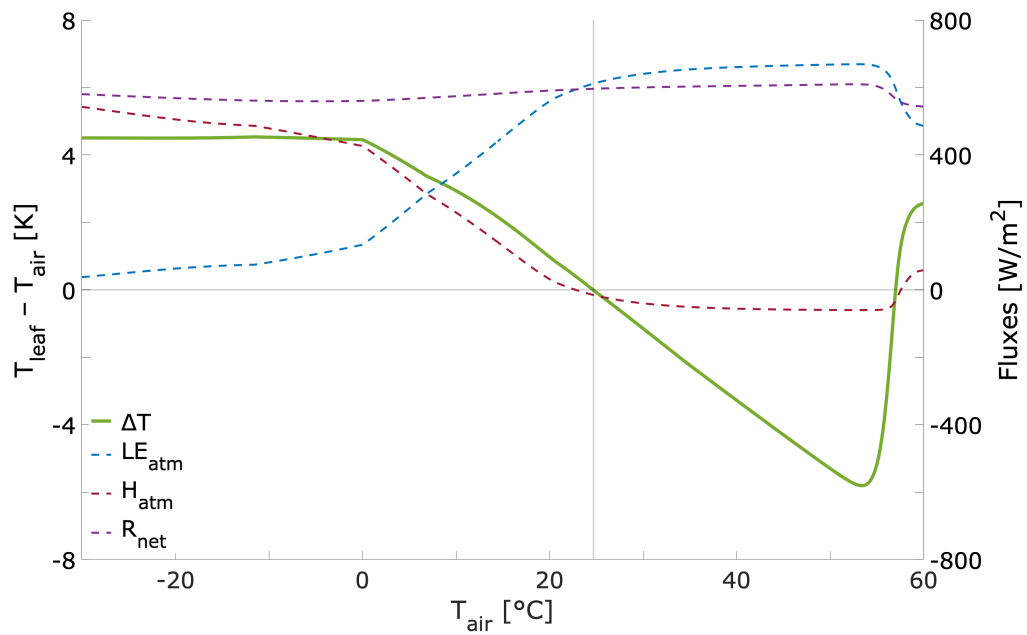
Fig. 4.6.: Example case for the steady-state solution of the CEBa energy balance equation depending on the air temperature at the reference level: Plotted are the leaf temperature excess, i.e., $T_{\text{leaf}} - T_{\text{air}}$ (green, solid line, left y-axis) and different types of fluxes (dashed lines, right y-axis): the total latent heat flux (blue), the total sensible heat flux (red) and the net radiation (violet)

dimensional experiment since the solution neither depends on space nor on time.

Figure 4.6 shows an example of how the steady-state solution of the CEBa energy balance equation depends on the air temperature at the reference level for a specific set of prescribed parameters. Plotted are the caclculated leaf temperature excess (green, solid line, left y-axis) and different fluxes (dashed lines, right y-axis): the total latent heat flux (blue), the total sensible heat flux (red) and the net radiation (violet). Since we assume a stationary case, there are neither heat or water mass storages. Also, no ground heat flux was allowed. In this case, the heat fluxes between the CAS and the LAL are the sums of the ground and canopy heat fluxes. Thus,

the third and fourth equation of (2.3.8) simplify to

$$H_{\mathrm{atm}} = H_{\mathrm{c}} + H_{\mathrm{g}}$$
$$LE_{\mathrm{atm}} = LE_{\mathrm{c}} + LE_{\mathrm{g}} \tag{4.4.1}$$

To obtain the total net radiation the partial radiative fluxes have to be weighted by the sky view factor χ:

$$R_{\mathrm{net}} = (1 - \chi)R_{\mathrm{c}} + \chi R_{\mathrm{g}} \tag{4.4.2}$$

For the sake of clarity, only the total heat and radiative fluxes (H_{atm}, LE_{atm} and R_{net}) and not the partial fluxes are shown in figure 4.6. In the following, the leaf temperature excess is defined as the temperature difference between T_{leaf} and T_{air}, although they are only indirectly coupled in the system of energy balance equations. It is debatable whether the measured air temperature data collected by Michaletz et al. (2016b) resemble more the temperature next to (or even under) the vegetation within the CAS T_{cas} or the air temperature above the canopy T_{air}. In this study we focus (in terms of figures) on the difference between T_{leaf} and T_{air} but also discuss the difference between T_{leaf} and T_{cas}.

For all steady-states experiments, we used the surface conditions of a forest with tall vegetation (i.e., $z_{\mathrm{veg}} = 30$ m, $z_0 = 4.8$ m, $LAI = 4.5$ m^2/m^2. Besides, we assume unlimited soil water availability when we specify the canopy resistance influencing transpiration, as well as for bare soil evaporation ($RH_{\mathrm{up}} = 1$). For the example case in Fig. 4.6, we chose typical atmospheric conditions: $S_{\mathrm{in}} = 800$ W/m^2, $RH = 50\%$ and $v = 3$ m/s. For these conditions, the leaf thermoregulation curve exhibits the expected negative correlation between leaf temperature excess and air temperature. For air temperatures under the freezing point – where no transpiration occurs – the leaf has a higher temperature than the air with a constant temperature difference of about $\Delta T \approx 4$ K. Hereafter, ΔT decreases almost linearly with increasing air temperature to about -6 K, before increasing rapidly at an air temperature of 55 °C. This limitation is caused by a high-temperature
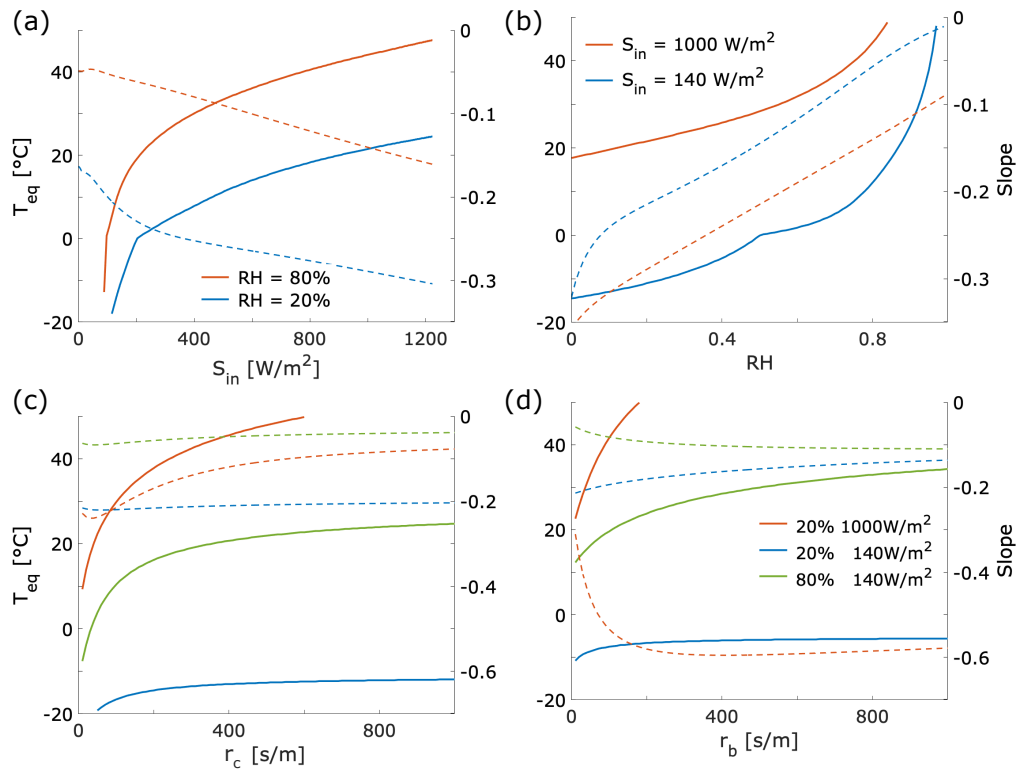
Fig. 4.7.: Variations of the leaf thermoregulation characteristics in terms of equivalence point (T_{eq}, solid lines, each left y-axis) and the slope (dashed-lines, each right y-axis) as a function of incoming solar radiation S_{in} (a), relative humidity RH (b), canopy resistance r_c (c), and aerodynamic resistance r_b (d).

inhibition (implemented in the calculation of the stomatal control) that prevents transpiration under high-temperature extremes. With increasing air temperature, the saturated specific humidity of the leaf surface increases exponentially (as explained in Sect. 4.1). Thus, the latent heat flux increases with increasing temperatures, whereas the sensible heat flux decreases. At a certain point, the latent heat flux exceeds the net radiation leading to a negative sensible heat flux (oasis effect). In this case the canopy air space releases energy towards the leaf. In the example of Fig. 4.6, this equivalence is reached at 24.7 °C. In the following, we investigate the regression line describing the leaf thermoregulation signal in terms of slope and equivalence point for different environmental parameters.

Figure 4.7 depicts the dependence of the equivalence point T_{eq} (which is the

root (zero point) of the leaf thermoregulation curve) and the slope of the leaf thermoregulation curve on different atmospheric conditions (i.e., relative humidity RH and incoming solar radiation S_{in}) and on internal canopy parameters (i.e., canopy resistance r_c and leaf aerodynamic resistance r_b), which are here prescribed as external variables. Here the solid lines represent the variations of the equivalence point T_{eq} (left y-axis), whereas the variations in the slope are depicted as dashed lines (right y-axis). As expected from the linearized solution of the leaf energy balance (Eq. 4.1.4), T_{eq} shifts towards higher temperatures for increased solar incoming radiation or relative humidity (Fig. 4.7a and b). However, the variations in the equivalence point show different behavior. They decrease depending on an increase in solar radiation or specific humidity: T_{eq} exhibits a logarithmic function for an increasing radiation flux (i.e., first a fast increase and then slow increase) and an exponential function for increasing relative humidity (i.e., first a slow increase and then a fast increase). This means, especially variations in weak solar incoming radiation (lower than 400 W/m^2) as well as in high relative humidity (higher than 80%) are crucial situations for the change of T_{eq}. The slope (dashed lines) of the negative correlation of LT displays a rather linear function. Surprisingly, it shows different behavior in regard to increasing atmospheric conditions: The absolute value of the negative slope increases with higher solar radiation, while it decreases with higher relative humidities.

In contrast to the strong influence of atmospheric conditions on T_{eq} and the slope, the canopy parameters, i.e., canopy resistance and aerodynamic leaf resistance, exhibit a relatively weak influence on the LT curve. T_{eq} increases logarithmically with increasing resistances for both r_s and r_b (Fig. 4.7c and d). So especially for cases with low resistances, the change in T_{eq} can be significant for small variations in the resistances. However, the slope of the thermoregulation curve at the equivalence point is almost independent of the canopy resistance. As an exception, under certain atmospheric conditions (high incoming solar radiation), variations in r_b can significantly impact the slope of the LT curve (Fig. 4.7d, red dashed line).

In summary, we found that the characteristics of leaf thermoregulation in terms of slope and equivalence point are strongly influenced by the atmospheric conditions, which means that the process cannot be attributed exclusively to the control and regulation of the plant itself. The solar radiation and the relative humidity are the most important determinants for leaf thermoregulation.

4.4.2. FLUXNET Sites

We want to determine whether, as in the simplified experiments, we are able to identify a negative correlation between leaf temperature excess and air temperature in realistic offline experiments over several years. Therefore, we analyze the results of model runs at two FLUXNET sites located in different vegetation zones. The first measurement tower is located in the needleleaf temperate forest Tharandt (Germany), providing data covering a wide range in temperature and humidity. The second site is located in the tropical evergreen forest of Brazil, which is characterized by a large number of warm days where high air temperatures prevail.

Since photosynthesis occurs only under the presence of sunlight, we analyze only daytime values (defined by inclination angles greater than 10°) of simulated leaf and air temperatures in the following experiments. Figure 4.8 shows the two-dimensional probability function of the leaf temperature excess (ΔT) and air temperature during the vegetation period (April to September) as the result of an offline experiment for the FLUXNET site located in the temperate needleleaf Tharandt forest in Germany. This plot has the advantage over a mere scatter-diagram to highlight the frequency of overlapping data of the air temperature and the leaf temperature excess distribution. The brightness of the color indicates how many percents of the data amount within an "area" of $1\,\mathrm{K} \times 1\,\mathrm{K} = 1\,\mathrm{K}^2$.
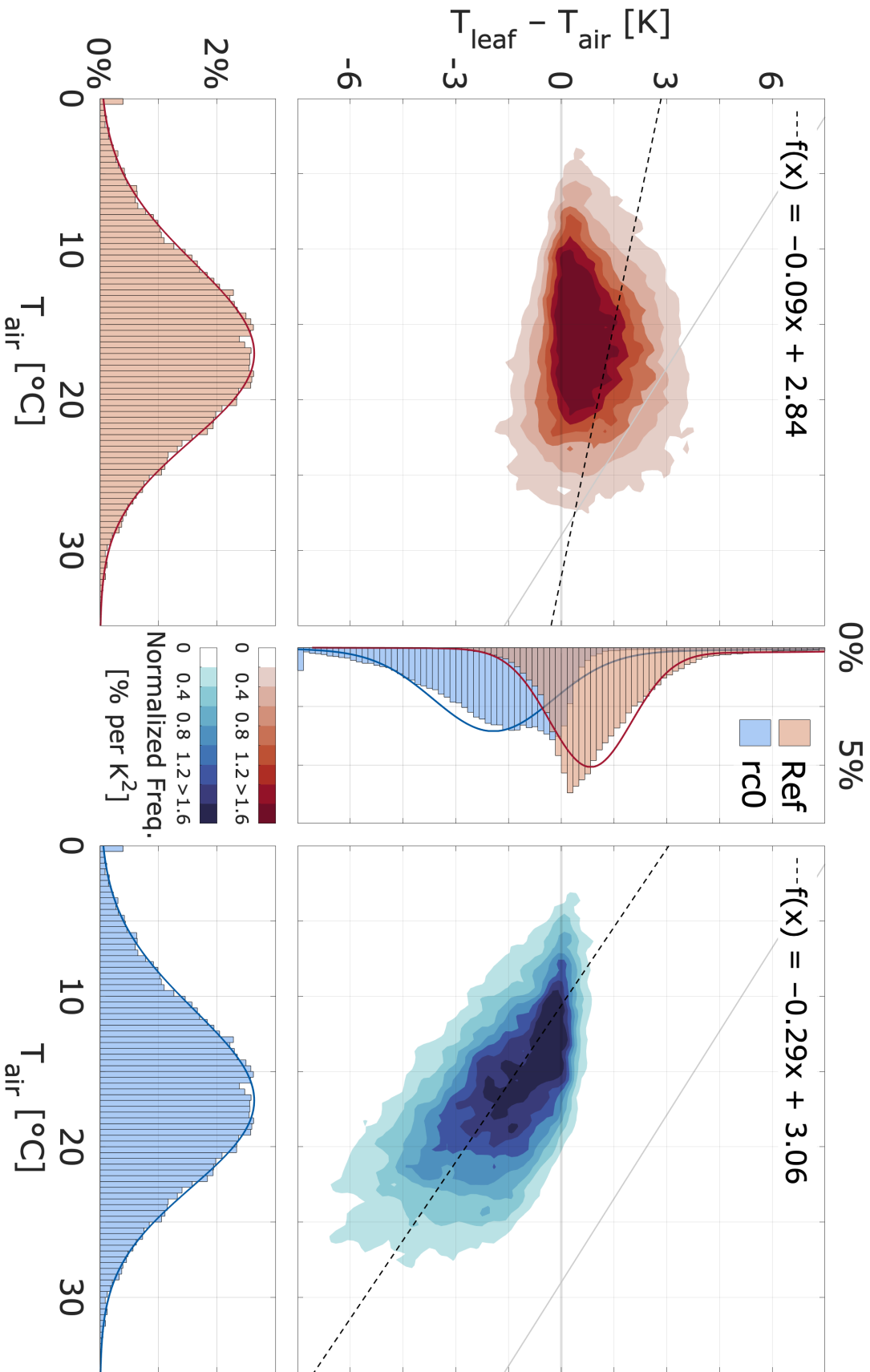
Fig. 4.8.: Two-dimensional probability function of daytime leaf temperature excess and air temperature. Data are from the vegetation period (April to September, 2006-2014) of the offline experiment for the FLUXNET site located in the temperate needleleaf Tharandt forest in Germany: Reference experiment (a) (Ref, red) and water-unlimited case (b) ($r_c = 0$, blue). Plotted are instantaneous values of the model output with 7.5 min time step. The dashed black line is the linear regression through all data of the model output; the gray solid line depicts the regression line derived in the study of Michaletz et al. (2016a)

Figure 4.8a illustrates the results of the real reference experiment, i.e., without any restrictions or modifications (of the leaf properties). The distribution of the air temperature is Gaussian, while the distribution of the leaf temperature excess shows a sharp drop in frequency for negative temperature differences. The two-dimensional probability function indicates a larger spread towards positive temperature differences ($3.7\,$K for frequencies larger than $0.2\%/$K^2) than towards negative temperature differences ($-1.6\,$K for frequencies larger than $0.2\%/$K^2). Nevertheless, the regression line between leaf temperature excess and air temperature, including all data, exhibits a negative correlation. The intersection of the regression line with the air temperature axis occurs at $31.7\,$°C and nearly agrees with the one found in the literature at around $30.1\,$°C. However, the slope of the regression line (-0.1) is significantly smaller compared to the slope of -0.27 found in Michaletz et al. (2016a).

To identify a possible cause for the underestimation of the LT signal at the canopy level, for the unlimited water case (Fig. 4.8b, blue), we set the canopy resistance to zero, and the moisture in the soil is kept saturated at soil field capacity. This modification implies that transpiration is considered as potential evaporation only limited by the turbulence conditions describing atmospheric conditions and by the leaf aerodynamic resistance. With this modification, the distribution of ΔT shifts significantly towards negative temperature differences. The largest significant ($> 0.2\%/$K^2) negative differences amount to $-6\,$K. The distribution of ΔT shows a strongly asymmetric behavior with an abrupt decline in frequencies for positive differences (only $0.7\,$K for frequencies larger than $0.2\%/$K^2). Due to the enhanced latent heat flux, which is not limited by water availability, in the form of transpiration in this sensitivity experiment, the available energy is mostly used for phase changes rather than to increase the leaf temperature. Therefore, the near-surface climate experiences a strong cooling leading to an equivalence point of $10.6\,$°C, which underestimates T_{eq} by almost $20\,$K compared to the literature. However, the slope of the $r_{\mathrm{c}} = 0$ experiment agrees with the one found in the observations and is even slightly higher
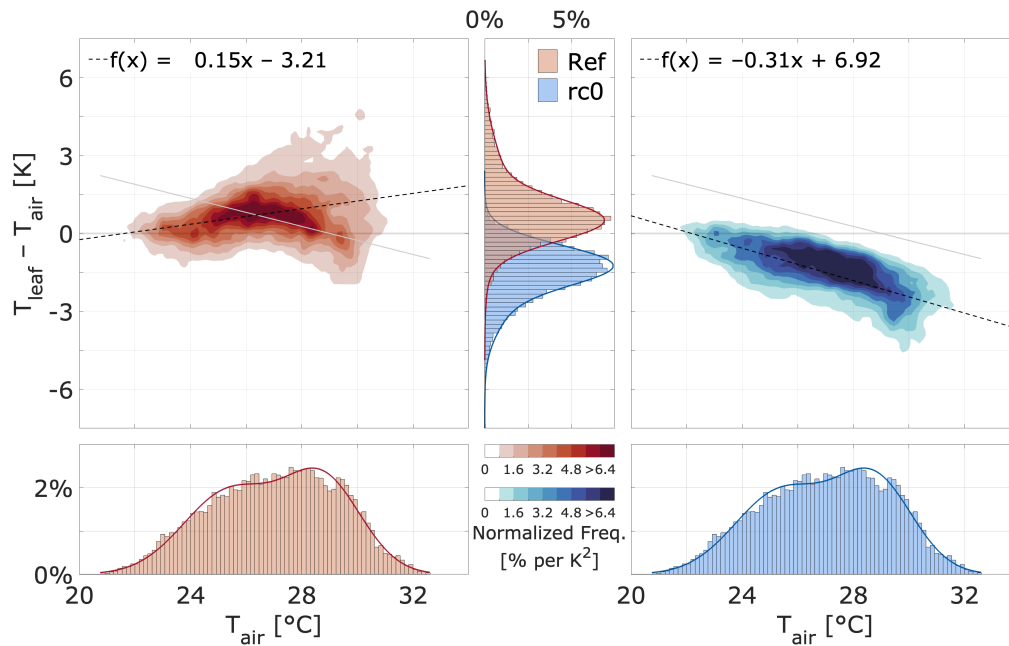
Fig. 4.9.: Two-dimensional probability function of daytime leaf temperature excess and air temperature. Data are from the offline experiment (September 2001 to October 2003) for the FLUXNET site located in a tropical evergreen forest in Brazil: Reference experiment (a) (Ref, red) and water-unlimited case (b) ($r_c = 0$, blue). Plotted are instantaneous values of the model output with 7.5 min time step. The dashed black line is the linear regression through all data of the model output; the gray solid line depicts the regression line of the findings of Michaletz et al. (2016a)

with −0.29.

The results of the second offline experiment using data from the FLUX-NET tower of a tropical evergreen forest in Brazil are depicted in Fig. 4.9. The reference experiment (Fig. 4.9a, left panel) shows a slight positive correlation disagreeing with the LT theory. Michaletz et al. (2016a) asked the question whether the common LT signal can be also found in the tropics. A possible explanation for the positive correlation found for the tropics is the high solar insolation combined with a large relative humidity. Only under idealized conditions, i.e., vanishing canopy resistance and unlimited soil moisture, a negative correlation can be found in the tropics. In this sensitivity experiment, the equivalence point (21.6 °C) and the slope (−0.31) are close to those values reported in the literature (compare Tab. 4.1).

Table 4.1.: Comparison of equivalence temperature and slope of the leaf thermoregulation curve simulated using offline experiments for the Tharandt site. The properties are distinguished between T_{air} and T_{cas} for two experiments: reference (Ref) and no water-limitation ($r_{\text{c}} = 0$)

Mode	T_{eq}		slope	
	T_{air}	T_{cas}	T_{air}	T_{cas}
Ref	31.7	32.3	−0.09	−0.06
$r_{\text{c}} = 0$	10.6	14.2	−0.29	−0.13
Literature	30.1		−0.27	

4.4.3. Global AMIP experiments

To investigate the process of leaf thermoregulation on the global scale for a decadal time period, we performed two 30-year AMIP experiments. The default output time intervals of this multi-year run correspond to monthly means. First, we consider hourly means for only one vegetation period of the AMIP run (April to September of the year 1976). This enables the possibility to compare the results of the AMIP run with those measured at the FLUXNET sites (Sect. 4.4.2). Due to a large number of grid cells (i.e., around 2000 CEBa points), this experiment delivers about 8.4 million hourly means of leaf temperature excess over a wide air temperature range from −15 to 35 °C over all latitudes (Fig. 4.10). The air temperature distribution shows a bimodal pattern. The right-hand peak around 25 °C is caused by the rather constant climate within the tropics. The reference AMIP experiment (without adjusted canopy resistance) exhibits a slight positive correlation of 0.02 and contradicts the prediction of leaf thermoregulation (Fig. 4.10a). The highest positive ΔT with about 3.75 K (for significant frequencies greater than 0.2%/K^2) can be found for the highest air temperatures (greater than 25 °C). In contrast, the negative leaf temperature excess for almost the entire air temperature range is limited to −0.75 K.

One explanation for the positive correlation is again the high insolation

combined with high relative humidity in the tropics. Another possible explanation for the absence of larger negative leaf temperature excesses under high air temperatures is the discrepancy between positive and negative temperature differences: In most cases, negative differences occur more often but have a much smaller absolute value than positive differences. Negative leaf temperature excesses occur during the morning with low net radiation values, and especially during the afternoon when weak insolation fluxes and relatively high air temperatures prevail. In contrast, positive leaf temperature excesses occur mainly during midday caused by the large net radiation fluxes during that time. When calculating the mean value (here a 1-hour average over eight instantaneous model output values), the larger absolute values of the positive differences dominate.

In contrast to the reference experiment, the idealized experiment (where
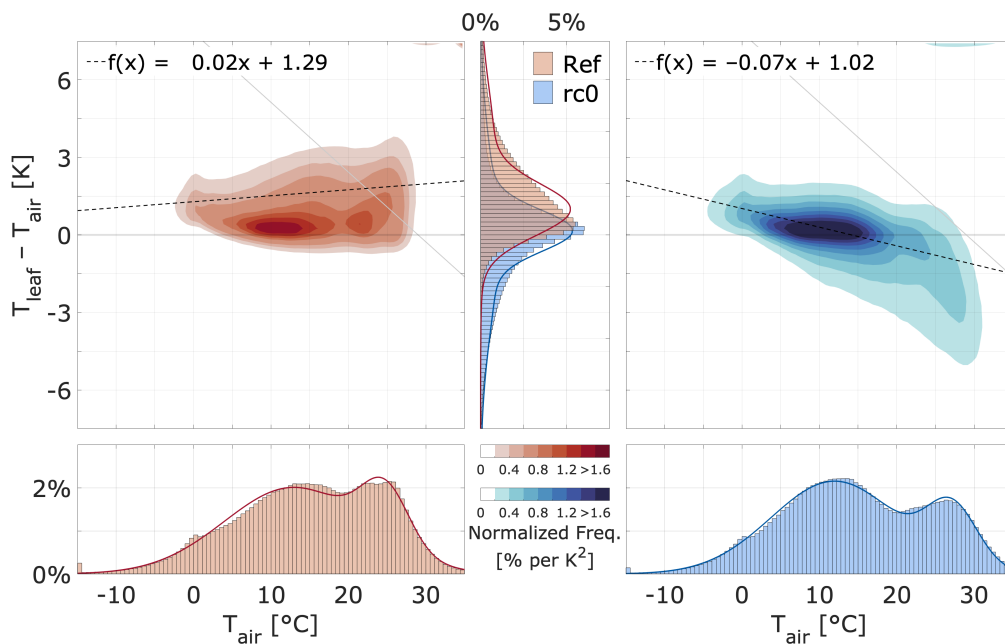
Fig. 4.10.: Two-dimensional probability function of daytime leaf temperature excess and air temperature. Data are from a short-term (hourly means during one vegetation period, April to September 1976) global AMIP experiment. Reference experiment (a) (Ref, red) and water-unlimited case (b) ($r_c = 0$, blue). The dashed black line is the linear regression through all data of the model output; the solid gray line depicts the regression line of the findings of Michaletz et al. (2016a)

the canopy resistance is artificially set to hero $r_c = 0$ and unlimited soil water availability is assumed) shows – similar to the site experiments – a negative correlation between the leaf temperature excess and the air temperature (Fig. 4.10b). This means that even in a coupled experiment, the atmospheric conditions allow the leaf to regulate its temperature (according to LT theory) as long as sufficient water is available. The largest negative temperature difference (of significant frequency) occurs for the highest air temperatures and amounts to -4.5 K. However, the slope of the regression line is with -0.07 significantly smaller compared to the results derived in the offline site experiments. One reason for this feature could be the negative feedback of the land–atmosphere coupling in an interactive experiment (as opposed to an offline run where the air temperature and specific humidity at the LAL are provided as a prescribed forcing). This different response of the atmosphere can be seen in the changed distribution of air temperature when comparing the reference experiment (Fig. 4.10a) and the idealized experiment (Fig. 4.10b). The latter exhibits a higher peak at lower air temperatures (around 10 to 15 °C) and a reduction in frequencies for the second peak (around 25 °C).

To establish whether we are able to find the effect of leaf thermoregulation in long-term simulations on a global scale, we also performed an AMIP experiment over 30 years (1979-2008). Figure 4.11 depicts the results from this run by showing a scatter plot of leaf temperature excess as a function of air temperature as the 30-year daytime (inclination angle greater than 10°) means of all 2000 CEBa grid points for the reference (red) and idealized (blue) experiment. In both experiments, we find the same pattern as for the short-term global experiment. The positive slope of the regression line in the reference experiment, however, is with 0.06 around three times steeper, whereas the negative slope of the regression line of the idealized experiment decreases to -0.03. For the reference experiment, only positive temperature differences can be found as a long-term mean: the smallest differences amount to 0.5 K. In contrast to the short-term AMIP experiment, the 30-year means in leaf temperature excess of the idealized experiment (blue)
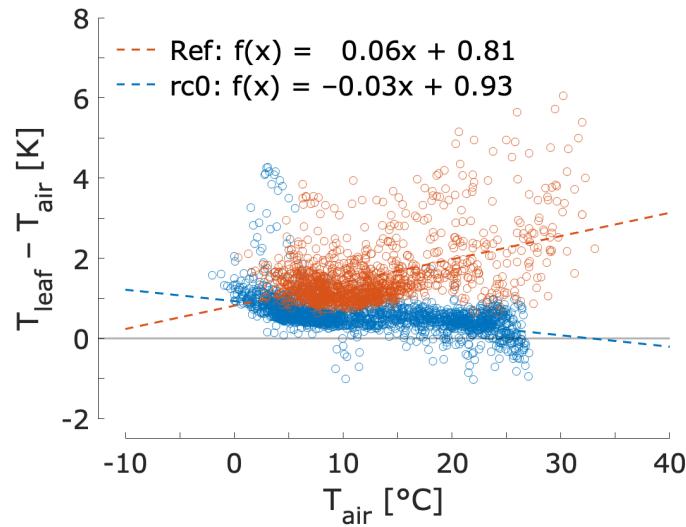
Fig. 4.11.: Scatter plot between the daytime leaf temperature excess and air temperature based on 30-year means. Data are derived from a long-term global AMIP experiment over 30 years (1979-2008): Reference experiment (Ref, red) and water-unlimited case (r_c = 0, blue). The dashed lines are the regression lines.

mostly represent positive values; only a small amount of data shows excesses that reach –1.0 K. This pattern agrees with our explanation of the findings related to the short-term experiment: The positive temperature differences are larger than the absolute values of the negative temperature differences and weighted disproportionately by averaging over decadal time periods.

Since the productivity of plants in the form of photosynthesis is temperature-dependent, we finally investigate the influence of the leaf temperature excess found in the global experiments on the simulated gross primary production. Therefore, we use the data both from the short-term and the long-term runs. Since we find the leaf thermoregulation signal only for the idealized experiment and not in the reference run, we also performed an idealized AMIP experiment with the JSBACH Classic scheme for the unlimited water case. The Classic scheme calculates the stomatal control and GPP based on the air temperature, whereas CEBa uses – as it is correctly done – the leaf temperature. Figure 4.12 depicts the correlation between the gross primary production (GPP in μmol CO_2/(m^{2}s)) of the CEBa and Classic scheme for the idealized experiment (water-unlimited case, r_c = 0).

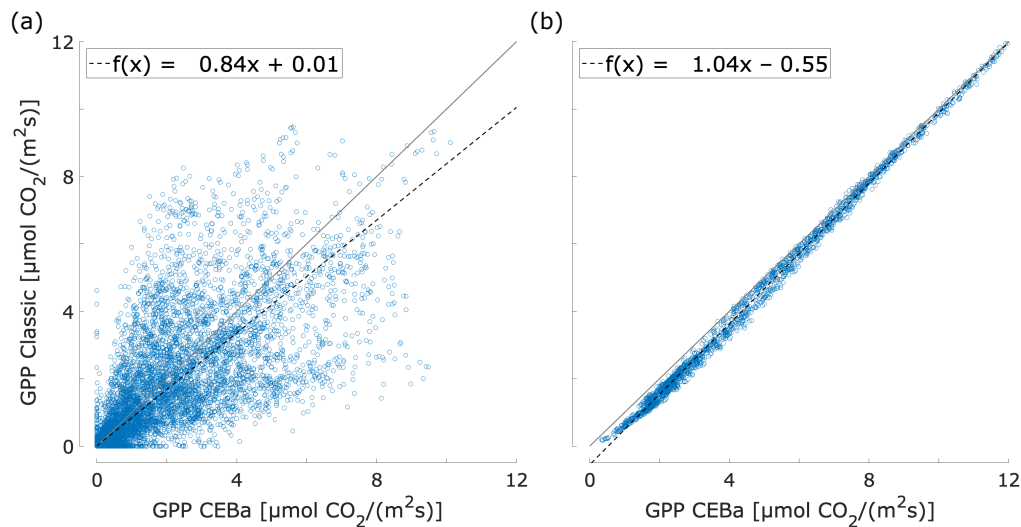**Fig. 4.12.: Correlation between the gross primary production (GPP) of CEBa and Classic** in μmol $CO_2/(m^2s)$ for the idealized experiment (water-unlimited case, $r_c = 0$): Plotted is the simulated model output for CEBa grid cells of the (a) short-term (hourly means of one vegetation period, April to September 1976) and (b) long-term (30-year means from 1979 to 2008) AMIP experiment.

The simulated model output for CEBa grid cells of the short-term experiment (Fig. 4.12a) shows a high degree of scattering. The slope of the linear regression amounts to 0.84, which means that in general, CEBa tends to simulate larger values for the GPP. That would support the hypothesis of the theory of leaf thermoregulation, which is the maximization of carbon gain. However, this signal can not be confirmed by the long-term averages of GPP (Fig. 4.12b). Here the slope of the regression line (1.04) is almost 1. Especially for larger GPP, both schemes simulate the same values in GPP. Only for small values of GPP, the CEBa scheme seems to be slightly more productive.

4.5. Discussion

In this chapter, we made a first approach to investigate the effect of leaf thermoregulation with an ESM in the canopy layer at larger spacial scale. We demonstrate that we can identify a negative correlation between leaf

temperature excess and air temperature on the site-level for a temperate forest. However, the extent in the form of the slope of this correlation is underestimated when comparing to the slope found in observations at the leaf scale. For the tropics as well as on a global scale, we find a positive correlation in the temperature difference, which contradicts the theory of leaf thermoregulation. However, under idealized conditions, i.e., unlimited water availability in the form of no canopy resistance, we discover a negative correlation together with a steep slope.

This raises the question of whether the current parameterization of the stomatal control overestimates canopy resistance, possibly, due to missing processes. The temperature dependence for the stomatal conductance as well as for the photosynthesis is assumed to follow an Arrhenius-type temperature dependence. This means in the context of JSBACH: the higher the temperature, the higher the stomatal conductance or the GPP (up to a certain temperature where a high-temperature inhibition sets it to zero). What is missing so far is a parameterization of a process that artificially regulates the stomata to the plant's temperature optimum.

Another limitation of this study is that only one single temperature curve determines the stomatal conductance and the GPP for all PFTs. The temperature optimum of plants is very different depending on the climate zone and should at least be differentiated for different plant functional types (PFT). Moreover, these temperature optima can adapt to different climatological conditions, which is a crucial aspect in a future warmer climate. In this context, the CEBa scheme is improvable, too, since, at the moment, the aerodynamic leaf resistance is not formulated for different PFTs and only described by one average leaf width.

We have shown that the effect of leaf thermoregulation (i.e., the amplitude of the leaf temperature excess) depends to a large extent on the relative humidity of the ambient air and the increasing solar insolation. Regarding the latter, it is crucial to estimate the distribution of radiation within the canopy layer correctly, i.e., how much radiation is absorbed or reflected

from the leaf and how much is transmitted to the ground surface. In this context, some studies have shown that leaves have the ability to reduce or enhance the absorption of solar radiation, e.g., by increasing the leaf or needle density, by rotating the leaf angle, or by reflective leaf hairs (Helliker and Richter, 2008).

It is debatable whether the current model version of JSBACH CEBa on a coarse grid (i.e.,1.9°) is sufficient to investigate the effect of leaf thermoregulation in full measure. We found that, especially during midday, the leaf temperature is almost always higher than the air temperature since it is completely illuminated. If, in this case of high insolation conditions, the leaf temperature would be lower than the air temperature, this would represent a stable condition, which is not realistic in convective conditions during the day. To avoid that, only a large heat flux from the ground surface could compensate that imbalance. Thus, it is debatable if leaf thermoregulation is even possible for extremely dense or closed canopy layers (e.g., in the tropics). In that regard, the absence of a flux aggregation method to solve the energy balance equation (Best et al., 2004; de Vrese and Hagemann, 2016) could represent a significant shortcoming.

In general, it is debatable whether a dual-source big leaf model as CEBa is, in principle, capable of correctly estimating the plant properties and leaf temperatures within the canopy layer. In this context, a multilayer model is probably more sufficient as it can use parameters measured at the leaf scale and at different heights to calculate the vertical distribution of leaf temperatures (Dai et al., 2004). Especially, the upscaling from the leaf to the canopy scale is a difficult task. Luo et al. (2018) suggest to avoid the big-leaf approach and advocates the use of a two-leaf scheme, which determines firstly the transpiration of sunlit and shaded leaves separately, and secondly, upscales the results from the leaf to the canopy scale.

4.6. Conclusion

In most present-day climate models, the air temperature (of the lowest atmospheric level) is used to calculate the stomatal control and plant productivity. However, in nature, it is the leaf temperature that controls photosynthesis. As found in long-term and short-term measurements, the leaf temperature can deviate significantly from its ambient temperature (e.g., Linacre, 1967; Helliker and Richter, 2008; Michaletz et al., 2016b). Moreover, the leaf temperature excess, which means the difference between leaf temperature and air temperature, follows a certain pattern. It shows a significant negative correlation with increasing air temperature: i.e., the leaf has the ability to be warmer than the air in cold environments, while it tends to stay colder than the air in warm environments. This implies that at a certain air temperature (the so-called equivalence point), the plant's transpiration equals the net radiation. Above this temperature, transpiration exceeds the net radiation, and a negative sensible heat flux occurs, causing a change in sign of the leaf excess. In this regard, we address the question of whether we can identify a negative correlation of leaf temperature excess and air temperature at the canopy scale in an Earth system model similar to the findings of Michaletz et al. (2016b), who reported and explained measurements at the leaf scale. Moreover, the goal of our research is to explore how atmospheric conditions and leaf properties influence the leaf's ability to regulate its temperature? Therefore, we extended the SkIn$^+$ scheme described in 3 to a dual-source canopy energy balance scheme (CEBa), which means that there are now separated sources (or sinks) for heat and water from canopy and soil. This allows distinguishing between the temperature of the ground, of the air within the canopy layer, and of the leaf itself. With the latter, it is now possible to simulate the process of leaf thermoregulation in JSBACH. With this newly developed land surface scheme, we first performed zero-dimensional (steady-state) as well as offline FLUXNET site experiments for a temperate evergreen forest in Germany and a tropical evergreen forest in Brazil forced with observations of temperature, wind, humidity, and radiation. Analyzing the process of

leaf thermoregulation we find:

- The effect of leaf thermoregulation in the form of slope and equivalence point is strongly influenced by the atmospheric conditions, which means that the process cannot be attributed exclusively to the control and regulation of the plant itself.

- The net radiation and the relative humidity of the ambient air are the most important determinants that regulate the amplitude of leaf thermoregulation. However, they influence the leaf temperature excess in different ways: While the equivalence temperature increases with larger values of insolation and relative humidity, the slope of the regression line decreases for larger insolation, but increases for higher relative humidities.

- The specific leaf properties, in terms of aerodynamic leaf resistance and the canopy resistance, can influence the slope and equivalence temperature significantly, especially for variations among small resistances. The aerodynamic leaf resistance widens the leaf temperature excess distribution, resulting in both larger positive as well as negative temperature differences.

When comparing the results of CEBa at the FLUXNET sites, we found:

- There is a negative correlation between leaf temperature excess and air temperature at the canopy scale in an offline experiment for a temperate forest site. However, the slope is significantly smaller compared to those reported by Michaletz et al. (2016a).

- Only for an idealized experiment with unlimited water availability, we are able to find a similar slope, as found in the observations at the leaf scale, but with a significantly cooler equivalence point temperature.

- We do not find a negative correlation for the tropical site, which is caused by the high insolation combined with high relative humidities. These conditions prevent leaf thermoregulation.

At this point, we conclude that the leaf thermoregulation signal can be found in a climate model at the canopy scale at the site level; however, only in an extenuated form. A similar negative correlation can only be found under idealized conditions.

In addition, we address the question of whether the leaf thermoregulation signal can also be found globally on decadal time scales, and if so, whether it has an impact of the photosynthesis in the form of gross primary production (GPP). To answer these questions, again the same global coupled land–atmosphere experiment covering the years from 1979 to 2008 with prescribed sea surface temperature was performed. Besides an analysis of the long-term 30-year means, we interpret hourly means of a single vegetation period run (April to September 1976). Finally, we compare the results of two idealized experiments regarding GPP. The first is simulated with the Classic scheme, which uses the air temperature as a proxy for the leaf temperature required for the calculation of photosynthesis. The second experiment uses the CEBa scheme, which calculates the photosynthesis depending on the leaf temperature. In these experiments, we find:

- The short-term as well as the long-term experiment exhibit a positive correlation between the leaf temperature excess and the air temperature, which contradicts the theory of leaf thermoregulation

- Again, only under unlimited water conditions a negative correlation can be found in both experiments. However, its slope is significantly smaller compared to those found at the offline site experiments, which could be caused by the negative feedback of the atmosphere in an interactive simulation.

- Consistent with these weak negative correlations we find no significant impact on the GPP when calculated with the leaf temperature in the CEBa scheme instead of the air temperature in the Classic scheme

In summary, the leaf thermoregulation signal at the canopy scale is even smaller on the global spatial scale as well as decadal time scales and needs

further investigations before concluding that the effect is negligible in a climate model.

5. Concluding remarks

In this thesis, we investigate two different processes in the context of the land–atmosphere interactions within the canopy layer. First, we analyze the effect of different heat storages – namely the soil and the canopy – on the diurnal cycle of near-surface temperatures, energy and moisture fluxes at the site level. Moreover, we determine whether the respective effects play a role in the global climate on decadal time scales. Secondly, we investigate the relation between air and leaf temperatures. As measurements at the leaf scale have shown, this relation is actively affected by the plant in the form of leaf thermoregulation. However, the resulting negative correlation between leaf temperature excess and air temperature has not yet been studied at the canopy scale. Here we develop the so-called CEBa scheme, which distinguishes between the temperature of the leaf and the air and makes it possible to simulate the process of leaf thermoregulation in JSBACH. With a series of experiments, we then determine whether leaf thermoregulation leads to significant leaf temperature excesses and whether it has an impact on climate and plant productivity on a global scale.

5.1. Summary and Conclusions

To investigate the effect of different heat storages, we implemented two new approaches for closing the surface energy balance into the land surface model JSBACH. The standard version of this model uses a prognostic procedure to close the surface energy balance within the uppermost soil layer of finite thickness and heat capacity. In the first step, the role of the

heat capacity of the soil is evaluated by comparing simulations with the standard model to simulations in which the newly developed SkIn scheme was implemented. In the latter, the energy balance is closed diagnostically at an infinitesimally thin surface layer that is located at the surface of the vegetated land (Viterbo and Beljaars, 1995). This comparison allows us to answer the first research question:

Does the elimination of the soil heat capacity in the energy balance substantially affect the diurnal cycle of surface temperature and heat fluxes in the case of shallow vegetation at the site level?

Analyzing the surface energy balance in both schemes, we find that:

- The surface temperature simulated with the reference scheme is underestimated in the case of heating during the day and overestimated in the case of cooling at night.

- SkIn removes these phase errors in the time-dependent behavior of the heat fluxes and surface temperatures that were caused by the dampening effect of the soil heat storage.

- With the new scheme, nocturnal heat releases, which unrealistically destroy the stable boundary layer previously, disappear.

Here we conclude that the elimination of the soil heat storage significantly improves the representation of exchange processes in our evaluation experiment. Thereby, the SkIn scheme leads to the removal of almost all biases on diurnal time scales in regions with shallow vegetation.

The importance of the canopy heat storage in connection with the solution of the energy balance equation has been estimated in several experimental studies at the site-level. Although the canopy heat storage can amount up to 40% of the net radiation, its impact on the Earth system for decadal time scales has not been studied in detail before. Here we performed an AMIP-type global coupled land–atmosphere experiment with the MPI-ESM covering the years from 1979 to 2008. For this global run, the standard heat

storage concept is replaced by a physically motivated approach describing the heat storage of the canopy layer in the surface energy balance (SkIn$^+$). This experiment is designed to answer the question:

What is the climatological effect of the canopy heat storage on near-surface temperature on the global scale?

We find that:

- The heat storage of the canopy layer must be taken into account in regions with tall vegetation (especially in the tropics). Here the heat storage of the canopy layer is larger than that of the uppermost (6.5 cm deep) soil layer.

- The turbulent exchange during daytime counteracts the delayed response in near-surface temperature, whereas, under stable conditions at night, a significant phase-shift occurs.

- For most regions – especially those with no or shallow vegetation and a pronounced diurnal cycle – the night effect of SkIn$^+$ prevails, leading to a cooling in the near-surface temperature relative to the standard scheme.

In summary, the canopy heat storage has a significant effect on the global climate on decadal time scales, and its implementation into the MPI-ESM leads to a significant reduction of the model's biases in regions with shallow vegetation. Here we show that the heat storage of the moist biomass accounts for the most significant contribution to the total canopy heat storage with around 60%. However, the latent heat storage and the heat storage of the canopy air amount to about 40% of the total canopy heat storage and can, therefore, not be neglected.

Photosynthesis rates are mainly controlled by the availability of water and by temperature, more specifically the temperature of the leaf. Short- and long-term measurements have shown that the leaf temperature can deviate significantly from the ambient temperature. In particular, the leaf temper-

ature is often warmer than the air in cold environments, while it tends to stay colder than the surrounding air in warm environments. To investigate this so-called leaf thermoregulation and its consequences for the turbulent energy fluxes and for the carbon cycle, we expand the SkIn$^+$ scheme to a dual-source canopy energy balance scheme (CEBa). This scheme allows the differentiation between the temperature of the ground, the air within the canopy layer, and the leaf itself. With this coupling scheme, we performed zero-dimensional (steady-state) and offline (forced with observations) FLUXNET site experiments for a temperate evergreen forest in Germany and tropical evergreen forest in Brazil. With these experiments, we are able to answer the following scientific questions:

How do atmospheric conditions and leaf properties influence the leaf's ability to regulate its temperature? Specifically, does the negative correlation between the leaf temperature excess and air temperature observed at the leaf scale hold at the canopy and regional scale?

We find that:

- The characteristics of leaf thermoregulation in the form of slope and equivalence point are strongly influenced by the atmospheric conditions, which means that the process cannot be attributed exclusively to the control and regulation of the plant itself.

- We find a negative correlation between the leaf temperature excess and the air temperature at the canopy scale in an offline experiment for a temperate forest site. However, the slope is significantly smaller: Only one-third of the slope found by Michaletz et al. (2016a).

- Only in an idealized experiment, where we assumed that water availability is not limited, we are able to find a similar slope as found in the observations at the leaf scale, but with a significantly lower equivalence temperature.

In summary, we conclude that the leaf thermoregulation signal can be found

in a climate model at the canopy scale, however, only in less pronounced form. A similar negative correlation can only be found under idealized conditions with unlimited water availability.

Furthermore, we performed a 30-year (1979-2008) AMIP experiment with the CEBa and the Classic scheme coupled to the MPI-ESM addressing the question:

What is the impact of leaf thermoregulation on global climate and plant productivity?

We find that:

- The short-term as well as the long-term experiment, exhibit a positive correlation between the leaf temperature excess and the air temperature, which contradicts the theory of leaf thermoregulation.

- Only under unlimited water conditions, a negative correlation between the leaf temperature excess and the air temperature can be found in both experiments. However, the slope of the regression line is significantly smaller compared to those derived from the site experiments.

- Consistent with these weak negative correlations, we find no significant difference in GPP when calculated using the leaf temperature in the CEBa scheme instead of the air temperature in the Classic scheme.

In summary, the conducted 30-year global experiment suggests that leaf thermoregulation does not substantially affect the surface or near-surface temperatures on climatological time scales. Due to the insignificant effect on the leaf temperature, the GPP remains unchanged as well. Nonetheless, the process of leaf thermoregulation needs further investigations (see next section) before concluding that the effect is negligible in an ESM.

5.2. Outlook

In this thesis, we have demonstrated the importance of heat storages in the canopy layer. One could have debated that the consideration of the heat storage induces only phase errors in the diurnal cycle of surface fluxes and near-surface temperatures, thus producing biases that cancel each other when averaged over decades. However, this assumption appears to be invalid. Moreover, the calculation of the correct timing of heat fluxes is of vital importance for the adequate simulation of the diurnal evolution of the boundary layer. Thereby, our scheme may also improve the representation of atmospheric phenomena such as cloud formation and convection.

Therefore, we recommend using the SkIn$^+$ scheme not only for models that operate on short time scales but also for Earth system models focusing on decadal time scales. In this context, the developed scheme is complete and fully functional and is currently implemented in JSBACH4 (Nabel et al., 2019), the land component of ICON-ESM (e.g., Giorgetta et al., 2018), the successor of MPI-ESM. Embedded within the newer ICON model, our developed scheme may show additional benefits compared to the old scheme. We believe that the canopy heat storage concept would take full effect in ICON, which takes into account the subgrid-scale surface temperature variations in a grid cell.

Moreover, as a non-hydrostatical model, ICON allows very high spatial resolutions and an explicit representation of convective processes. In contrast to low-resolution, parameterized convection, we expect a stronger sensitivity to the diurnal exchange fluxes between the land and the boundary layer. The SkIn$^+$ scheme may, therefore, provide an added value compared to the old scheme through its substantial improvement of biases in heat fluxes in terms of phase and amplitude.

For exploring the role of the leaf temperature in the canopy, we made a first approach to investigate the effect of leaf thermoregulation using an Earth system model at the canopy scale. We show that we are indeed

able to detect a negative correlation between leaf temperature excess and air temperature, but its magnitude is underestimated when compared to observations found at the leaf scale. This finding raises the question of whether the current parameterization of the stomatal control is even capable of correctly reproducing the leaf's behavior in nature. A first approach in this regard could be the implementation of a process that artificially regulates the stomatal resistance such that the plant can stay close to its temperature optimum.

We have shown that the effect of leaf thermoregulation is highly dependent on the relative humidity of the ambient air and the increasing solar radiation. With regard to the latter, it is crucial to estimate the distribution of radiation within the canopy layer correctly. In this context, some studies have shown that leaves have the ability to reduce or increase the absorption of solar radiation, e.g., by increasing the leaf or needle density, by rotating the leaf angle, or by reflective leaf hairs (Helliker and Richter, 2008).

Another limitation of this study is that only one temperature curve determines stomatal conductance and the GPP for all PFTs. The optimum temperature of plants varies depending on the climate zone and should at least be differentiated for different plant functional types (PFT). In this context, the CEBa scheme is still improvable since, at the moment, the aerodynamic leaf resistance is currently not formulated for different PFTs and, for example, only described by one average leaf width. Furthermore, these temperature optima can adapt to different climatological conditions (Berry and Bjorkman, 1980), which is a crucial aspect in a future warmer climate. In this sense, it would be valuable to further study the phenomenon of leaf thermoregulation, because, in a warming climate, many plants may come close to their temperature limits. Thus, they would increasingly be dependent on the cooling effect due to the leaf's ability to regulate its temperature. Therefore, estimates of carbon uptake by the biosphere may crucially depend on the accurate representation of leaf thermoregulation.

A. Formal remark about the use of "we" in this thesis

Since most of the research has been conducted under the supervision of Prof. Dr. Felix Ament and Dr. Andreas Chlond, the author prefers to choose the first person plural.

Nonetheless, this PhD thesis can mainly be viewed as a solitary work as substantial parts of the research ideas, and experiment design were developed by the doctoral candidate. Furthermore, nearly all work in terms of model code development and experiment execution, as well as data analysis and manuscript writing, was conducted by the doctoral candidate.

B. Comparison of model biases

(a) ΔT(SkIn$^+$ — Observations) [K]

(b) ΔT(Classic — Observations) [K]
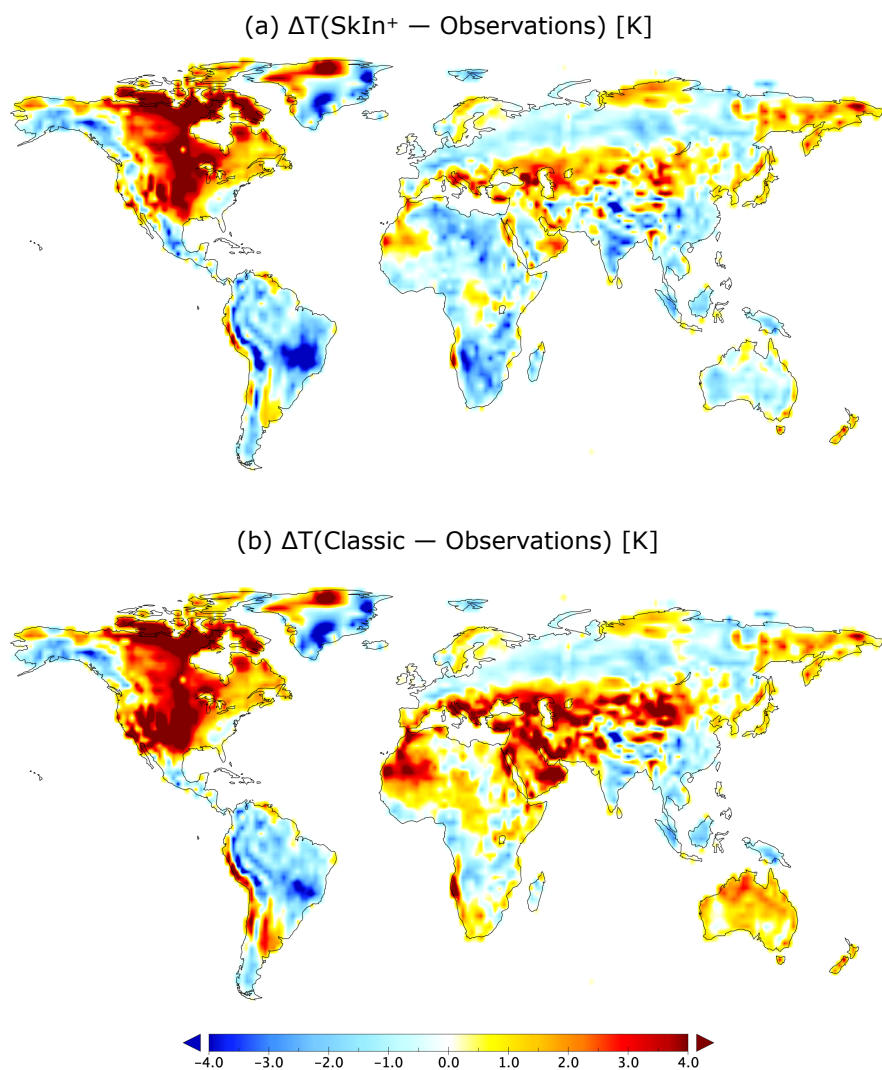
Fig. B.1.: Comparison of the model bias of SkIn$^+$ and JSBACH Classic on regional scales: Thirty-year (1979-2008) summer half-year (Apr-Sep) average of the difference of near-surface temperatures between SkIn$^+$ and observations (a) as well as between JSBACH Classic and observations (b).

List of Figures

Bibliography

Askenasy, E. (1875). Ueber die Temperatur, welche Pflanzen in Sonnenlicht annehmen. *Bot. Zeit*, 33(1875):441–444.

Aston, A. (1985). Heat storage in a young eucalypt forest. *Agricultural and Forest Meteorology*, 35(1-4):281–297.

Ball, J. T., Woodrow, I. E., and Berry, J. A. (1987). A model predicting stomatal conductance and its contribution to the control of photosynthesis under different environmental conditions. In *Progress in photosynthesis research*, pages 221–224. Springer.

Balsamo, G., Beljaars, A., Scipal, K., Viterbo, P., van den Hurk, B., Hirschi, M., and Betts, A. K. (2009). A revised hydrology for the ECMWF model: Verification from field site to terrestrial water storage and impact in the Integrated Forecast System. *Journal of hydrometeorology*, 10(3):623–643.

Balsamo, G., Pappenberger, F., Dutra, E., Viterbo, P., and Van den Hurk, B. (2011). A revised land hydrology in the ECMWF model: a step towards daily water flux prediction in a fully-closed water cycle. *Hydrological Processes*, 25(7):1046–1054.

Berry, J. and Bjorkman, O. (1980). Photosynthetic response and adaptation to temperature in higher plants. *Annual Review of plant physiology*, 31(1):491–543.

Best, M., Beljaars, A., Polcher, J., and Viterbo, P. (2004). A proposed structure for coupling tiled surfaces with the planetary boundary layer. *Journal of hydrometeorology*, 5(6):1271–1278.

Betts, A. K., Ball, J. H., and Beljaars, A. (1993). Comparison between the land surface response of the ECMWF model and the FIFE-1987 data. *Quarterly Journal of the Royal Meteorological Society*, 119(513):975–1001.

Betts, R. A. (2000). Offset of the potential carbon sink from boreal forestation by decreases in surface albedo. *Nature*, 408(6809):187.

Blackadar, A. K. (1976). Modeling the nocturnal boundary layer. In *Preprints, Third Symp. on Atmospheric Turbulence, Diffusion, and Air Quality, Raleigh.* Amer. Meteor. Soc.

Bonan, G. B. (1996). Land surface model (LSM version 1.0) for ecological, hydrological, and atmospheric studies: Technical description and users guide. Technical note. Technical report, National Center for Atmospheric Research, Boulder, CO (United States).

Brovkin, V., Boysen, L., Raddatz, T., Gayler, V., Loew, A., and Claussen, M. (2013). Evaluation of vegetation cover and land-surface albedo in MPI-ESM CMIP5 simulations. *Journal of Advances in Modeling Earth Systems*, 5(1):48–57.

Brovkin, V., Raddatz, T., Reick, C. H., Claussen, M., and Gayler, V. (2009). Global biogeophysical interactions between forest and climate. *Geophysical Research Letters*, 36(7).

Brutsaert, W. (1975). The roughness length for water vapor sensible heat, and other scalars. *Journal of the Atmospheric Sciences*, 32(10):2028–2031.

Budyko, M. (1956). The Heat Balance of the Earth's Surface, translated by NA Stepanova, 1958. *US Dept. of Commerce, Washington DC*, 259.

Burns, S., Blanken, P., Turnipseed, A., Hu, J., and Monson, R. (2015). The influence of warm-season precipitation on the diel cycle of the surface energy balance and carbon dioxide at a Colorado subalpine forest site. *Biogeosciences*, 12(23):7349–7377.

Campbell, G., Norman, J., et al. (1989). The description and measurement of plant canopy structure. In *Plant canopies: their growth, form and function*, volume 31, pages 1–19. Cambridge University Press Cambridge.

Chahine, M. T. (1992). The hydrological cycle and its influence on climate. *Nature*, 359(6394):373.

Chase, T. N., Pielke, R. A., Kittel, T. G., Nemani, R., and Running, S. W. (1996). Sensitivity of a general circulation model to global changes in leaf area index. *Journal of Geophysical Research: Atmospheres*, 101(D3):7393–7408.

Chen, T. H., Henderson-Sellers, A., Milly, P., Pitman, A., Beljaars, A., Polcher, J., Abramopoulos, F., Boone, A., Chang, S., Chen, F., et al. (1997). Cabauw experimental results from the project for intercomparison of land-surface parameterization schemes. *Journal of Climate*, 10(6):1194–1215.

Choudhury, B. J. and Monteith, J. (1988). A four-layer model for the heat budget of homogeneous land surfaces. *Quarterly Journal of the Royal Meteorological Society*, 114(480):373–398.

Claussen, M., Selent, K., Brovkin, V., Raddatz, T., and Gayler, V. (2013). Impact of CO2 and climate on Last Glacial maximum vegetation–a factor separation. *Biogeosciences*, 10:3593–3604.

Collatz, G. J., Ball, J. T., Grivet, C., and Berry, J. A. (1991). Physiological and environmental regulation of stomatal conductance, photosynthesis and transpiration: a model that includes a laminar boundary layer. *Agricultural and Forest meteorology*, 54(2-4):107–136.

Collatz, G. J., Ribas-Carbo, M., and Berry, J. (1992). Coupled photosynthesis-stomatal conductance model for leaves of C4 plants. *Functional Plant Biology*, 19(5):519–538.

da Silva, V., Almeida, R., Dantas, V., da Costa, A., Singh, V., et al. (2012). Sensible and Latent Heat Storage Fluxes within the Canopy Air-Space in the Amazon Rainforest. *Forest Res*, 1(106):2.

Dai, Y., Dickinson, R. E., and Wang, Y.-P. (2004). A two-big-leaf model for canopy temperature, photosynthesis, and stomatal conductance. *Journal of Climate*, 17(12):2281–2299.

Dai, Y., Zeng, X., Dickinson, R. E., Baker, I., Bonan, G. B., Bosilovich, M. G., Denning, A. S., Dirmeyer, P. A., Houser, P. R., Niu, G., et al. (2003). The common land model. *Bulletin of the American Meteorological Society*, 84(8):1013–1024.

de Vrese, P. and Hagemann, S. (2016). Explicit representation of spatial subgrid-scale heterogeneity in an ESM. *Journal of Hydrometeorology*, 17(5):1357–1371.

Deardorff, J. (1978). Efficient prediction of ground surface temperature and moisture, with inclusion of a layer of vegetation. *Journal of Geophysical Research: Oceans*, 83(C4):1889–1903.

Delpierre, N., Soudani, K., Francois, C., Köstner, B., Pontailler, J.-Y., Nikinmaa, E., Misson, L., Aubinet, M., Bernhofer, C., Granier, A., et al. (2009). Exceptional carbon uptake in European forests during the warm spring of 2007: a data–model analysis. *Global Change Biology*, 15(6):1455–1474.

Dickinson, R., Henderson-Sellers, A., Kennedy, P., and Wilson, M. (1986). Biosphere–atmosphere transfer scheme (BATS) for the NCAR Community Climate Model. NCAR Tech. *Note Tn-275+ STR*, 72.

Dirmeyer, P. A., Dolman, A., and Sato, N. (1999). The pilot phase of the global soil wetness project. *Bulletin of the American Meteorological Society*, 80(5):851–878.

dos Santos Michiles, A. A. and Gielow, R. (2008). Above-ground thermal energy storage rates, trunk heat fluxes and surface energy balance in a central Amazonian rainforest. *Agricultural and Forest Meteorology*, 148(6-7):917–930.

Ehlers, J. H. (1915). The temperature of leaves of Pinus in winter. *American Journal of Botany*, 2(1):32–70.

Ershadi, A., McCabe, M., Evans, J. P., Chaney, N. W., and Wood, E. F. (2014). Multi-site evaluation of terrestrial evaporation models using FLUXNET data. *Agricultural and Forest Meteorology*, 187:46–61.

Farquhar, G. D. and Sharkey, T. D. (1982). Stomatal conductance and photosynthesis. *Annual review of plant physiology*, 33(1):317–345.

Farquhar, G. v., von Caemmerer, S. v., and Berry, J. (1980). A biochemical model of photosynthetic CO_2 assimilation in leaves of C3 species. *Planta*, 149(1):78–90.

Fauset, S., Freitas, H. C., Galbraith, D. R., Sullivan, M. J., Aidar, M. P., Joly, C. A., Phillips, O. L., Vieira, S. A., and Gloor, M. U. (2018). Differences in leaf thermoregulation and water use strategies between three co-occurring Atlantic forest tree species. *Plant, cell & environment*, 41(7):1618–1631.

Feddes, R. A., Hoff, H., Bruen, M., Dawson, T., De Rosnay, P., Dirmeyer, P., Jackson, R. B., Kabat, P., Kleidon, A., Lilly, A., et al. (2001). Modeling root water uptake in hydrological and climate models. *Bulletin of the American meteorological society*, 82(12):2797–2810.

Garai, A., Kleissl, J., and Smith, S. G. L. (2010). Estimation of biomass heat storage using thermal infrared imagery: application to a walnut orchard. *Boundary-layer meteorology*, 137(2):333–342.

Gates, D. M. (1962). Leaf temperature and energy exchange. *Archiv für Meteorologie, Geophysik und Bioklimatologie, Serie B*, 12(2):321–336.

Gates, D. M. (1965). Energy, plants, and ecology. *Ecology*, 46(1-2):1–13.

Gates, W. L. (1992). AMIP: The atmospheric model intercomparison project. *Bulletin of the American Meteorological Society*, 73(12):1962–1970.

Giorgetta, M. A., Brokopf, R., Crueger, T., Esch, M., Fiedler, S., Helmert, J., Hohenegger, C., Kornblueh, L., Köhler, M., Manzini, E., et al. (2018). ICON-A, the Atmosphere Component of the ICON Earth System Model: I. Model Description. *Journal of Advances in Modeling Earth Systems*, 10(7):1613–1637.

Hagemann, S. (2002). An improved land surface parameter dataset for global and regional climate models. *MPI Reports*.

Hagemann, S. and Stacke, T. (2015). Impact of the soil hydrology scheme on simulated soil moisture memory. *Climate Dynamics*, 44(7-8):1731–1750.

Haverd, V., Cuntz, M., Leuning, R., and Keith, H. (2007). Air and biomass heat storage fluxes in a forest canopy: Calculation within a soil vegetation atmosphere transfer model. *Agricultural and Forest Meteorology*, 147(3-4):125–139.

Helliker, B. R. and Richter, S. L. (2008). Subtropical to boreal convergence of tree-leaf temperatures. *Nature*, 454(7203):511.

Henderson-Sellers, A., Yang, Z., and Dickinson, R. (1993). The project for intercomparison of land-surface parameterization schemes. *Bulletin of the American Meteorological Society*, 74(7):1335–1349.

Huete, A., Artiola, J., and Pepper, I. (2004). Environmental monitoring with remote sensing. *Environmental Monitoring and Characterization*, 11:183.

Hurtt, G. C., Chini, L. P., Frolking, S., Betts, R., Feddema, J., Fischer, G., Fisk, J., Hibbard, K., Houghton, R., Janetos, A., et al. (2011). Harmonization of land-use scenarios for the period 1500–2100: 600 years of

global gridded annual land-use transitions, wood harvest, and resulting secondary lands. *Climatic change*, 109(1-2):117.

Ingwersen, J., Imukova, K., Högy, P., and Streck, T. (2015). On the use of the post-closure methods uncertainty band to evaluate the performance of land surface models against eddy covariance flux data. *Biogeosciences*, 12(8):2311–2326.

Jacobs, A. F., Heusinkveld, B. G., and Holtslag, A. A. (2008). Towards closing the surface energy budget of a mid-latitude grassland. *Boundary-layer meteorology*, 126(1):125–136.

Jarvis, P. (1976). The interpretation of the variations in leaf water potential and stomatal conductance found in canopies in the field. *Philosophical Transactions of the Royal Society of London. B, Biological Sciences*, 273(927):593–610.

Kilinc, M., Beringer, J., Hutley, L. B., Haverd, V., and Tapper, N. (2012). An analysis of the surface energy budget above the world's tallest angiosperm forest. *Agricultural and forest meteorology*, 166:23–31.

Knauer, J., Werner, C., and Zaehle, S. (2015). Evaluating stomatal models and their atmospheric drought response in a land surface scheme: a multibiome analysis. *Journal of Geophysical Research: Biogeosciences*, 120(10):1894–1911.

Knorr, W. (2000). Annual and interannual CO2 exchanges of the terrestrial biosphere: Process-based simulations and uncertainties. *Global Ecology and Biogeography*, 9(3):225–252.

Koster, R. D., Sud, Y., Guo, Z., Dirmeyer, P. A., Bonan, G., Oleson, K. W., Chan, E., Verseghy, D., Cox, P., Davies, H., et al. (2006). GLACE: the global land–atmosphere coupling experiment. Part I: overview. *Journal of Hydrometeorology*, 7(4):590–610.

Kowalczyk, E., Stevens, L., Law, R., Dix, M., Wang, Y., Harman, I., Haynes, K., Srbinovsky, J., Pak, B., and Ziehn, T. (2013). The land surface model component of ACCESS: description and impact on the simulated surface climatology. *Aust. Meteorol. Oceanogr. J*, 63(1):65–82.

Krinner, G., Viovy, N., de Noblet-Ducoudré, N., Ogée, J., Polcher, J., Friedlingstein, P., Ciais, P., Sitch, S., and Prentice, I. C. (2005). A dynamic global vegetation model for studies of the coupled atmosphere-biosphere system. *Global Biogeochemical Cycles*, 19(1).

Kusano, S. (1901). Transpiration of evergreen trees in winter. *The journal of the College of Science, Imperial University of Tokyo*, 15:313–366.

Lawrence, D. M., Thornton, P. E., Oleson, K. W., and Bonan, G. B. (2007). The partitioning of evapotranspiration into transpiration, soil evaporation, and canopy evaporation in a GCM: Impacts on land–atmosphere interaction. *Journal of Hydrometeorology*, 8(4):862–880.

Lee, X. (2018). *Fundamentals of boundary-layer meteorology*. Springer.

Linacre, E. (1964). A note on a feature of leaf and air temperatures. *Agricultural Meteorology*, 1(1):66–72.

Linacre, E. (1967). Further notes on a feature of leaf and air temperatures. *Archiv für Meteorologie, Geophysik und Bioklimatologie, Serie B*, 15(4):422–436.

Linacre, E. and Harris, W. (1970). A thermistor leaf thermometer. *Plant physiology*, 46(2):190–193.

Lindroth, A., Mölder, M., and Lagergren, F. (2010). Heat storage in forest biomass improves energy balance closure. *Biogeosciences*, 7(1):301–313.

Loew, A., van Bodegom, P., Widlowski, J.-L., Otto, J., Quaife, T., Pinty, B., and Raddatz, T. (2014). Do we (need to) care about canopy radiation schemes in DGVMs? Caveats and potential impacts. *Biogeosciences*, 11:1873–1897.

Louis, J. (1982). A short history of PBL parameterization at ECMWF. In *paper presented at the Workshop on Planetary Boundary Layer Parameterization, Eur. Cent. For Medium-Range Weather Forecasts, Reading, England, 1982*.

Louis, J.-F. (1979). A parametric model of vertical eddy fluxes in the atmosphere. *Boundary-Layer Meteorology*, 17(2):187–202.

Luo, X., Chen, J. M., Liu, J., Black, T. A., Croft, H., Staebler, R., He, L., Arain, M. A., Chen, B., Mo, G., et al. (2018). Comparison of big-leaf, two-big-leaf, and two-leaf upscaling schemes for evapotranspiration estimation using coupled carbon-water modeling. *Journal of Geophysical Research: Biogeosciences*, 123(1):207–225.

Manabe, S. (1969). Climate and the ocean circulation. *Mon. Wea. Rev*, 97(11):739–774.

Mauritsen, T., Bader, J., Becker, T., Behrens, J., Bittner, M., Brokopf, R., Brovkin, V., Claussen, M., Crueger, T., Esch, M., et al. (2019). Developments in the MPI-M Earth System Model version 1.2 (MPI-ESM1. 2) and its response to increasing CO2. *Journal of Advances in Modeling Earth Systems*, 11(4):998–1038.

Meyers, T. P. and Hollinger, S. E. (2004). An assessment of storage terms in the surface energy balance of maize and soybean. *Agricultural and Forest Meteorology*, 125(1-2):105–115.

Michaletz, S., Blonder, B., Chambers, J., Enquist, B., Faybishenko, B., Grossiord, C., Jardine, K., Negron Juarez, R., Varadharajan, C., McDowell, N., et al. (2016a). Do general patterns of leaf thermoregulation hold in the tropics? In *AGU Fall Meeting Abstracts*.

Michaletz, S. T., Weiser, M. D., McDowell, N. G., Zhou, J., Kaspari, M., Helliker, B. R., and Enquist, B. J. (2016b). The energetic and carbon economic origins of leaf thermoregulation. *Nature plants*, 2(9):16129.

Mintz, Y. (1984). 1984: The sensitivity of numerically simulated climates to land-surface boundary conditions. In Houghton, JT, editor, The global climate, Cambridge: Cambridge University Press, 79-105.

Moore, C. and Fisch, G. (1986). Estimating heat storage in Amazonian tropical forest. *Agricultural and Forest Meteorology*, 38(1-3):147–168.

Nabel, J. E., Naudts, K., and Pongratz, J. (2019). Accounting for forest age in the tile-based dynamic global vegetation model JSBACH4 (4.20 p7; git feature/forests)–a land surface model for the ICON-ESM. *Geoscientific Model Development*.

Niu, G.-Y., Yang, Z.-L., Mitchell, K. E., Chen, F., Ek, M. B., Barlage, M., Kumar, A., Manning, K., Niyogi, D., Rosero, E., et al. (2011). The community Noah land surface model with multiparameterization options (Noah-MP): 1. Model description and evaluation with local-scale measurements. *Journal of Geophysical Research: Atmospheres*, 116(D12).

Nobel, P. (2009). *Physicochemical and Environmental Plant Physiology.* Elsevier Science.

Oki, T. and Kanae, S. (2006). Global hydrological cycles and world water resources. *science*, 313(5790):1068–1072.

Otto, J., Raddatz, T., and Claussen, M. (2011). Strength of forest-albedo feedback in mid-Holocene climate simulations. *Climate of the Past*, 7(3):1027–1039.

Pitman, A. (2003). The evolution of, and revolution in, land surface schemes designed for climate models. *International Journal of Climatology*, 23(5):479–510.

Polcher, J., Cox, P., Dirmeyer, P., Dolman, H., Gupta, H., Henderson-Sellers, A., Houser, P., Koster, R., Oki, T., Pitman, A., et al. (2000). GLASS: Global land-atmosphere system study. *GEWEX News*, 10(2):3–5.

Pongratz, J., Reick, C., Raddatz, T., and Claussen, M. (2008). A reconstruction of global agricultural areas and land cover for the last millennium. *Global Biogeochemical Cycles*, 22(3).

Raddatz, T., Reick, C., Knorr, W., Kattge, J., Roeckner, E., Schnur, R., Schnitzler, K.-G., Wetzel, P., and Jungclaus, J. (2007). Will the tropical land biosphere dominate the climate–carbon cycle feedback during the twenty-first century? *Climate Dynamics*, 29(6):565–574.

Rameaux (1843). Des températures végétales. *Paris, Ann. Sc.*, 8:30.

Reick, C., Raddatz, T., Brovkin, V., and Gayler, V. (2013). Representation of natural and anthropogenic land cover change in MPI-ESM. *Journal of Advances in Modeling Earth Systems*, 5(3):459–482.

Rey-Sánchez, A. C., Slot, M., Posada, J. M., and Kitajima, K. (2016). Spatial and seasonal variation in leaf temperature within the canopy of a tropical forest. *Climate Research*, 71(1):75–89.

Richtmyer, R. and Morton, K. (1967). Interscience tracts in pure and applied mathematics, Vol. 4, Difference Methods for Initial Value Problems, 2nd edn., ed. L. Bers, R. Courant, & J. Stoker, J.

Roeckner, E., Bauml, G., Bonaventura, L., Brokopf, R., Esch, M., Giorgetta, M., Hagemann, S., Kirchner, I., Kornblueh, L., Manzini, E., et al. (2003). The atmospheric general circulation model EHAM5. Part I: model description. *MPI Reports*.

Samuelsson, P., Gollvik, S., and Ullerstig, A. (2006). *The land-surface scheme of the Rossby Centre regional atmospheric climate model (RCA3)*. SMHI.

Schimel, D. S., House, J. I., Hibbard, K. A., Bousquet, P., Ciais, P., Peylin, P., Braswell, B. H., Apps, M. J., Baker, D., Bondeau, A., et al. (2001). Recent patterns and mechanisms of carbon exchange by terrestrial ecosystems. *Nature*, 414(6860):169.

Schulz, J.-P., Dümenil, L., and Polcher, J. (2001). On the land surface–atmosphere coupling and its impact in a single-column atmospheric model. *Journal of Applied Meteorology*, 40(3):642–663.

Sellers, P., Dickinson, R., Randall, D., Betts, A., Hall, F., Berry, J., Collatz, G., Denning, A., Mooney, H., Nobre, C., et al. (1997). Modeling the exchanges of energy, water, and carbon between continents and the atmosphere. *Science*, 275(5299):502–509.

Sellers, P., Mintz, Y., Sud, Y. e. a., and Dalcher, A. (1986). A simple biosphere model (SiB) for use within general circulation models. *Journal of the Atmospheric Sciences*, 43(6):505–531.

Sellers, P., Randall, D., Collatz, G., Berry, J., Field, C., Dazlich, D., Zhang, C., Collelo, G., and Bounoua, L. (1996). A revised land surface parameterization (SiB2) for atmospheric GCMs. Part I: Model formulation. *Journal of climate*, 9(4):676–705.

Sellers, P. J. (1985). Canopy reflectance, photosynthesis and transpiration. *International Journal of Remote Sensing*, 6(8):1335–1372.

Seneviratne, S. I., Corti, T., Davin, E. L., Hirschi, M., Jaeger, E. B., Lehner, I., Orlowsky, B., and Teuling, A. J. (2010). Investigating soil moisture–climate interactions in a changing climate: A review. *Earth-Science Reviews*, 99(3-4):125–161.

Shuttleworth, W. J. and Wallace, J. (1985). Evaporation from sparse crops-an energy combination theory. *Quarterly Journal of the Royal Meteorological Society*, 111(469):839–855.

Steeneveld, G., Van de Wiel, B., and Holtslag, A. (2006). Modeling the evolution of the atmospheric boundary layer coupled to the land surface for three contrasting nights in CASES-99. *Journal of the atmospheric sciences*, 63(3):920–935.

Stevens, B., Giorgetta, M., Esch, M., Mauritsen, T., Crueger, T., Rast, S., Salzmann, M., Schmidt, H., Bader, J., Block, K., et al. (2013). Atmospheric component of the MPI-M Earth System Model: ECHAM6. *Journal of Advances in Modeling Earth Systems*, 5(2):146–172.

Svensson, G., Holtslag, A., Kumar, V., Mauritsen, T., Steeneveld, G., Angevine, W., Bazile, E., Beljaars, A., De Bruijn, E., Cheng, A., et al. (2011). Evaluation of the diurnal cycle in the atmospheric boundary layer over land as represented by a variety of single-column models: the second GABLS experiment. *Boundary-Layer Meteorology*, 140(2):177–206.

Taha, H., Akbari, H., and Rosenfeld, A. (1991). Heat island and oasis effects of vegetative canopies: micro-meteorological field-measurements. *Theoretical and Applied Climatology*, 44(2):123–138.

Thornley, J. (1971). Energy, respiration, and growth in plants. *Annals of Botany*, 35(4):721–728.

Trigo, I., Boussetta, S., Viterbo, P., Balsamo, G., Beljaars, A., and Sandu, I. (2015). Comparison of model land skin temperature with remotely sensed estimates and assessment of surface-atmosphere coupling. *Journal of Geophysical Research: Atmospheres*, 120(23).

Twine, T. E., Kustas, W., Norman, J., Cook, D., Houser, P., Meyers, T., Prueger, J., Starks, P., and Wesely, M. (2000). Correcting eddy-covariance flux underestimates over a grassland. *Agricultural and Forest Meteorology*, 103(3):279–300.

Vamborg, F., Brovkin, V., and Claussen, M. (2011). The effect of dynamic background albedo scheme on Sahel/Sahara precipitation during the Mid-Holocene. *Climate of the Past*, 7:117–131.

Verseghy, D., McFarlane, N., and Lazare, M. (1993). CLASS – A Canadian land surface scheme for GCMs, II. Vegetation model and coupled runs. *International Journal of Climatology*, 13(4):347–370.

Vidale, P. and Stöckli, R. (2005). Prognostic canopy air space solutions for land surface exchanges. *Theoretical and applied climatology*, 80(2-4):245–257.

Viterbo, P. and Beljaars, A. C. (1995). An improved land surface parameterization scheme in the ECMWF model and its validation. *Journal of Climate*, 8(11):2716–2748.

Weedon, G. P., Balsamo, G., Bellouin, N., Gomes, S., Best, M. J., and Viterbo, P. (2014). The WFDEI meteorological forcing data set: WATCH Forcing Data methodology applied to ERA-Interim reanalysis data. *Water Resources Research*, 50(9):7505–7514.

Wohl, K. and James, W. (1942). The energy changes associated with plant respiration. *New Phytologist*, 41(4):230–256.

Xue, Y., Sellers, P., Kinter, J., and Shukla, J. (1991). A simplified biosphere model for global climate studies. *Journal of Climate*, 4(3):345–364.

Zheng, W., Best, M., Lock, A., and Ek, M. (2013). Initial Results from the Diurnal Land/Atmosphere Coupling Experiment (DICE). In *AGU Fall Meeting Abstracts*.

Danksagung

First of all, I would like to thank my two supervisors, Felix Ament and Andreas Chlond, not only for the last four years of productive collaboration, supervision, and support but rather for accompanying my scientific career for almost 10 years. I want to thank Felix Ament for giving me a huge boost of motivation through his positive way of thinking, all over again. A special thanks goes to Andreas Chlond for the almost daily cooperation and occasional discussions about hours in which he always kept a calm mind and lived up to his role as "Doktorvater".

Furthermore. I want to thank Martin Claußen, who has also accompanied me for almost 10 years in my scientific career, for the productive panel meetings in which he ensured the smooth progress of my doctoral thesis. In particular, I would like to thank him for making it possible to have a first look into the world of teaching.

Special thanks go to Antje Weitz, who has been available at all times since my first day at the IMPRS to give advice and support to the other doctoral students and me. If the term "doctoral mother" exists, it should be assigned for her!
In summary, I would like to thank all four persons mentioned once again for their understanding and support during a more difficult phase at the end of my doctoral thesis.

I would also like to thank Bjorn Stevens for the joyful collaboration from time to time and for his unique lectures, which, through his enthusiasm and passion for science (and especially water), are a model for my possible future career in teaching.

Another thanks goes to my (former) work colleagues from the Schäferkampsallee crew, Goran Georgievski, Stefan Hagemann (who is also part of my panel), Tobias Stacke and Philipp de Vrese for the nice welcome in the working group. Additional thanks go to Tobias and Philipp for all their help and answers to questions about the model, as well as for the spontaneous proofreading of this work.

A very special thanks goes to Alexander Lemburg, who has been a good friend since the beginning of our studies, for his constant help and fun at work, especially on nights before a deadline (which I really appreciate)!

Last but not least, I want to thank my parents who were always there for me in the past – especially when I needed them the most.

Versicherung an Eides statt

Declaration of oath

Hiermit versichere ich an Eides statt, dass ich die vorliegende Dissertation mit dem Titel: „Studying land–atmosphere interactions in an Earth system model – The role of canopy heat storage and leaf thermoregulation" selbstständig verfasst und keine anderen als die angegebenen Hilfsmittel – insbesondere keine im Quellenverzeichnis nicht benannten Internet-Quellen – benutzt habe. Alle Stellen, die wörtlich oder sinngemäß aus Veröffentlichungen entnommen wurden, sind als solche kenntlich gemacht. Ich versichere weiterhin, dass ich die Dissertation oder Teile davon vorher weder im In- noch im Ausland in einem anderen Prüfungsverfahren eingereicht habe und die eingereichte schriftliche Fassung der auf dem elektronischen Speichermedium entspricht.

Hamburg, den 05.02.2020   ....
                                            Marvin Heidkamp

Hinweis / Reference

Die gesamten Veröffentlichungen in der Publikationsreihe des MPI-M
„Berichte zur Erdsystemforschung / Reports on Earth System Science",
ISSN 1614-1199

sind über die Internetseiten des Max-Planck-Instituts für Meteorologie erhältlich:
http://www.mpimet.mpg.de/wissenschaft/publikationen.html

All the publications in the series of the MPI -M
„Berichte zur Erdsystemforschung / Reports on Earth System Science",
ISSN 1614-1199

are available on the website of the Max Planck Institute for Meteorology:
http://www.mpimet.mpg.de/wissenschaft/publikationen.html